# Aspects of Preheating after Inflation

Patrick Bradley Greene

December 17, 2001

# Abstract

Aspects of Preheating after Inflation

Patrick Bradley Greene

Doctor of Philosophy
Graduate Department of Physics
University of Toronto
2002

We review several aspects of preheating after inflation. Topics covered include the structure of bosonic parametric resonance in conformal theories, the parametric excitation of fermions both with and without expansion of the universe, and tachyonic preheating at the end of supersymmetric hybrid inflation.

# Acknowledgments

Many praises are due to all of my collaborators. Their ideas and insights fill these pages. I thank them for sharing their knowledge with me and stimulating my own research and excitement in cosmology and particle physics.

I'd particularly like to thank my advisor, Lev "the Levitino" Kofman, and Andrei Linde for their encouragement and tutelage. "All things move according to the whim of the Great Magnet"; I'm very fortunate to have had the opportunity to work with them. Lev has been a conscientious shepherd and a real friend, two things that I've heard many advisors are not.

I would also like to thank my many, many good friends on several continents who have shared their company with me over the years and have been there when I needed them. I am grateful for so many memories of nice people, fine food, and too much drink. Desert trips, communal meals in the Santa Cruz co-op, Thanksgiving dinners in Hawaii, cook-outs in the St. George courtyard, wings and beer at the Ferret... have all meant a lot to me. I don't recall who said it, but I'd agree

> *He who has but once dined his friends has tasted whatever it is to be Caesar.*

Finally, I'd like to dedicate this work to my wife, Sigrid Kümpel Greene, and my parents, Malbone Watson Greene and Betty Morse Greene.

# Contents

# Chapter 1

# Introduction

Substantial observational evidence suggests that the standard Big Bang cosmological model correctly describes the history of the Universe for the last 13 or so billion years. Tests support the model back at least to the epoch of primordial nucleosynthesis, at which time the primordial nucleon soup was at a temperature of a few MeV. Our understanding of the Standard Model of particle physics encourages us to push this back even further, in spite of a lack of direct observational evidence, and try to understand, for example, electroweak symmetry breaking as a thermal phase transition in the early universe. Nevertheless, the success of the Big Bang and Standard models requires us to deal seriously with their well known shortcomings. These include, on the cosmological side, explaining the large scale smoothness and small scale inhomogeneity of the universe, its apparent spatial flatness, and the nature of the initial singularity. On the particle physics side, the Standard Model does not provide an explanation of the observed dark matter and dark energy components of the Universe. Furthermore, within the simplest extensions of the Standard Model that incorporate grand unification, there is no easy way to understand the absence of certain relics and defects, like magnetic monopoles, that the expanding and cooling universe should have left behind in abundance.

There can be no doubt that inflation is the dominant paradigm for understanding the origin of the hot Big Bang universe and thereby addressing some of the shortcomings listed above. Inflation does this by hypothesizing that, at some stage in the evolution of the early universe, the Hubble expansion was quasi-exponential rather than the gradual power law expansion we see today and that would be expected of a hot, radiation dominated universe. This exponential period of expansion smoothes out inhomogeneities, flattens spatial sections, and dilutes the abundance of relics and defects. Furthermore, the mechanism of inflation can be understood within the Standard Model as an "effective cosmological constant" created by the expectation value of a scalar field (either fundamental or composite) shifted away from its true vev (vacuum expectation value). In these models, quantum fluctuations of this field, amplified and stretched outside of the Hubble radius during inflation, serve as the source of primordial inhomogeneities. These later fall back into the Hubble radius leading eventually to structure formation and explaining the slight anisotropy observed in the cosmic microwave background radiation.

From the beginning, the theory of inflation has been associated with four basic predictions. The first is that the visible universe should be spatially flat to a high degree of precision. The second is that the primordial spectrum of adiabatic density perturbations should be nearly flat ($n = 1$). The third is that there should be an appreciable gravitational wave background remnant from inflation. The fourth prediction is that all matter in the visible universe must have been created after inflation. Recent high precision observations indicate that the first two of these predictions are remarkably accurate. It is hoped that a signal of the gravitational wave background will be found very shortly.

The fourth prediction, that all matter is created after inflation, is the subject of this thesis. The success of the Hot Big Bang model shows that any viable model of inflation must eventually lead to the creation of a hot, Friedmann universe with a temperature greater than at least a few MeV. The question of how this can be arranged within the usual models of inflation is more difficult than it might seem. The necessity of matter creation after inflation is due to the fact that the expansion brought about by inflation exponentially dilutes the energy density of all matter in the universe, except for the inflaton scalar field. At the end of inflation, the inflaton's energy must somehow be converted into a relativistic gas of hot particles. Indeed, this "graceful exit" or reheating problem killed Guth's original theory of inflation (c.f. [1] for a recent review of early inflation theory with references therein).

Guth's original theory [2] used the false vacuum energy of a scalar field trapped in a metastable state to drive inflation. Inflation was supposed to end through bubble nucleation to the true vacuum. These bubbles would then collide, dissipating their energy to other fields, reheating the universe. The problem was that the bubble collisions either didn't happen, because the tunneling rate was too small, or, if they were produced and collided, the collisions produced unacceptable inhomogeneities. Guth's "old inflation" model was soon replaced by another for which bubble nucleation was not an essential feature [3, 4]. Soon after these "new inflation" models were proposed came a new solution to the reheating problem [5, 6]. New inflation ended with the inflaton field oscillating about the minimum of its potential near its true vev. The coherently oscillating inflaton field could be considered as a collection of many inflaton particles with couplings to other fields. These massive particles would then perturbatively decay into lighter particles, reheating the universe.

As we will discuss shortly, the interaction of the inflaton was expected to lead to an effective perturbative decay rate $\Gamma_{\rm tot}$. Perturbative reheating would only occur once the expansion rate after inflation decreased to the order of the perturbative decay rate: $H \sim \Gamma_\phi$. This lead to tight bounds on the maximum reheating temperature after inflation. It also implied that nothing interesting happened for the first $O(m_\phi \Gamma_\phi^{-1}) \gg 1$ inflaton oscillations after inflation.

This basic reheating scenario survived in subsequent inflationary models, like chaotic and hybrid inflation, which we will discuss here. These models are of the most interest currently because they do not require that the universe was ever in thermal equilibrium prior to inflation, unlike both old and new inflation, c.f. [7]. The modern picture, embodied in these models, is that inflation occurred as a natural relaxation process of scalar fields in the early universe. There is no reason to assume that any fundamental scalars present in the early universe would be found at their low energy vevs. Once any such region of the early universe began to expand, for whatever reason, it would naturally evolve into an inflating universe. Such inflating regions would be exponentially larger than all others. Inflation would end in a given patch when the scalar fields relax sufficiently close to their true vevs. They would then oscillate around these vevs, just as in new inflation.

However, about a decade after the original perturbative reheating scenario was developed, Traschen and Brandenberger [8], Kofman, Linde and Starobinsky [9], and others realized that reheating due to the coherent oscillations of the inflaton typically begins with a stage of explosive particle creation, which Kofman, Linde and Starobinsky called *preheating*. It was found that, even if the inflaton field interacts only weakly with other bosons, its coherent oscillations can induce a resonant decay process, creating exponentially large numbers of the other bosons or fluctuations of itself. Thus, even for a small coupling constant and $\Gamma_\phi / m_\phi \ll 1$, this resonance can lead to the rapid decay of much of the inflaton's energy.

Preheating typically leads to the growth of large amplitude, long wavelength bosonic fluctuations, far from thermal equilibrium, which can be treated as classical fields. These waves will scatter off one another and decay into particles of other fields. This leads to thermalization, but it occurs on a time scale different from what would be expected in the original theory.

This thesis is a collection of some of the author's contributions to the theory of preheating. With his collaborators, the author has sought to understand general features of preheating and when and where preheating will occur. These investigations have lead to some surprising new results, which will be the topic of this thesis.

Inflation has rightly been called “a scenario in search of a model” [10]. In practice, no one has a good idea which fundamental or composite scalar field might have caused inflation or at exactly what energy scale this occurred. No one knows what the reheating temperature was, and thus, how far back the Hot Big Bang should be taken seriously. The study of inflationary “toy” models is important for classifying the kinds of scalar field theories (i.e. effective Lagrangians) that seem to allow viable inflation and reheating. One guiding principle in the author and his collaborators' approach has been to try to understand how reheating fits into the bigger cosmological picture. This has meant examining in what theories and in what guises preheating might occur. For example, in considering models of inflation that follow from supersymmetry or supergravity, we have been lead to consider the role of fermions in preheating and preheating in so-called “hybrid” models of inflation which involve several scalar fields shifted from their vevs. Both of these issues will be addressed in this thesis.

The organization of this thesis is as follows: Chapter 2 reviews [11] on bosonic preheating in the class of conformal theories characterized by the interaction Lagrangian

$$-\mathcal{L}_{\rm int} = \frac{1}{4}\lambda\phi^4 + g_i^2\phi^2\chi_i^2\,, \tag{1.1}$$

where several real scalar fields $\chi_i$ interact with the inflaton field $\phi$ through a four-legs type interaction. Inflation in this theory is supported by the quartic inflaton potential $V(\phi) = \frac{1}{4}\lambda\phi^4$ and has the interesting property of conformal invariance that allows us to transform away all the effects of expansion. The resulting equation that describes the resonant amplification of $\chi$-field modes is the well known Lamé equation [9]. In finding both numerical and analytic solutions for the particle production governed by the Lamé equation, we gain a better understanding of preheating. Among other things, we find that the strength of the resonance is a non-monotonic function of the coupling parameters. Thus, the fields with larger $g_i$ will not necessarily be more strongly produced. As we discuss in Chapter 2, this has implications for some earlier attempts at understanding preheating by considering certain particular values of $g^2$ and $\lambda$.

The next two chapters deal with the non-perturbative production of fermions during preheating. It was originally thought that fermion creation would not be particularly interesting as Pauli blocking prohibits the occupation number of fermions from becoming exponentially large–or greater than one for that matter. However, in [12] the author and his collaborator discovered that fermion creation is quite pronounced nonetheless. We found that fermions will very quickly saturate a broad band in momentum space. Even for very small Yukawa coupling constant, the production of fermions during preheating differs markedly from the perturbative theory. This rapid and strong growth in occupation number was termed "parametric excitation of fermions" and "fermionic preheating". In addition to the numerical investigation of this effect (coincidentally undertaken and appreciated by another group [13]), the author and his collaborator were able to extend and apply some analytic results–known for many years in the study of $e^+e^-$ pair production in strong electric fields–to the problem of fermionic preheating. These analytic results are useful for understanding fermionic preheating in models where expansion can be neglected or transformed away. The application and extension of these results, as well as the numerical investigation of fermionic preheating when expansion can be neglected or removed are the subject of Chapter 3.

In Chapter 4 we review the results of [14] which extended our analysis to non-conformal theories with massive fermions for which the role of expansion is very important. Here, expansion makes the previous analytic results no longer useful. Nevertheless, we were able to extend the method of successive parabolic scatterings, a very useful technique in the bosonic case, to the study of fermions. This method, originally developed in [15], is also applied to the bosonic conformal theory in Chapter 2 [11]. It allows an analytic investigation of preheating in the broad resonance case. For fermions, the net result is that particles are only created when their effective mass vanishes due to the oscillations of the inflaton field. Between these moments, the number of fermions does not change. We find an analytic expression for the change in fermion occupation number between two zeros and compare it to the bosonic result.

Another important observation is that fermions much more massive than the inflaton can be created during preheating. In the bosonic case, particles with a mass $m_b \sim q^{1/4} m_\phi$ can be created [15]. Here, $q \gg 1$ is a dimensionless parameter characterizing the strength of the resonance. In the fermionic case, the analogous limit is $m_\psi \sim q^{1/2} m_\phi \gg m_b$. Particles created in this manner can have masses as large as $O(10^{17})$ GeV! This result was first noticed in [16] and numerically investigated in [17]. Following [14], we present an analytic formula for the final spectrum of produced supermassive fermions in Chapter 4.

The final body Chapter of this thesis deals with preheating in hybrid models of inflation. In particular, we consider a couple of different models motivated by attempts to find supersymmetric models for inflation. Hybrid models can have many fields shifted away from their true vevs during inflation. Inflation in these models ends when the slow motion of one of these fields towards its vev triggers spontaneous symmetry breaking (SSB) in another field or multiplet of fields. Originally, it was thought that these fields would roll towards their vevs in a classical manner, executing oscillations around the minimum. These oscillations would then lead to p/reheating as in the simple one field models. In fact, we have found that typically these oscillations never occur [18, 19]. SSB occurs due to the appearance of a negative mass-square, or tachyonic mass, for some of the fields. This tachyonic mass develops quickly and the system is quenched. The result is that long wavelength modes are exponentially amplified, breaking the symmetry and creating a very inhomogeneous background. This can be the case even if the typical separation between defects is large.

Because the quenched transition in hybrid inflation results in large amplitude and long wavelength, semi-classical fluctuations of the scalar fields, the end result looks qualitatively and quantitatively like the effect of bosonic parametric resonance in bosonic preheating. We therefore refer to this effect as *tachyonic preheating*. In Chapter 5 we investigate this effect first through a linear analysis of the fluctuations and then via lattice simulations. The linear analysis reveals that, within a single oscillation of the would-be background fields, fluctuations are amplified by the tachyonic instability to a level where their backreaction must be incorporated. Fortunately, the rapid growth of fluctuations means that these modes may be treated as semi-classical waves and solved on a lattice. The results of these calculations confirm that most of the scalar field's initial potential energy from the false vacuum state is lost to fluctuations within a single oscillation. It is thus meaningless to talk of a mean background field plus fluctuations around this. Furthermore, the theory of tachyonic preheating will be important whenever one considers quenched phase transitions in the early universe (or elsewhere).

In the remainder of this introduction, we will discuss a simple model of chaotic inflation due to Linde [20]. In this model, inflation is supported by a simple mass term for the inflaton field $\phi$. As the rest of this thesis is concerned with the stage of oscillations of the inflaton field which occurs after inflation, in the next section, we will take the opportunity to familiarize the reader with the inflationary stage in this one example. In particular, we will show that the amplitude of adiabatic density perturbations generated during inflation can be used to determine the inflaton's mass, once the COBE normalization is applied [7, 10].

After this, we discuss perturbative reheating in this simple model and show why preheating actually occurs long before perturbative reheating can take place. We follow [15] in this discussion. We conclude the introduction with some remarks on the current status of reheating and the role of preheating in inflationary theory.

## 1.1 A Simple Model of Inflation

As we said above, the standard way to achieve inflation, and the only one considered here, is through the vacuum energy of a slowly evolving, homogeneous scalar field. Take, for example, a scalar field, $\phi$, minimally coupled to gravity in a flat Friedmann-Robertson-Walker (FRW) universe[1]. The scalar field's evolution is

[1]Refer to Appendix A for our notation.

governed by the Klein-Gordon equation generalized to curved space-time:

$$\ddot{\phi} + 3H\dot{\phi} = -\frac{\partial V}{\partial \phi}\,, \tag{1.2}$$

where $H$ is the Hubble parameter, $V(\phi)$ is the field's potential, and we have taken the scalar field to be homogeneous $\phi = \phi(t)$. For an FRW universe, the expansion of the universe is determined by the Friedmann equation

$$H^2 = \left(\frac{\dot{a}}{a}\right)^2 = \frac{8\pi}{3M_p^2}\left(\frac{1}{2}\dot{\phi}^2 + V(\phi)\right)\,, \tag{1.3}$$

with $a(t)$ the scale factor of the universe. Here we have assumed that the inflaton field alone is the dominant source of energy-momentum in the early universe.

We will consider the inflaton to be simply a massive field: $V(\phi) = \frac{1}{2}m_\phi^2\phi^2$. It is not difficult to follow this same development through for an arbitrary power-law dependence $V \sim \phi^n$ [7], but we will forego such generality.

Suppose the inflaton field starts out shifted away from its true vev at zero. This might occur due to quantum fluctuations in the early universe, for example. If $\phi(t) \gg M_p$, the damping term in (1.2) dominates the evolution of the inflaton as it tries to roll back to the minimum of its potential[2]. During this slow-roll stage, the Klein-Gordon and Friedmann equations become approximately

$$3H\dot{\phi} \approx -m_\phi^2\phi \tag{1.4}$$

and

$$H^2 \approx \frac{8\pi}{3M_p^2}\left(\frac{1}{2}m_\phi^2\phi^2\right) \tag{1.5}$$

which just describe the over-damped evolution of the $\phi$-field. These equations are easily solved to give the motion of the inflaton:

$$\phi(t) = \phi_0 - \frac{m_\phi M_p}{2\sqrt{3\pi}}t\,. \tag{1.6}$$

Substituting this solution into the Friedmann equation, we obtain an equation for the scale factor of the universe. To this approximation we find quasi-exponential

[2] Here and elsewhere we will use the field to represent its expectation value. As the field amplitude is large, we can treat it semi-classically and there is no need to distinguish between the two.

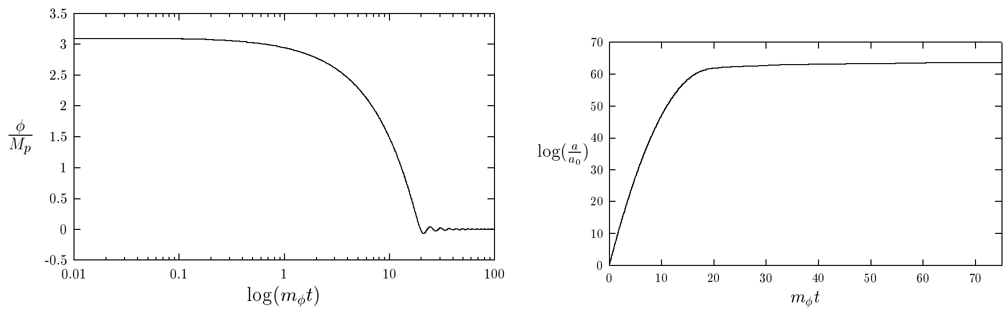


Figure 1.1: The left panel shows the evolution of the inflaton field during and after the stage of inflation as a function of time in the chaotic inflation model with a quadratic potential. We have actually used a logarithmic time scale to stretch out the inflationary period relative to that of oscillations. Inflation ends "quickly" relative to the oscillatory time scale $m_\phi^{-1}$, but the field amplitude changes very slowly during the inflationary epoch due to Hubble damping. The right panel shows the evolution of the scale factor, $a(t)$, for the same model. We plot the natural log of the scale factor as a function of time, measured in units of $m_\phi^{-1}$. Note that the inflationary stage appears linear with this scaling, and ends at $t \approx 10 m_\phi^{-1}$. During the stage of oscillations, the scale factor grows like that of a matter dominated universe: $a(t) \sim t^{2/3}$.

expansion

$$a(t) = a_0 \exp\left(\frac{2\pi}{M_p^2}[\phi_0^2 - \phi^2(t)]\right) . \tag{1.7}$$

The slow-roll approximation will break down once the inflaton field rolls down sufficiently close to the minimum of its potential. Specifically, once the curvature of the potential becomes comparable to the damping, inflation will end. This simple estimate gives $3H_e \approx m_\phi$ or $\phi_e \approx (\sqrt{12\pi})^{-1} M_p \approx \frac{1}{6} M_p$ at the end of the inflationary stage. (For a more careful derivation of these results, see [7].) For later use, it is convenient to express the amplitude of the inflaton field as a function of the number of e-foldings, $N$, of expansion remaining before the end of inflation: $N = \ln(a_e/a)$. From (1.7) we have

$$\phi_N \approx \sqrt{\frac{N}{2\pi}} M_p \,. \tag{1.8}$$

It is a straight forward matter to solve the Klein-Gordon equation (1.2) and Friedman equation (1.3) numerically for this example. In the left panel of figure 1.1 we plot the time development of the inflaton field, $\phi(t)$. We have chosen

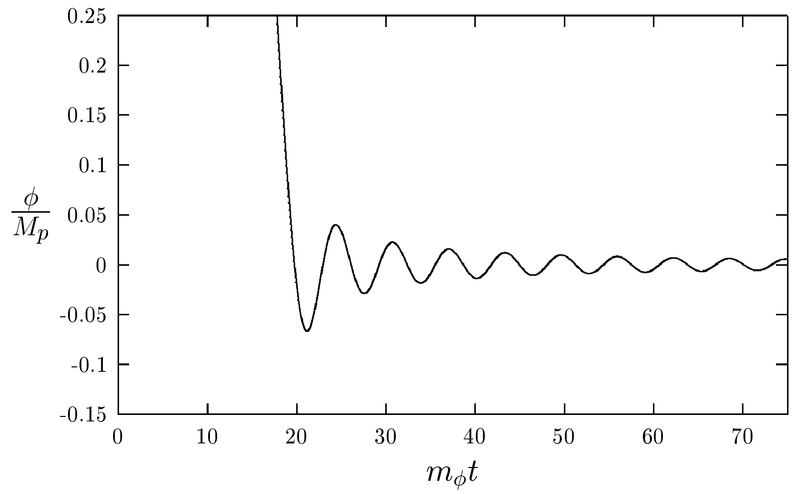


Figure 1.2: The evolution of the inflaton field, $\phi$, as a function of time in the simple chaotic inflation model with a quadratic potential. Field amplitude is measured in units of $M_p$ and time in units of $m_\phi^{-1}$. Soon after the end of the inflationary stage, the inflaton field begins to oscillate about the minimum of its potential. These oscillations are damped due to the expansion of the Universe.

the initial value $\phi_0 = 3.1 M_p$ and measure time from this moment, in units of $m_\phi^{-1}$. In the right panel of figure 1.1 we plot the time development of the scale factor for this example. We have chosen $a(0) = 1$ and plot the natural log of the scale factor as a function of time, again in units of $m_\phi^{-1}$. We see that the scale factor grows by roughly 60 e-foldings, as predicted by (1.7), and that the inflationary phase ends somewhat before $\phi = \frac{1}{6} M_p$. In figure 1.2 we show the evolution of the inflaton field at the stage of oscillations.

It is not obvious from the right panel of figure 1.1, but during the stage of oscillations, the scale factor grows approximately as for a matter dominated universe: $a(t) \sim t^{2/3}$. One can see this in a simple way. Covariant conservation of the energy-momentum in a comoving volume element of the expanding universe leads to the equation:

$$\frac{d}{dt}\left(a^3 \rho_\phi\right) = -P_\phi \frac{d}{dt}\left(a^3\right) \tag{1.9}$$

where $\rho_\phi = \frac{1}{2}\dot{\phi}^2 + \frac{1}{2}m_\phi^2\phi^2$ is the energy density of the homogeneous inflaton field and $P_\phi = \frac{1}{2}\dot{\phi}^2 - \frac{1}{2}m_\phi^2\phi^2$ is its pressure. Since, during the stage of oscillations, $H < m_\phi$, the inflaton field makes several oscillations during a Hubble time $H^{-1}$. It then makes sense to average the energy density and pressure of the oscillating inflaton field over a period of its oscillation, and use these averages in equation (1.9) and the Friedman equation (1.3). As is well known for a harmonic oscillator, $\left\langle \frac{1}{2}\dot{\phi}^2 \right\rangle = \left\langle \frac{1}{2} m_\phi^2 \phi^2 \right\rangle$. We see immediately that the average pressure vanishes, like in a matter dominated universe, and from equation (1.9), we conclude that the energy density scales like $a^{-3}$. The Friedmann equation then tells us that $(\frac{\dot{a}}{a})^2 \propto a^{-3}$ from which the observed evolution $a \propto t^{2/3}$ follows immediately.

Let us now discuss the observational constraints on this model. A successful model of inflation must give sufficient inflation to "flatten" the universe and create the many domains which will eventually become our visible universe. From (1.7), we see that this is merely a constraint on the initial amplitude of $\phi$. For $\phi_0 = 3.1 M_p$, for example, we get about 60 e-foldings worth of inflation. Typically [7, 10], one requires about this many e-foldings to solve the cosmological "problems".

Quantum fluctuations, $\delta\phi$, of the inflaton field are generated by the expansion during inflation. When reheating occurs, these inhomogeneities will show up as fluctuations in the energy density of radiation filling the early universe. The uniformity of the cosmic microwave background radiation indicates that these fluctuations must have been very small. The constraint which the amplitude of CMB fluctuations places on the slow-roll potential may be written [7]

$$\left(\frac{8\pi}{M_p^2}\right)^{3/2} \left(\frac{V^{3/2}}{V_{,\phi}}\right) \approx 5.3 \times 10^{-4} \, . \tag{1.10}$$

The left hand side of this equation should be evaluated at the time when fluctuations that would later be galaxy sized are pushed outside the Hubble radius during inflation. Taking our potential and this time to be roughly $\phi_{60}$ (60 e-foldings before the end of inflation), we get the constraint

$$m_\phi \approx 2 \cdot 10^{13} \, \mathrm{GeV} \, . \tag{1.11}$$

For future reference, we note that, if we had done all this for the potential $\frac{1}{4}\lambda\phi^4$, we would have obtained the value $\lambda \approx 2 \cdot 10^{-13}$. As the inflaton field has an amplitude of order the Planck mass during inflation, we see that the inflationary potential is very flat: $V_{,\phi\phi} \ll \phi^2$. This is a general property of inflationary potentials.

We now address reheating in this model. Our analysis will follow closely that of Kofman, Linde, and Starobinsky in [15] (see also [7]).

## 1.2 The Theory of Perturbative Reheating

In order to have reheating, the inflaton field must be coupled to other fields. In every case which shall interest us, it is convenient to define the particular model being considered in terms of its Lagrange density, $\mathcal{L}$. Moreover, as all of our examples will utilize minimal kinetic terms, we can divide the Lagrangian into a kinetic part and an interacting part. The interacting part $\mathcal{L}_{\text{int}}$ will contain all masses, self interactions, and other couplings between fields. In particular, it will contain the inflaton potential $V(\phi)$.

Suppose the inflaton couples to several scalar, $\chi_i$, and fermion fields, $\psi_i$. We will take the interacting Lagrangian to be

$$-\mathcal{L}_{\text{int}} = \frac{1}{2}m_\phi^2\phi^2 + \nu_i v \phi \chi_i^2 + \frac{1}{2}g_i^2\phi^2\chi_i^2 + h_i\phi\bar{\psi}_i\psi_i\,, \tag{1.12}$$

where the $\nu_i$, $g_i$, and $h_i$ are dimensionless coupling constants, and $v$ is a constant of mass dimension one. We have left out any mass terms as we will assume that the fields other than the inflaton must be much lighter than the inflaton if the inflaton is to decay into them at an appreciable rate. (We have already mentioned that this is no longer true when preheating is taken into account, but it is true perturbatively.)

In order that these interactions not induce radiative corrections that spoil the flatness of the inflaton potential, we must require that all the coupling constants are small. We might, therefore, believe that the decay of the inflaton is perturbative and calculate decay rates for $\phi \to \chi_i\chi_i$ etc. Formally, the addition of the interacting terms to the fundamental Lagrangian modifies the Klein-Gordon equation (1.2). It becomes

$$\ddot{\phi} + 3H\dot{\phi} + (m_\phi^2 + \Pi)\phi = 0\,, \tag{1.13}$$

where $\Pi$ is the polarization (self-energy) operator for the inflaton field. The real part of $\Pi$ gives a small correction to the effective mass of the inflaton field. However, when decay into the other fields present is possible, the polarization operator gets an imaginary part. The imaginary part is related to the decay width by the familiar expression: $Im\{\Pi\} = m_\phi\Gamma_{\text{tot}}$. We assume that $m_\phi$ is much larger than both $\Gamma_{\text{tot}}$ and $H$ at the end of inflation. Then we may solve the Klein-Gordon equation (1.13) at the stage of oscillations treating both $H$ and $\Gamma_{\text{tot}}$ as constant during one oscillation. The solution is

$$\phi(t) = \phi_0 e^{-\frac{1}{2}\int(3H+\Gamma_{\text{tot}})dt}\cos(m_\phi\Delta t)\,, \tag{1.14}$$

where $\Delta t$ is the time from the start of oscillations. Recall that the Hubble parameter decreases in time like $\frac{2}{3}t^{-1}$. As long as $H > \Gamma_{\text{tot}}$, the damping of the inflaton's energy density due to the Hubble expansion (like $a^{-3}$) will dominate over its decay into other particles. Furthermore, as the energy density of radiation red-shifts like $a^{-4}$, any decay products will be quickly red-shifted away.

Reheating can only take place after a time $t_{\rm rh}$ when $3H \lesssim \Gamma_{\rm tot}$. Taking these to be equal, we get the energy in the inflaton field at the time of reheating to be

$$\rho_{\rm rh} \sim 10^{-3} M_p^2 \Gamma_{\rm tot}^2\,, \tag{1.15}$$

where we have taken the initial amplitude of oscillations to be $\phi_0 \approx M_p/20$, see figure 1.2. If all of this energy is converted into radiation at the time $t_{\rm rh}$, we have $\rho_{\rm rh} = \frac{\pi^2}{30} g_* T_{\rm rh}^4$, where $T_{\rm rh}$ is the reheat temperature and $g_*$ is the effective number of light degrees of freedom at this temperature. Thus, we find an upper bound on the perturbative reheat temperature

$$T_{\rm rh} \lesssim \frac{0.2}{g_*^{1/4}} \sqrt{\Gamma_{\rm tot} M_p} \ll 10^{15}\,{\rm GeV}\,, \tag{1.16}$$

where the last inequality follows from requiring $\Gamma_{\rm tot} \ll m_\phi$.

Considering only the three-legs interactions (i.e. set $g_i = 0$), the decay rates are well known. For light scalars and fermions we have

$$\begin{aligned} \Gamma_{\phi\to\chi_i\chi_i} &= \frac{\nu_i^2 v^2}{8\pi m_\phi} \\ \Gamma_{\phi\to\psi_i\psi_i} &= \frac{h_i^2 m_\phi}{8\pi}\,. \end{aligned} \tag{1.17}$$

With $h \sim 10^{-2}$, the decay rate into fermions is $O(10^8)\,$GeV, the reheat temperature is $O(10^{13})\,$GeV, and the inflaton makes $O(10^5)$ oscillations before reheating can occur. For bosons with a coupling $\nu_i \sim 10^{-2}$ and $v \sim 10^{11}\,$GeV, the decay rate is only $O(10^3)\,$GeV, the reheat temperature is $O(10^{10})\,$GeV, and the inflaton makes $O(10^{10})$ oscillations before reheating occurs!

For bosons with a four-legs interaction, the decay rate is

$$\Gamma_{\phi\phi\to\chi_i\chi_i} = \frac{g_i^2 \phi^2}{8\pi m_\phi}\,, \tag{1.18}$$

which is time dependent because it is proportional to the square of the inflaton field's amplitude. As $\phi^2 \sim a^{-3} \sim t^{-2}$, the decay rate through the four-legs interaction decreases faster than the expansion rate $H \sim t^{-1}$. Thus, perturbative reheating can never occur through the four-legs interaction, as first noted in [15].

## 1.3 The Advent of Preheating

The discovery of preheating was made by returning to the fundamental Lagrangian (1.12) and considering the quantum evolution of the scalar fields to which the inflaton couples. Suppose we have only one such field with a simple four-legs interaction with coupling $g$. Now consider the quantum evolution of the $\chi$ field in the background of the oscillating inflaton field, $\phi(t)$. Let us ignore the expansion of the universe for a moment. In the Heisenberg representation of quantum field theory, the $\chi$ field becomes a field operator which can be decomposed into eigenmodes

$$\hat{\chi}(t,\mathbf{x}) = \int \frac{d^3k}{(2\pi)^3} \left(\hat{a}_k \chi_k(t)\, e^{-i\mathbf{k}\cdot\mathbf{x}} + \hat{a}_k^\dagger \chi_k^*(t)\, e^{i\mathbf{k}\cdot\mathbf{x}}\right), \qquad (1.19)$$

where $a_k^\dagger$ and $a_k$ are the creation and annihilation operators. The temporal part of the eigenmodes, $\chi_k(t)$, will obey an oscillator-like equation

$$\ddot{\chi}_k + \left(k^2 + g^2\phi^2(t)\right)\chi_k = 0\,. \qquad (1.20)$$

In the absence of expansion, the inflaton field simply oscillates harmonically with (angular) frequency $m_\phi$. Changing variables to $\tau = m_\phi t$ and substituting $\phi(t) = \phi_o \cos(m_\phi t)$, the mode equation (1.20) becomes

$$\ddot{\chi}_k + \left(\kappa^2 + q\cos^2(\tau)\right)\chi_k = 0\,, \qquad (1.21)$$

where we have introduced the dimensionless momentum and resonance parameters

$$\kappa^2 = \frac{k^2}{m_\phi^2} \qquad , \qquad q = \frac{g^2\phi_0^2}{m_\phi^2}\,. \qquad (1.22)$$

Equation (1.21) is the master equation for bosonic preheating. It is a Schroedinger-like equation for a particle in a negative periodic potential of depth $q$. As is well known, for a given value of the resonance parameter $q$, equation (1.21) will possess exponentially growing solutions for certain bands of the momentum parameter $\kappa$. In the analogous solid state problem of particle propagation through a lattice, these unstable solutions correspond to the “forbidden” bands. In our problem, these forbidden bands of $\kappa$ will have exponentially growing fluctuations as a function of time: $\chi_k \sim exp\{\mu_k\tau\}$. As the occupation number of bosons in the mode $k$ goes like the square of the field amplitude, we get $n_k \sim exp\{2\mu_k\tau\}$ for certain ranges of momentum. This exponential growth in the number of particles is preheating.

In mechanics, the instability of an oscillator due to the periodic variation of its frequency, as is the case here, is known as parametric resonance. Parametric resonance is easily understood by considering the following example: Let us consider a mass hanging on a spring whose spring constant, $k$, is periodically increased slightly—say, by heating it up and cooling it back down at some frequency $\Omega$. Newton's equation for this system is:

$$\ddot{x} + \left[\omega_0^2 + \Delta \sin(\Omega t)\right] x = 0\,, \tag{1.23}$$

where $\omega_0$ is the natural frequency of oscillation and $\Delta$ describes how strongly the spring constant is varied. We ask, "what happens to the amplitude of the mass as a function of time for a given natural frequency and perturbing frequency?" First, imagine that the spring constant is increased twice each oscillation of the mass so that $\Omega \approx 2\omega_0$. Then, we easily see two possibilities depending on the phase of the oscillations. If the spring constant increases as the mass reaches each of its maxima, the changing spring constant will tend to amplify the mass' oscillations: relaxing near equilibrium and pulling harder near the maxima. If, on the other hand, the spring constant increases near equilibrium and relaxes near the maxima, the oscillations will tend to be damped.

These two possibilities reflect the two independent solutions when $\Omega \approx 2\omega_0$: one growing and one decaying. It is easy to see that, if $\Omega \approx 4\omega_0$, or more generally $\Omega \approx n\omega_0$ for n an even integer, there will also be growing and decaying modes, only with less effect for larger n. If, on the other hand, $\Omega$ happens to be between one of these unstable values, it is possible for the oscillator to undergo stable oscillations, though with a period different from $\Omega$.

When the effective frequency varies harmonically, as here, the equation of motion (1.21) is known as the Mathieu equation, whose properties have been frequently studied, c.f. [15] and references therein. For any value of the resonance parameter $q$, the Mathieu equation possesses an infinite number of unstable bands at higher and higher momenta. For small $q \ll 1$, these bands are narrow and centered at $k = nm_\phi$. The maximum magnitude of the characteristic exponent $\mu_k$ decreases as one goes to higher bands, so that the lowest band dominates the decay. For small $q$, the fact that $k \sim m_\phi$ can be interpreted as saying that, when inflatons decay through a four-legs interaction, each $\chi$ particle carries away the rest energy of one of the inflatons.

The role of parametric resonance in the theory of particle creation by strong external fields was considered many years ago, c.f. [21, 22, 23, 24]. The first examinations of parametric resonance in the process of reheating after inflation were made by Dolgov and Kirilova [25] and Traschen and Brandenberger [8] for narrow resonance in the context of the New Inflation scenario. In [25], the authors conjectured that parametric resonance in the expanding universe would not lead to efficient reheating. The authors of [8] reached the important conclusion that parametric resonance in New Inflation could be efficient. The role of parametric resonance in chaotic inflation scenarios was first considered by Kofman, Linde, and Starobinsky in [9]. They realized that reheating in these theories typically begins with a stage of broad parametric resonance, $q \gg 1$, during which the production of particles is very efficient. They named this stage preheating to distinguish it from the stages of perturbative decay and thermalization.

We can see that a broad resonance regime must be considered by looking at the values of $\phi_0$ and $m_\phi$ found above for $\frac{1}{2}m_\phi^2\phi^2$ chaotic inflation. Equations (1.8), (1.11), and (1.22) give

$$q \approx g^2\, 10^{10}\,. \tag{1.24}$$

Thus, as long as $g \gtrsim 10^{-5}$, the resonance will be strong. It turns out that, in order for the inflaton field to self-consistently dominate the energy density of the universe during inflation, $g$ can't be much smaller than $10^{-5}$ [26]. The reason for this is the following: During inflation, the Hubble expansion will excite and amplify all fields with masses $m_\chi < H$. For the $\chi$ fields above, their effective mass is just $g\phi$. Thus, we require $g\phi \gtrsim H \sim 3 \cdot 10^{-6}\phi$, where the last result follows from the Friedmann equation and the value of $m_\phi$. When this constraint is violated, the $\chi$ field will be produced in abundance during inflation and will actually come to dominate the energy density of the universe.

Thus, generally we expect that, at the start of inflaton oscillations, scalar fields to which the inflaton couples are being produced in a regime of broad parametric resonance. For $q \gg 1$, bosons with momenta as large as $q^{1/4}m_\phi \sim \sqrt{h}\,10^{15}\,\mathrm{GeV}$ are being exponentially produced. The characteristic exponent can be as large as $\mu_{\max} = \frac{1}{\pi}\ln(1+\sqrt{2}) \approx 0.28$ [9, 15]. This means that the energy in the produced particles can be an appreciable fraction of the inflaton field's total energy in only a few oscillations.

So far, we have neglected the expansion of the universe. One might think that, because parametric resonance seems to require the careful matching of phases through the periodic background, any disturbance to the background could kill the resonance. In fact, in the broad resonance case, expansion of the universe can actually make preheating more efficient [15]. Particle production in this case was called "stochastic resonance" in [15] because the creation process is like a random walk, changing the particle number after each half inflaton oscillation. Furthermore, it was found that the addition of a homogeneous or inhomogeneous noise component to the background field oscillations could also enhance rather than diminish the particle production efficiency [27, 28, 29].

In general, the introduction of expansion simply makes the two parameters $\kappa$ and $q$ time dependent. $\kappa$ red-shifts like $a^{-1}$ as it describes the physical momentum of a particle. $q$ red-shifts like $a^{-3}$ because it depends on the square of the inflaton field's amplitude. Even when $q$ is not much greater than one, the resonance will still occur. The time dependence of parameters means that different modes will be pulled into and out of the resonance bands. However, once $q$ red-shifts to become much less than one, the perturbative decay will eventually become more efficient than parametric resonance, as we have already mentioned.

## 1.4 What does Preheating Mean for Reheating?

Several different mechanisms have been found for preheating. Parametric resonance can amplify bose and fermi fields due to the non-adiabatic evolution of their effective masses. A related effect is *instant preheating* [30] where a single instance of non-adiabaticity is sufficient to dissipate most of the inflaton's energy. Meanwhile, in tachyonic preheating [18, 19], the negative mass-squared of the "Higgs" field leads to exponential particle creation even while the evolution is adiabatic (in the sense that a WKB-like approximation for the modes is valid). Such tachyonic effects can enhance particle production in models other than hybrid inflation [31, 32].

Naturally, the next question to be asked is, what is the end result of incorporating preheating into our understanding of inflation? One might wonder if preheating is irrelevant since the final result should be a thermal state at some temperature. Initially, it was thought that what one should try to identify in the new theory is a bound on the new reheating temperature. This is useful because one already knows several constraints that can be applied to the maximum temperature the universe has had since inflation. For one, it shouldn't be above the GUT scale of $O(10^{15} - 10^{16})$ GeV because then one has to worry about the production of monopoles and other defects again. Also, if one thinks that supergravity should ultimately provide the correct high energy theory beyond the standard model, then the reheat temperature shouldn't exceed about $10^9$ GeV because thermal collisions would over-produce gravitinos which would then destroy the successful predictions of Big Bang nucleosynthesis, c.f. [33, 34, 35].

Several of these "dangerous relic" constraints can be applied to the thermal history of the universe. What preheating indicates, however, is that the non-thermal history of an inflationary universe is very important as well. During preheating, very large amplitude fluctuations of both scalar, and as we will see, fermionic fields are produced. These can result in the direct or indirect (through rescattering) production of copious relics far from equilibrium. These relics will not necessarily ever reach thermal equilibrium with the rest of the universe, and so a reheating temperature is useless for describing their properties. This is even the case in the context of the old perturbative theory of reheating where it has been found that the effective maximum temperature after inflation is actually larger than the final reheat temperature [36]. Of course, not all relics are bad. It may be that the far from equilibrium particle production that occurs during preheating is exactly what one needs to explain the baryon asymmetry of the universe, for example.

Being a generally occurring, far from equilibrium phase of the inflationary universe, preheating might be essential for understanding such problems as baryo- and leptogenesis in the early universe. We will see that preheating can create bosons and fermions much more massive than the inflaton–a process which is impossible perturbatively. These might serve as dark matter candidates. They might open up new kinematic regions, decaying themselves to other particles whose masses are larger than the equilibrium temperature has ever been.

Furthermore, even if we ignore the problem of relic production, the eventual thermalization of the universe is still far from trivial to extract from the theory. It is known that bosonic preheating does not generally lead to the complete decay of the inflaton field [15, 37, 38, 11]. Fortunately, because the preheated bose fields have a large amplitude (or large occupation number), they can be treated classically once they are produced. The relativistic wave equations that follow from the Lagrangian (1.12) can be put on a lattice and solved, as originally done in [37]. Generally, the stage of resonant particle production is terminated by the backreaction of produced particles. This leaves a combination of the inflaton field and large amplitude, long wavelength fluctuations of it and the other bose fields to which it couples, either directly or indirectly. These waves can then rescatter, leading to thermalization. However, in [39] it was found that different sectors of the theory can reach a quasi-equilibrium at different effective temperatures. This happens when there is a hierarchy in the coupling strengths between fields. One can imagine a prolonged epoch of the early universe in which different sectors (multiplets) of some GUT are excited to various quasi-equilibrium temperatures. Such asymmetries might also help to explain baryo- and leptogenesis.

In some circumstances, preheating has also been found to trigger the non-thermal restoration of symmetry [40, 41]. This can occur when the large amplitude fluctuations generated by preheating induce a positive effective mass-square for a field whose true vev is a spontaneously broken state. This means, for example, that preheating might create defects even if the reheating temperature is never large enough to restore symmetry thermally.

Finally, we note that, in addition to rescattering, the inflaton and other bose fields can decay through perturbative channels [15, 11] and the non-perturbative production of fermions [12, 14]. This last effect, and indeed the general role of fermions in the reheating process, is not well understood. The principle problem here is the inability to place fermions on the lattice with the bosonic fluctuations. The presence of copious numbers of fermions will, no doubt, greatly influence the rates of thermalization.

# Chapter 2

# Preheating of Bosons

In this chapter we consider preheating in the theory

$$\mathcal{L}_{\text{int}} = \frac{1}{4}\lambda\phi^4 + \frac{1}{2}g^2\phi^2\chi^2 \,, \tag{2.1}$$

where the classical oscillating inflaton field, $\phi(t)$, decays into scalar $\chi$- and $\phi$-particles. A salient feature of these models with vanishing bare masses is that they are conformally equivalent to theories in Minkowski space-time. This trivializes the role of expansion and makes a detailed analytic treatment of preheating possible.

We find that the strength of the parametric resonance depends crucially on the ratio $\frac{g^2}{\lambda}$. For example, in the cases $\frac{g^2}{\lambda} = 1$ and 3, there is only one resonance band. However, changing $\frac{g^2}{\lambda}$ only slightly away from these values leads to an infinite tower of resonance bands stretching to higher and higher momenta. Furthermore, while $\frac{g^2}{\lambda} = 1$ and 3 each have only band, the value of the characteristic exponent $\mu_k$, describing the efficiency of the resonance, is very different for each. In general, we find that the characteristic exponent for the fastest growing mode, $\mu_{\max}$, is a non-monotonic function of $\frac{g^2}{\lambda}$. For these reasons, it is dangerous to extrapolate results obtained for one choice of parameters to another choice.

To better understand the nature of preheating in these models, we will present a stability/instability plot for the conformally invariant theories. This contour plot of $\mu_k$ in the $(\frac{g^2}{\lambda}, k^2)$-plane shows clearly all of the features described above. In particular, if one imagines several fields, $\chi_i$, interacting with the inflaton field with various coupling strengths, $g_i$, then the stability/instability plot tells us which field dominates the decay of the inflaton, at least in the linear regime.

Certain aspects of the theory (2.1) have been studied by numerous groups [9, 42, 43, 37, 44, 45, 46, 47]. In this chapter, we present the results of Greene, Kofman, Linde, and Starobinsky [11]. Though this model is not well motivated from particle physics, it has two properties that make it particularly interesting to study. The first is that it leads to a conformally invariant theory so that all the complications of expanding FRW space-time can be transformed away. The second is that the model with $g^2 = 0$–that is, the model with just the self interacting inflaton field–is the simplest conceivable model of inflation in which preheating can occur.

## 2.1 Evolution of the Inflaton Field

In the model we consider, inflation is driven by the non-vanishing vacuum expectation value of the scalar field $\phi$ displaced from the minimum of its potential. The Friedman equation governs the evolution of the resulting (flat) FRW universe:

$$H^2 = \frac{8\pi}{3M_p^2}\left(\frac{1}{2}\dot{\phi}^2 + \frac{1}{4}\lambda\phi^4\right) , \tag{2.2}$$

where $H = \dot{a}/a$ is the Hubble parameter. Let us note one more useful relationship between $H(t)$ and $\phi(t)$ which follows from the Einstein equations

$$\dot{H} = -\frac{4\pi\dot{\phi}^2}{M_p^2} . \tag{2.3}$$

The Klein-Gordon equation for the classical field $\phi(t)$ is

$$\ddot{\phi} + 3H\dot{\phi} + \lambda\phi^3 = 0 . \tag{2.4}$$

For sufficiently large initial values of $\phi > M_p$, the friction term, $3H\dot{\phi}$, in (2.4) dominates over $\ddot{\phi}$ and the potential term in (2.2) dominates over the kinetic term. This leads to an inflationary stage during which the universe expands quasi-exponentially: $a(t) = a_0 \exp(\int dtH(t))$. Under the influence of the drag term and potential, the $\phi$ field slowly rolls towards its vev. Once $\phi$ falls below $O(M_p)$, the drag term $3H\,\dot{\phi}$ becomes less important and inflation terminates at $\phi \sim M_p/2$. After a short stage of fast rolling down, the inflaton field begins to rapidly oscillate around the minimum of $V(\phi)$ with an initial amplitude $\Phi_0 \sim 0.1M_p$, see figure 2.1.

The character of the classical oscillations of the homogeneous scalar field depends on the shape of its potential $V(\phi)$. As we saw in the introduction, for a quadratic potential $V(\phi) = \frac{1}{2}m_\phi^2\phi^2$, the fluctuations are almost harmonic, $\phi(t) = \Phi(t)\sin m_\phi t$, with an amplitude decreasing like $\Phi(t) \approx \frac{M_p}{\sqrt{3\pi}m_\phi t} \propto a^{-3/2}$. The scale factor at the stage of oscillations is $a(t) \approx a_0 t^{2/3}$, and the energy density of the

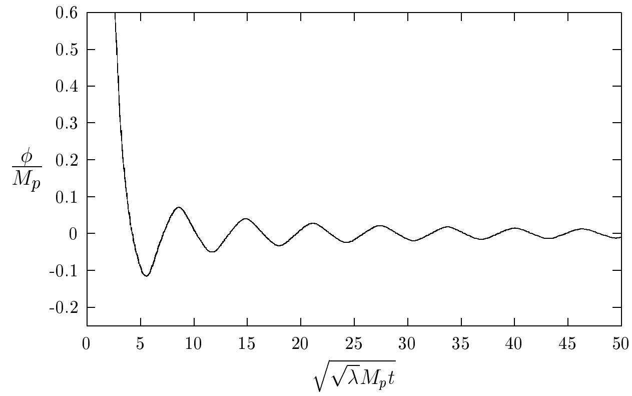


Figure 2.1: Oscillations of the field $\phi$ after inflation in the theory $\frac{1}{4}\lambda\phi^4$ as a function of the conformal time $\sim \sqrt{t}$. The value of the scalar field is measured in units of $M_p$, time is measured in units of $(\sqrt{\lambda}M_p)^{-1}$.

inflaton field decreases in the same way as the energy density of nonrelativistic matter $\propto a^{-3}$.

In the present theory with potential $V(\phi) = \frac{1}{4}\lambda\phi^4$, the inflaton oscillations are not given by harmonic functions but rather elliptic ones. The oscillations of $\phi$ at the end of inflation are shown for this model in figure (2.1). The amplitude $\Phi(t)$ of the oscillations of the scalar field $\phi$ at late times approaches the asymptotic regime

$$\Phi(t) \approx \frac{1}{\sqrt{t}}\left(\frac{3M_p^2}{8\pi\lambda}\right)^{1/4} \sim \frac{M_p}{10N} \propto a^{-1}, \tag{2.5}$$

where $N$ is the number of oscillations after the end of inflation.

To make calculations in this theory, and in particular, to find the form of the oscillations, it is convenient to make a conformal transformation of the space-time metric and the fields. For this we use the conformal time

$$\eta = \int \frac{dt}{a(t)} , \tag{2.6}$$

and the conformal field,

$$\varphi = a\phi . \tag{2.7}$$

In the coordinates $(\eta, \mathbf{x})$ the Klein-Gordon equation (2.4) for $\varphi$ is

$$\varphi'' + \lambda\varphi^3 - \frac{a''}{a}\varphi = 0 , \tag{2.8}$$

where $'$ stands for the derivative with respect to the conformal time, $\frac{d}{d\eta}$. The Friedmann equation (2.2) in these variables is

$$a'^2 = \frac{8\pi}{3M_p^2}\left(\frac{1}{2}\left(\varphi' - \varphi\frac{a'}{a}\right)^2 + \frac{\lambda\varphi^4}{4}\right) . \tag{2.9}$$

As one can see from equation (2.8), the equation of motion for the field $\varphi$ in the time variable $\eta$ does not look exactly as the equation for the theory $\frac{1}{4}\lambda\varphi^4$ in Minkowski space. This is because we have considered minimal couplings to the curvature in our original Lagrangian. Had we added a term $\frac{1}{2}\xi R\phi^2$ to the Lagrangian with $\xi = \frac{1}{6}$, the third term on the LHS of (2.8) would not occur. In fact, this subtlety is not very important. First off, soon after the end of inflation, one has $\frac{1}{4}\lambda\phi^4 \gg \frac{1}{12}|R|\phi^2$, and $\lambda\varphi^3 \gg \frac{a''}{a}\varphi$. Moreover, it is known that the energy-momentum tensor of the field $\phi$ in the theory $\frac{1}{4}\lambda\phi^4$, when averaged over several oscillations, is traceless ($p = \rho/3$), c.f. [10]. In this case, one has $R = 0$, $a(\eta) \sim \eta$, and $a'' = 0$, so that the last term in equation (2.8) vanishes identically. In any event, we are justified in taking

$$\varphi'' + \lambda\varphi^3 = 0 \tag{2.10}$$

as our new Klein-Gordon equation.

The Friedmann equation (2.9) averaged over several oscillations of the field $\phi$ in the regime $\phi \ll M_p$ also takes a very simple form:

$$a'^2 = \frac{8\pi}{3M_p^2}\left(\frac{1}{2}\varphi'^2 + \frac{1}{4}\lambda\varphi^4\right) \equiv \frac{8\pi\rho_\varphi}{3M_p^2} , \tag{2.11}$$

where we have introduced the conformal energy density, $\rho_\varphi = \frac{1}{2}\varphi'^2 + \frac{1}{4}\lambda\varphi^4$.

It is convenient to express $\rho_\varphi$ in terms of the amplitude $\tilde{\varphi}$ of the oscillations of the field $\varphi$: $\rho_\varphi = \frac{1}{4}\lambda\tilde{\varphi}^4$. Equation (2.10) has an oscillatory solution with a constant amplitude and the conformal energy $\rho_\varphi$. Then from (2.11) we find

$$a(\eta) = \sqrt{\frac{2\pi\lambda}{3}}\frac{\tilde{\varphi}^2}{M_p}\eta , \qquad t = \sqrt{\frac{\pi\lambda}{6}}\frac{\tilde{\varphi}^2}{M_p}\eta^2 . \tag{2.12}$$

As expected, in this regime the term $\frac{a''}{a}\varphi$ in equation (2.8) vanishes.

Equation (2.10) can be reduced to the canonical equation for an elliptic function. Introducing a dimensionless conformal time variable

$$x \equiv \sqrt{\lambda}\tilde{\varphi}\eta = \left(\frac{6\lambda M_p^2}{\pi}\right)^{1/4}\sqrt{t} , \tag{2.13}$$

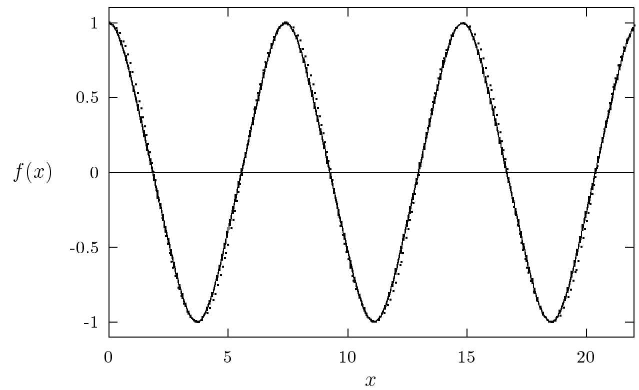


Figure 2.2: The solution (2.14) for the oscillations of the inflaton field after inflation in the conformally invariant theory $\frac{1}{4}\lambda\phi^4$. We show the field in rescaled conformal field and time variables, $f(x) = \frac{\varphi}{\tilde{\varphi}}$ (solid curve) and the first term, $\cos(0.8472x)$, in its harmonic expansion (2.15) (dotted curve).

we can rescale the function $\varphi \equiv a\phi = \tilde{\varphi} f(x)$. The function $f(x)$ has unit amplitude and obeys the canonical equation for an elliptic function. The integral of this equation, $f'^2 = \frac{1}{2}(1 - f^4)$, has a solution in terms of the Jacobi elliptic cosine

$$f(x) = cn\Big(x - x_0\,,\ \frac{1}{\sqrt{2}}\Big)\ . \tag{2.14}$$

As claimed, oscillations in this theory are not sinusoidal but are given by an elliptic function. The energy density of the field $\phi$ decreases as $a^{-4}$, the same as radiation. The solution (2.14) has some interesting properties which are not usually elucidated in the literature. It matches the solution describing the slow rolling of the field $\varphi$ at the end of inflation if one takes $x_0 \approx 2.44$. The period of the oscillations (in units of $x$) is $T = 4K(\frac{1}{\sqrt{2}}) = \frac{\Gamma^2(1/4)}{\sqrt{\pi}} \approx 7.416$, $K$ stands for the complete elliptic integral of the first kind. The effective frequency of oscillations is $2\pi/T \approx 0.8472$ [9]. The value of $f^4$ averaged over a period is $\frac{1}{3}$. The potential energy density $\frac{1}{4}\lambda\varphi^4$ averaged over a period of oscillation is equal to $\frac{1}{3}\rho_\varphi$, and the average kinetic energy $\frac{1}{2}\varphi'^2$ is given by $\frac{2}{3}\rho_\varphi$.

The elliptic cosine can be represented as follows:

$$f(x) = \frac{8\pi\sqrt{2}}{T}\sum_{n=1}^{\infty}\frac{e^{-\pi(n-1/2)}}{1+e^{-\pi(n-1/2)}}\cos\frac{2\pi(2n-1)x}{T}\ . \tag{2.15}$$

The amplitude of the first term in this sum is 0.9550; the amplitude of the second term is much smaller, 0.04305. The full solution (2.14) is plotted in figure (2.2) (solid curve), alongside the leading harmonic term in the series (2.15), $\cos(0.8472x)$ (dotted curve). Although the first harmonic term is very close to the actual form of the oscillations, it turns out to be crucial for the investigation of the general structure of stability/instability bands in this theory that $f(x)$ is not exactly equal to $\cos\frac{2\pi x}{T}$.

## 2.2 Equations for Fluctuations in the $\phi$ and $\chi$ Fields

We consider here the interaction between the *classical* inflaton field, $\phi$, and the massless, *quantum* scalar field, $\hat{\chi}$, with the Lagrangian (2.1). We decompose the $\chi$-field operator as

$$\hat{\chi}(t,\mathbf{x}) = \int \frac{d^3k}{(2\pi)^3} \left(\hat{a}_k \chi_k(t)\, e^{-i\mathbf{k}\cdot\mathbf{x}} + \hat{a}_k^\dagger \chi_k^*(t)\, e^{i\mathbf{k}\cdot\mathbf{x}}\right) . \tag{2.16}$$

The temporal part of the eigenfunction with comoving momentum $\mathbf{k}$ obeys the following equation:

$$\ddot{\chi}_k + 3\frac{\dot{a}}{a}\dot{\chi}_k + \left(\frac{k^2}{a^2} + g^2\phi^2\right)\chi_k = 0 \ . \tag{2.17}$$

As we mentioned in the previous section, at the stage of oscillations when $\phi \ll M_p$ the average value of the curvature $R$ vanishes, so one can neglect the term $\sim \xi\phi^2 R$.

The self-interaction $\frac{1}{4}\lambda\phi^4$ also leads to the generation of fluctuations of the field $\phi$. We may decompose the $\phi$-field operator into a classical part and a quantized, fluctuation part

$$\hat{\phi}(t,\mathbf{x}) = \phi(t) + \int \frac{d^3k}{(2\pi)^3} \left(\hat{a}_k \phi_k(t)\, e^{-i\mathbf{k}\cdot\mathbf{x}} + \hat{a}_k^\dagger \phi_k^*(t)\, e^{i\mathbf{k}\cdot\mathbf{x}}\right) , \tag{2.18}$$

where $\left\langle \hat{\phi} \right\rangle = \phi(t)$ is the classical part. To lowest order in fluctuations, the equation for the eigenmodes $\phi_k(t)$ depends only on the classical background:

$$\ddot{\phi}_k + 3\frac{\dot{a}}{a}\dot{\phi}_k + \left(\frac{k^2}{a^2} + 3\lambda\phi^2\right)\phi_k = 0 \ . \tag{2.19}$$

Note that this equation is identical to equation (2.17) with $g^2 = 3\lambda$. Therefore, the study of the fluctuations $\phi_k$ in the $\frac{1}{4}\lambda\phi^4$ model is a particular case of the general equation for fluctuations (2.17).

The physical momentum, $\mathbf{p} = \frac{\mathbf{k}}{\mathbf{a(t)}}$, in equation (2.17) is red-shifted in the same manner as the background field amplitude, $\phi(t) = \frac{\varphi}{a(t)}$. Therefore, the red-shifting of momenta can be eliminated from the evolution of $\chi_k$. Indeed, let us use the conformal transformation of the mode function $X_k(t) = a(t)\chi_k(t)$ and rewrite the mode equation for $X_k(t)$ with the dimensionless conformal time $x$:

$$X_k'' + \left(\kappa^2 + \frac{g^2}{\lambda} cn^2\Big(x, \frac{1}{\sqrt{2}}\Big)\right) X_k = 0 \ , \tag{2.20}$$

where for simplicity we drop the initial value $x_0 = 2.44$. In this form the equation for fluctuations does not depend on the expansion of the universe. This is a peculiar, though expected, feature of the conformally invariant theory $\frac{1}{4}\lambda\phi^4 + \frac{1}{2}g^2\phi^2\chi^2$.

For the fluctuations of the inflaton field, one takes $\varphi_k = a\phi_k$ and equation (2.19) becomes

$$\varphi_k'' + \left(\kappa^2 + 3cn^2\Big(x, \frac{1}{\sqrt{2}}\Big)\right)\varphi_k = 0 \ , \tag{2.21}$$

which is again just (2.20) with $g^2 = 3\lambda$.

Equation (2.20) is the master equation for our investigation of the resonance in the conformally invariant theory. The comoving momentum $k$ enters the equation in the combination

$$\kappa^2 = \frac{k^2}{\lambda\tilde{\varphi}^2} \ . \tag{2.22}$$

Therefore, the natural scale of the momentum $k$ is $\sqrt{\lambda}\tilde{\varphi} \sim O(10^{11}\mathrm{GeV})$, where the numerical value follows from $\lambda \sim 10^{-13}$ and $\tilde{\varphi} \sim 0.1M_p$. Equation (2.20) describes oscillators, $X_k$, with a variable frequency

$$\omega_k^2 = \kappa^2 + \frac{g^2}{\lambda} cn^2\left(x, \frac{1}{\sqrt{2}}\right) \ , \tag{2.23}$$

which periodically depends on time, $x$. It is well known that in this case the solutions $X_k$ are exponentially unstable: $X_k(x) \propto e^{\mu_k x}$. If we choose the vacuum positive-frequency initial condition, $X_k(x) \simeq \frac{e^{-i\kappa x}}{\sqrt{2\kappa}}$, we then expect the exponentially fast creation of $\chi$-particles ($n_k \propto e^{2\mu_k x}$) as the inflaton field oscillates. The strength of interaction with the periodic oscillations $cn^2(x, \frac{1}{\sqrt{2}})$ is given by the dimensionless coupling parameter $\frac{g^2}{\lambda}$. This means that the condition for broad parametric resonance does not require a large initial amplitude of the inflaton field, $\Phi_0$, as was the case with the quadratic potential [9, 48]. As we will see, the combination of parameters $\frac{g^2}{\lambda}$ ultimately defines the structure of the parametric resonance in the theory. It turns out that the strength of the resonance depends rather non-trivially (non-monotonically) on this parameter.

From a mathematical point of view, the mode equation (2.20) belongs to the class of Lamé equations [49]. In the context of preheating this was first noticed in [48], and then thoroughly studied for the $O(N)$ symmetric theory in the limit $N \to \infty$ (i.e. for $g^2 = \lambda$) in [45] and for the $\frac{1}{4}\lambda\phi^4$ theory ($g^2 = 3\lambda$) in [46]. Here, we follow [11] and present the results of a numerical and analytic investigation of the parametric amplification of fluctuations in the conformally invariant theory $\frac{1}{4}\lambda\phi^4 + \frac{1}{2}g^2\phi^2\chi^2$ for an arbitrary parameter $\frac{g^2}{\lambda}$. In the next section, we present the two dimensional chart of the stability/instability bands for the Lamé equation (2.20) in terms of the dimensionless variables $\kappa^2$ and $\frac{g^2}{\lambda}$. In subsequent sections, we give an analytic treatment of the Lamé equation in the case $\frac{g^2}{\lambda} = \frac{n(n+1)}{2}$ for integer $n$. We also present an analytic investigation of the resonance for $\frac{g^2}{\lambda} \ll 1$ and for $\frac{g^2}{\lambda} \gg 1$.

## 2.3 Stability/Instability Plot for the Lamé Equation

As we have seen, the equation for vacuum fluctuations interacting with the inflaton oscillations in the conformal theories can be reduced to a problem in Minkowski space-time. The equation for fluctuations (2.20) in this case contains only two parameters. The first parameter is $\frac{g^2}{\lambda}$, which characterizes the strength of the interaction. The second parameter is the momentum of vacuum fluctuations $\kappa$ in units of the frequency of the inflaton oscillations. As is well known, the solutions $X_k$ of this equation may be stable or unstable depending on the particular values for $\kappa$ and $\frac{g^2}{\lambda}$ considered.

As long as we neglect the backreaction of the unstable fluctuations on the homogeneous inflaton field, equation (2.20) is an equation with periodic coefficients, which belongs to the class of the Lamé equations. The stability/instability chart of another equation with periodic coefficients, the Mathieu equation, is well known and can be found in many textbooks, see e.g. [50]. The stability/instability chart for the Lamé equation first appeared in [11]. In this section, we present the stability/instability chart in the variables $\left(\kappa^2, \frac{g^2}{\lambda}\right)$, which was obtained by solving the Lamé equation numerically.

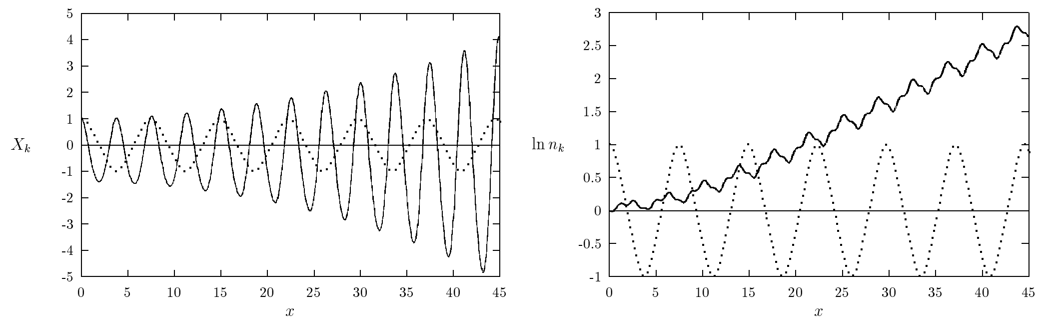


Figure 2.3: The left panel shows the numerical solution of the mode equation (2.20) for the particular choice of rescaled comoving momentum $\kappa^2 = 1.6$, and resonance parameter $\frac{g^2}{\lambda} = 3$. Shown are the background field $f(x)$ (dotted) and the real part of the eigenmode $X_k(x)$ (solid). Note the the eigenmode is being amplified. The left panel is similar, except this plot shows the logarithm of the comoving particle number density, $n_k$, (solid) calculated with formula (2.24). The number of particles grows exponentially, $\log n_k \approx 2\mu_k x$. In this case, $\mu_k \approx 0.035$.

Figure 2.3 shows a typical resonant solution of equation (2.20). Though we have plotted the particular case $\kappa^2 = 1.6$, $\frac{g^2}{\lambda} = 3$, the form of the resonant solution is generic. The left panel of figure 2.3 shows the amplification of the real part of the eigenmode $X_k(x)$ (solid curve) and the oscillations of the inflaton background (dotted curve).

As emphasized in [15], it is convenient for analytical and numerical work to consider the evolution of the comoving number density of created $\chi$-particles, $n_k$, with comoving momentum $k$. This can be defined from the comoving energy density and the energy per particle, $\omega_k$:

$$n_k = \frac{\omega_k}{2}\left(|X_k|^2 + \frac{|\dot{X}_k|^2}{\omega_k^2}\right) - \frac{1}{2}\,. \tag{2.24}$$

The right panel of figure 2.3 shows the logarithm of $n_k$ (solid curve) and the inflaton field (dotted curve). For the growing solutions–and after an initial transient period–the number of particles increases exponentially, $\ln n_k \approx 2\mu_k x$, where $\mu_k$ is the characteristic exponent of the unstable solution. In the particular case shown, $\mu_k \approx 0.035$.

For arbitrary values of $\kappa$ and $\frac{g^2}{\lambda}$, we can obtain a numerical solution of equation (2.20) and exploit the simple relation $\ln n_k \approx 2\mu_k x$ to extract the characteristic exponent for the growing modes. For the regions of stability, the characteristic exponent formally is imaginary. In this way, the stability/instability chart for the

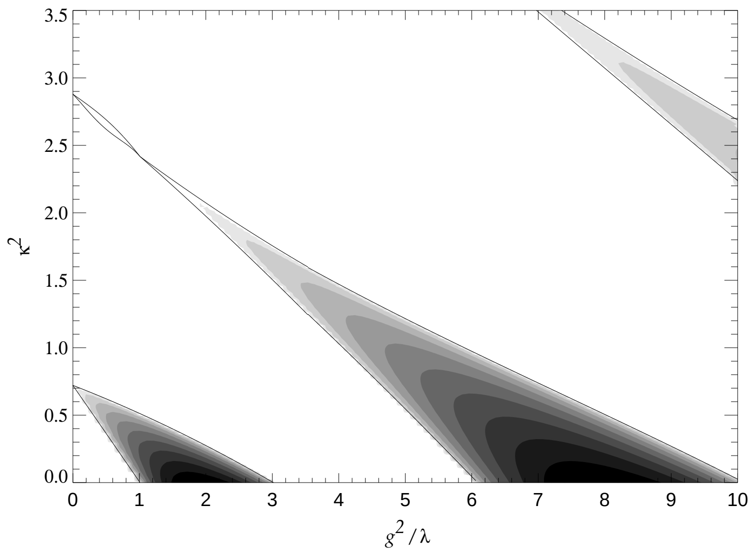


Figure 2.4: The stability/instability chart for the Lamé equation for fluctuations $X_k(x)$ in the variables $(\kappa^2, \frac{g^2}{\lambda})$, obtained from the numerical solution of equation (2.20). Shaded (unshaded) areas are regions of instability (stability). For instability bands, the darker shade implies a larger characteristic exponent $\mu_k$. Altogether, there are 10 color steps. One color step corresponds to the increment $\Delta\mu_k = 0.0237$, so the darkest shade corresponds to maximal $\mu_k = 0.237$, the least dark shade in the instability bands corresponds to $\mu_k = 0.009$. For positive $\kappa^2$, there is only one instability band for the particular values of the parameter $\frac{g^2}{\lambda} = 1$ and 3. This occurs because the higher bands shrink into nodes as $\frac{g^2}{\lambda}$ approaches 1 and 3.

Lamé equation, figure 2.4, is constructed. Shaded (unshaded) regions of the chart indicate values of $\kappa^2$ and $\frac{g^2}{\lambda}$ for which the solutions are unstable (stable). For the instability bands, a darker shade indicates a larger characteristic exponent. An immediate result is that, for a given range of $\frac{g^2}{\lambda}$, the largest characteristic exponent will occur for $\kappa^2 = 0$ between the integer values $\frac{g^2}{\lambda} = n(2n-1)$, and $n(2n+1)$, with $n$ integer.

This is demonstrated in figure 2.5, where slices of the stability/instability chart show the characteristic exponent as a function of $\kappa^2$ for various values of $\frac{g^2}{\lambda}$. The left panel of figure 2.5 shows the cases $\frac{g^2}{\lambda} = 1.0, 1.5, 2.0, 2.5, 3.0$, labeled $a$ through $e$ respectively. $\frac{g^2}{\lambda} = 1$ corresponds to $n = 1$, $\frac{g^2}{\lambda} = 3$ corresponds to $n = 2$. As claimed, we see that the largest value of the characteristic exponent occurs for $\kappa^2 = 0$ at a value of $\frac{g^2}{\lambda}$ between the limits 1 and 3 (curve $c$). Similarly, the right

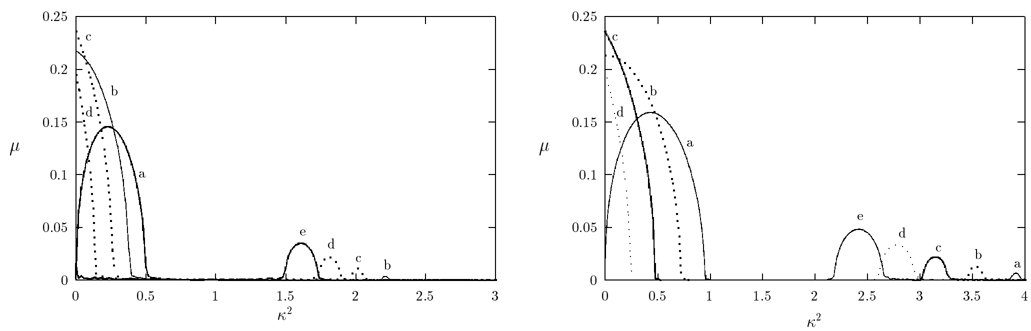


Figure 2.5: The left panel shows slices of the stability/instability chart, figure 2.4, reveal the dependence of the characteristic exponent, $\mu_k$, on $\kappa^2$ for several particular values of $\frac{g^2}{\lambda}$. Here $\frac{g^2}{\lambda} = 1.0,\ 1.5,\ 2.0,\ 2.5,$ and $3.0$, labeled $a$ through $e$ respectively. The numerical curves $a$ and $e$ for $\frac{g^2}{\lambda} = 1$ and $\frac{g^2}{\lambda} = 3$ are identical to the analytic predictions (2.36) and (2.42) of Section 2.4. The right panel is the same, only now for $\frac{g^2}{\lambda} = 6.0$, 7.0, 8.0, 9.0, and 10, labeled $a$ through $e$ respectively.

panel shows the cases $\frac{g^2}{\lambda} = 6.0, 7.0, 8.0, 9.0, 10.0$, labeled $a$ through $e$ respectively. The values $\frac{g^2}{\lambda} = 6$ and 10 correspond to $n = 3$ and 4. Again we see that the largest value of the characteristic exponent occurs for $\kappa^2 = 0$ at a value of $\frac{g^2}{\lambda}$ between the limits 6 and 10 (curve $c$).

This stability/instability chart is very similar to the stability/instability chart of the Mathieu equation. Nevertheless, there are important differences as well. For the Mathieu equation there are infinitely many instability bands corresponding to each value of the parameter $q$, which is analogous to our parameter $\frac{g^2}{\lambda}$. Meanwhile for the Lamé equation some of the instability bands may occasionally shrink to a point. As a result, for $\frac{g^2}{\lambda} = 1$ and for $\frac{g^2}{\lambda} = 3$ (left panel of figure 2.5, curves $a$ and $e$ respectively) there is only one instability band. This will be shown analytically in section 2.4. From the stability/instability chart for the Lamé equation we see that, topologically, this occurs because all the higher instability bands shrink to nodes as $\frac{g^2}{\lambda}$ approaches 1 and 3.

Similarly, there are a finite number of instability bands for positive $\kappa^2$ whenever $\frac{g^2}{\lambda} = \frac{n(n+1)}{2}$. Again, it occurs as other higher instability bands shrink to nodes. However, as for the Mathieu equation, all other values of $\frac{g^2}{\lambda}$ have an infinite number of instability bands. This is true in particular for $\frac{g^2}{\lambda} \ll 1$ where, as we will show in section 2.4.2, the Lamé equation (2.20) may be formally transformed into the Mathieu equation (2.45) with the parameters $A \approx 1.3932\kappa^2$ and $q \approx 0.3464\frac{g^2}{\lambda} \ll 1$. Thus, with this change of variables and in the limit $\frac{g^2}{\lambda} \ll 1$, the stability/instability chart for the Lamé equation is found to coincide exactly with that for the Mathieu equation [48, 15].

As was shown in [48, 15], the maximum value of the characteristic exponent $\mu_{max}$ for the Mathieu equation (2.45) (for $A \geq 2q$) is $\mu_{max} \approx 0.28$. As we will see below, similarly, the maximum value of the characteristic exponent for the Lamé equation (2.20) is $\mu_{max} \approx 0.2377$. This limit can be easily related to that of the Mathieu equation. Indeed, $0.2377 = 0.28\left(\frac{T_M}{T_L}\right)$, where $T_M$ and $T_L$ are the periods for harmonic oscillations, $\cos(x)$, and Jacobi-elliptic oscillations, $cn(x, \frac{1}{\sqrt{2}})$. That is, $T_M = 2\pi$ and $T_L \approx 7.416$.

As pointed out before, oscillations $cn(x, \frac{1}{\sqrt{2}})$ differ only insignificantly from the leading harmonic term $\cos(0.8472x)$ of the series (2.15). Meanwhile, in general the solutions of the Lamé equation cannot be obtained by perturbative corrections to the solutions of the Mathieu equation. Over all, the stability/instability chart of the Lamé equation, figure 2.4, is quite different from that of the Mathieu equation. This is one of the manifestations of the non-perturbative nature of the parametric resonance.

## 2.4 Some Special Solutions of the Lamé Equation

We now proceed to develop the analytic results for preheating in the physically interesting theories with $\frac{g^2}{\lambda} = \frac{n(n+1)}{2}$ and in the limiting cases when $\frac{g^2}{\lambda} \ll 1$ or $\frac{g^2}{\lambda} \gg 1$. These solutions where presented in detail in [11].

### 2.4.1 Existence of a Closed Form solution when $\frac{g^2}{\lambda} = \frac{n(n+1)}{2}$

We saw in the last section that something is special about the solutions to the Lamé equation when $\frac{g^2}{\lambda} = \frac{n(n+1)}{2}$ for positive, integer values of $n$. It is known that the Lamé equation can be solved in terms of the transcendental Jacobi-elliptic functions, which in turn are given by series expansions in harmonic functions. Earlier, the result $\mu_{\max} = 0.0359$ for the creation of $\delta\phi$ fluctuations in $\lambda\phi^4$ theory was presented in [48, 43]. Analytic investigations of the resonance using these transcendental functions has given the width of the unstable zone and the maximum of the characteristic exponent, $\mu_k$, in the physically interesting cases of the $O(N)$ symmetric theory in the limit $N \to \infty$ (which is equivalent to $\frac{g^2}{\lambda} = 1$ in our convention) and the $\frac{1}{4}\lambda\phi^4$ self-interacting theory ($\frac{g^2}{\lambda} = 3$) [45, 46].

However, calculations involving these transcendental functions are extremely tedious. Fortunately, in [11] it was found that for

$$\frac{g^2}{\lambda} = \frac{n(n+1)}{2} \;, \tag{2.25}$$

with $n$ an integer, one can obtain simple, closed-form solutions to the master equation (2.20). This includes in particular the most interesting cases $g^2 = \lambda$ and $g^2 = 3\lambda$. This result is derived here.

To find the solutions of the fluctuation equation (2.20) for $\frac{g^2}{\lambda} = \frac{n(n+1)}{2}$, we rewrite equation (2.20) in the so-called algebraic form. We will use the "time" variable $z$ instead of $x$:

$$z(x) = cn^2\Big(x, \frac{1}{\sqrt{2}}\Big) \;, \quad \frac{d}{dx} = -\sqrt{2z(1-z^2)}\frac{d}{dz} \;. \tag{2.26}$$

Equation (2.20) for fluctuations becomes

$$2z(1-z^2)\frac{d^2X_k}{dz^2} + (1-3z^2)\frac{dX_k}{dz} + (\kappa^2 + \frac{g^2}{\lambda}z)X_k = 0 \;. \tag{2.27}$$

Omitting the lower index $k$ for simplicity, let $X_1(z)$ and $X_2(z)$ be two linearly-independent solutions of (2.27). For $\kappa^2$ in a resonance band, one of these fundamental solutions grows exponentially while the other decays exponentially. Let us also introduce the bilinear combinations $X_1^2$, $X_2^2$, and $X_1X_2$. From (2.27) it follows that these bilinear combinations obey a third order equation

$$2z(z^2-1)\frac{d^3M}{dz^3} + (9z^2-3)\frac{d^2M}{dz^2} - 2\left[\Big(2\frac{g^2}{\lambda} - 3\Big)z + 2\kappa^2\right]\frac{dM}{dz} - 2\frac{g^2}{\lambda}M = 0 \;. \tag{2.28}$$

The three solutions, $M(z)$, of this equation correspond to the three bilinear combinations of $X_1$ and $X_2$. However, for $\frac{g^2}{\lambda} = \frac{n(n+1)}{2}$ the third order equation (2.28) admits a polynomial solution of degree $n$. In the particular cases $n = 1$ and $n = 2$, we have

$$\begin{aligned} n = 1 : &\quad M_1(z) = z - 2\kappa^2 \;, \\ n = 2 : &\quad M_2(z) = z^2 - \frac{2}{3}\kappa^2 z - 1 + \frac{4}{9}\kappa^4 \;. \end{aligned} \tag{2.29}$$

Clearly, such a polynomial function $M(z)$ can only correspond to the product of an exponentially growing solution with an exponentially decreasing one, i.e. $M(z) = X_1(z)X_2(z)$, when in a resonance zone. From this, as we show next, one can construct closed-form solutions for $X(z)$. We now calculate these solutions for the physically interesting cases $n = 1$ and $n = 2$. In particular, we will find the form of the characteristic exponent $\mu_k$ as a function of $\kappa^2$ in each case.

In the case $g^2 = \lambda$ equation (2.28) in the resonance band gives

$$X_1(z)X_2(z) = M_1(z) \ , \tag{2.30}$$

where

$$M_1(z) = z - 2\kappa^2 \ . \tag{2.31}$$

The Wronskian of equation (2.27) for $X(z)$ is

$$X_1 \frac{dX_2}{dz} - X_2 \frac{dX_1}{dz} = \frac{C}{\sqrt{z(1-z^2)}} \ , \tag{2.32}$$

where $C$ is some constant, $C = C_1$, to be defined. From (2.30) and (2.32) we immediately obtain the closed form solutions

$$X_{1,2}(z) = \sqrt{|M_1(z)|} \exp\left( \pm \frac{C_1}{2} \int \frac{dz}{\sqrt{z(1-z^2)} M_1(z)} \right) \ ., \tag{2.33}$$

unique up to normalization, c.f. [51] Substituting this solution back into equation (2.27) for $X(z)$, we find the constant $C_1$:

$$C_1 = \sqrt{2\kappa^2(1-4\kappa^4)} \ . \tag{2.34}$$

For exponentially growing solutions, $C_1$ must be real; therefore the exponentially growing solutions for fluctuations with $\kappa^2 > 0$ take place in a single instability band for which

$$0 < \kappa^2 < \frac{1}{2} \ , \tag{2.35}$$

in agreement with the result of [45]. The growing solution of (2.20) has the form $X(x) = e^{\mu_k x} P[z(x)]$, where $P[z(x)]$ is a periodic function of the conformal time $x$. Using (2.33), we can now find the characteristic exponent $\mu_k$ as a function of $\kappa$. The technical details can be found in the Appendix to [11].

The final answer is

$$\mu_k(\kappa) = \frac{2}{T} \sqrt{2\kappa^2(1-4\kappa^4)} I(\kappa) \ , \tag{2.36}$$

where the auxiliary function $I(\kappa)$ is

$$I(\kappa) = \int_0^{\pi/2} d\theta \frac{\sin^{1/2}\theta}{1 + 2\kappa^2 \sin\theta} . \tag{2.37}$$

Recall that $T \approx 7.416$. Equation (2.36) is one of the most important analytic results of [11]. Some numerical values of $\mu_k$ as function of $\kappa^2$ for $\frac{g^2}{\lambda} = 1$ calculated with (2.36) are listed in the upper half of the table below.

| $g^2/\lambda$ | $\kappa^2$ | $\mu_k$ |
|---|---|---|
| 1 | 0.0 | 0.000 |
| 1 | 0.1 | 0.1238 |
| 1 | 0.2 | 0.1460 |
| 1 | 0.21 | 0.1466 |
| 1 | 0.22 | 0.1469 |
| 1 | 0.228 | 0.1470 |
| 1 | 0.23 | 0.1470 |
| 1 | 0.24 | 0.1468 |
| 1 | 0.25 | 0.1465 |
| 1 | 0.3 | 0.1411 |
| 1 | 0.4 | 0.1117 |
| 1 | 0.5 | 0.000 |
| 3 | 1.5 | 0.000 |
| 3 | 1.55 | 0.02981 |
| 3 | 1.60 | 0.03570 |
| 3 | 1.61 | 0.03595 |
| 3 | 1.615 | 0.03598 |
| 3 | 1.62 | 0.03594 |
| 3 | 1.625 | 0.03583 |
| 3 | 1.65 | 0.03427 |
| 3 | 1.70 | 0.02460 |
| 3 | 1.732 | 0.00 |

The analytic form (2.36) is in excellent agreement with the numerical results for this case plotted in the left panel of figure 2.5 as curve $a$. The maximum value of the characteristic exponent for $\frac{g^2}{\lambda} = 1$ is $\mu_{max} \approx 0.1470$ at $\kappa^2 \approx 0.228$, in agreement with the numerical value for $\mu_{max}$ of figure 2.6.

The method of obtaining a closed-form analytic solution, $X_k(z)$, in the case $g^2 = 3\lambda$ is similar to that in the previous case. In the resonance zone with $g^2 = 3\lambda$, equation (2.28) gives

$$X_1(z)X_2(z) = M_2(z) \ , \tag{2.38}$$

where now

$$M_2(z) = z^2 - \frac{2}{3}\kappa^2 z - 1 + \frac{4}{9}\kappa^2 \tag{2.39}$$

The Wronskian of equation (2.27) is the same as in (2.32), but with a new constant, $C = C_2$. Therefore, the closed form solutions are the same as in (2.33), but with $M_2(z)$ in place of $M_1(z)$. Substituting this solution into equation (2.27), we find the constant $C_2$ in this case:

$$C_2 = \sqrt{\frac{32}{81}\kappa^2\Big(\kappa^4 - \frac{9}{4}\Big)(3-\kappa^4)} \ . \tag{2.40}$$

Therefore, in the case $\frac{g^2}{\lambda} = 3$ for $\kappa^2 > 0$, there is also only a single instability band corresponding to

$$\frac{3}{2} < \kappa^2 < \sqrt{3} \ , \tag{2.41}$$

in agreement with [46].

We plotted the resonant solution $X_k(x)$ in figure 2.3. Notice that $X_k(x)$ oscillates twice within one inflaton oscillation. Using the solution (2.33) with $M_2(z)$ and $C_2$, we can find $\mu_k$ in this case. Details are in the Appendix to [11].

The resulting characteristic exponent for $\frac{g^2}{\lambda} = 3$ is

$$\mu_k = \frac{8\sqrt{2}}{9T}\sqrt{\kappa^2\Big(\kappa^4 - \frac{9}{4}\Big)(3-\kappa^4)}\ J(\kappa) \ , \tag{2.42}$$

where the auxiliary function $J(\kappa)$ is

$$J(\kappa) = \int_0^{\pi/2} d\theta \frac{\sin^{3/2}\theta}{1 + \frac{2}{3}\kappa^2\sin\theta + (\frac{4}{9}\kappa^4 - 1)\sin^2\theta} \tag{2.43}$$

in this case. Equation (2.42) is another important result of [11]. Some numerical values of $\mu_k$ as a function of $\kappa^2$ for $\frac{g^2}{\lambda} = 3$ calculated with (2.42) are listed in the lower half of the table above. The analytic form (2.42) is in agreement with the numerical results for this case plotted in figure 2.5 as curve $e$. The maximum value of the characteristic exponent for $\frac{g^2}{\lambda} = 3$ is $\mu_{max} \approx 0.03598$ at $\kappa^2 \approx 1.615$, in agreement with the numerical value for $\mu_{max}$ of figure 2.6 and [48]

### 2.4.2 Narrow Resonance: $\frac{g^2}{\lambda} \ll 1$

In this section we investigate the equation for fluctuations (2.20) in the limiting case $\frac{g^2}{\lambda} \ll 1$. Let us recall that $f(x)$ is given by the series (2.15), and hence, $f^2(x)$ in equation (2.20) can be decomposed as

$$f^2(x) = F_0 + F_1 \cos\Big(\frac{4\pi x}{T}\Big) + F_2 \cos\Big(\frac{8\pi x}{T}\Big) + \dots\ , \tag{2.44}$$

where $F_0 = 0.4570$, $F_1 = 0.4973$, $F_2 = 0.04290$ and so on, but $\sum_{k=0}^{\infty} F_k = 1$. One can seek $X_k(x)$ in the form of a harmonic series of terms $\cos\left(\frac{2n\pi x}{T}\right)$ with slowly varying coefficients. If $\frac{g^2}{\lambda}$ is a small parameter, one can develop an iterative solution with respect to $\frac{g^2}{\lambda}$. It is easy to show that the leading contribution to $X_k(x)$ comes from the lower harmonic: $\cos\left(\frac{4\pi x}{T}\right)$. Keeping only this term, the equation for $X_k(x)$ can be reduced to the Mathieu equation

$$\frac{d^2 X_k}{d\tau^2} + (A + 2q\cos 2\tau)\, X_k = 0\ , \tag{2.45}$$

where $\tau = \frac{2\pi x}{T}$, $A = \left(\frac{T\kappa}{2\pi}\right)^2$, and $q = \frac{g^2}{2\lambda}\left(\frac{T}{2\pi}\right)^2 F_1$. Thus, our theory is effectively reduced to the Mathieu equation only in the limit $q \ll 1$, where it has instabilities in very narrow resonant bands around $\kappa^2 = \frac{2\pi m}{T}$, $m = 1, 2, \dots$. The results of the numerical investigation of the instability zones plotted in figure 2.4 indeed show that for $\frac{g^2}{\lambda} \ll 1$ the parametric resonance corresponds to that of the Mathieu equation. The exponentially growing solution of the Mathieu equation, $X_k(x) \propto e^{\mu_k x}$, has a maximum characteristic exponent (in the first zone)

$$\mu_{\max} = \frac{g^2}{4\lambda}\left(\frac{T}{2\pi}\right)^2 F_1 \approx 0.1467\frac{g^2}{\lambda}\ . \tag{2.46}$$

In figure 2.6 we plot the maximum value of the characteristic exponent as a function of $\frac{g^2}{\lambda}$ together with the prediction (2.46) for $\mu_{max}$ from the Mathieu equation. As one can see from figure 2.6, equation (2.46) works extremely well even up to $\frac{g^2}{\lambda} \simeq 1$.

### 2.4.3 Broad Resonance: $\frac{g^2}{\lambda} \gg 1$

In this section we consider the limiting case when the parameter $\frac{g^2}{\lambda}$ is very large. Physically, this case is very interesting. We have seen that the normalization of perturbations from inflation in the $\frac{1}{4}\lambda\phi^4$ theory requires $\lambda \sim 10^{-13}$. One can imagine many scalar fields $\chi_i$ coupled to the inflaton with coupling constants $g_i$ not

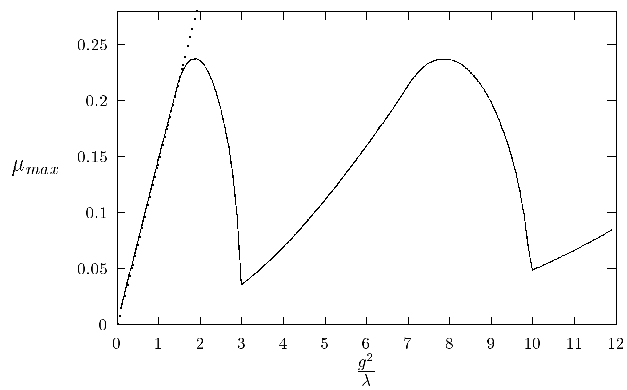


Figure 2.6: The maximum value of the characteristic exponent $\mu_{max}$ extracted from the stability/instability chart, figure 2.4, is plotted as a function of $\frac{g^2}{\lambda}$ (solid curve). The function $\mu_{max}(\frac{g^2}{\lambda})$ is non-monotonic. The universal upper limit of $\mu_{max}$ is 0.2377. The local minima of the function are gradually increasing with $\frac{g^2}{\lambda}$, and asymptotically approach 0.2377. The dotted line is the prediction $\mu_{max} \approx 0.1467\frac{g^2}{\lambda}$ for $\frac{g^2}{\lambda} \ll 1$, when the mode equation (2.20) is effectively reduced to the Mathieu equation (2.45).

much smaller than $O(10^{-2})$ or so; merely small enough that radiative corrections don't spoil the flatness of the inflaton potential. In this case, we readily expect $\frac{g_i^2}{\lambda} \sim O(10^{10})$, which is certainly much bigger than one [9, 48].

As an example of such a case–with only a moderately large value of $\frac{g^2}{\lambda}$–in the left panel of figure 2.7 we plot the numerical solution of equation (2.20) for $\frac{g^2}{\lambda} = 5050$ and $\kappa^2 = 29.0$. The solid line shows the time evolution of of the real part of $X_k(x)$ while the dotted curve shows the background oscillations $f(x)$, as in figure 2.3. In the right panel we plot the log of the number of particles $n_k(x)$ in a given mode as a function of time $x$ calculated from $X_k(x)$ with equation (2.24). The basic observation is that, for $\frac{g^2}{\lambda} \gg 1$, the evolution of the modes $X_k(x)$ is adiabatic and the number of particles $n_k(x)$ is constant between the zeros of the background field. Changes in the number density of particles occur only near times $x = x_j$ when the amplitude of the inflaton field crosses zero, i.e. $\varphi(x_j) = 0$. To describe the effect of a single kick at $x = x_j$, it is enough to consider the evolution of $X_k(x)$ in the interval when $\varphi^2(x)$ is small and can therefore be represented by its quadratic part $\propto (x - x_j)^2$. This process looks like wave propagation in a parabolic potential. Outside of these time intervals, $X_k(x)$ has a simple, adiabatic (or semi-classical) form. We can combine the action of the subsequent parabolic potentials to find the net effect of particle creation. This method of successive parabolic scattering

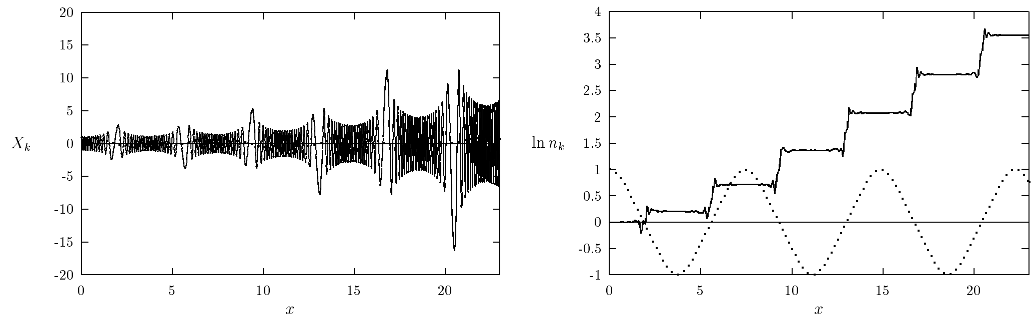


Figure 2.7: The left panel is the same as in figure 2.3 but for a value of $\frac{g^2}{\lambda} \gg 1$. Here, we show the particular choice $\frac{g^2}{\lambda} = 5050$ and $\kappa^2 = 29.0$. The figure shows the time-dependence of the real part of the eigenmode $X_k(x)$ (solid line). Oscillations of the background field are also shown (dotted line) and are exactly the same as figure 2.3. The eigenmode $X_k(x)$ makes many oscillations during each half inflaton oscillation, characteristic of the adiabatic (or semi-classical) regime. The right panel shows $\log n_k$ as a function of time $x$ (solid line) for the same parameters. We also plot the background field oscillations $f(x)$ (dotted line). Particle creation occurs in a step-like manner only in the vicinity of the zeros of the inflaton field where adiabaticity is broken; $n_k$ is an adiabatic invariant of the fluctuation equation (2.20). The magnitude of $\log n_k$ grows approximately as $2\mu_k x$. The characteristic exponent for this example is $\mu_k \approx 0.1$.

was formulated and applied to the broad parametric resonance for the quadratic inflaton potential in [15] and as developed here in [11].

We expect that the semi-classical solution to be valid everywhere except near the times $x_j$. Thus, prior to scattering at $x_j$, the mode function $X_k(x)$ has the adiabatic form

$$X_k^j(x) = \frac{\alpha_k^j}{\sqrt{2\omega_k}}\, e^{-i\int_0^x \omega_k dx} + \frac{\beta_k^j}{\sqrt{2\omega_k}}\, e^{+i\int_0^x \omega_k dx} \ , \tag{2.47}$$

where the coefficients $\alpha_k^j$ and $\beta_k^j$ are constant for $x_{j-1} < x < x_j$. Positive frequency initial conditions tell us that $\alpha_k^0 = 1$ and $\beta_k^0 = 0$ while our normalization yields $|\alpha_k|^2 - |\beta_k|^2 = 1$. After scattering at $x = x_j$, $X_k(x)$ in the interval $x_j < x < x_{j+1}$ again has the adiabatic form of equation (2.47) but with new constant coefficients, $\alpha_k^{j+1}$ and $\beta_k^{j+1}$.

Now, the key observation is that the outgoing amplitudes, $\alpha_k^{j+1}$ and $\beta_k^{j+1}$, can be expressed in terms of the incoming amplitudes, $\alpha_k^j$ and $\beta_k^j$, with the help of the reflection and transmission amplitudes for scattering off an inverted parabolic potential [15]. To find these coefficients, we need only consider the asymptotic expansion of the mode functions around a single parabolic potential. From these we can read off the scattering amplitudes in the usual way that it is done in quantum mechanics. In the vicinity of any $x_j$, $cn\left(x, \frac{1}{\sqrt{2}}\right) \approx \frac{1}{\sqrt{2}}(x - x_j)$. Then equation (2.20) around $x_j$ is reduced to the simple equation

$$\frac{d^2X_k}{dx^2} + \left(\kappa^2 + \frac{g^2}{2\lambda}(x - x_j)^2\right) X_k = 0 \ , \tag{2.48}$$

which is simply a Schroedinger equation for a unit mass particle of energy $E = \kappa^2$ in the inverted parabolic potential $V(x) = -\frac{g^2}{2\lambda}(x - x_j)^2$. Exact solutions of this equation are obtainable in terms of parabolic cylinder functions and the reflection and transmission coefficients obtained from their asymptotic expansions [15, 52].

Here, we will simply state the results of such an analysis: the mapping of $\alpha_k^j$, $\beta_k^j$ into $\alpha_k^{j+1}$, $\beta_k^{j+1}$ in terms of the parameters in equation (2.48) reads

$$\begin{pmatrix} \alpha_k^{j+1} \\ \\ \beta_k^{j+1} \end{pmatrix} = \begin{pmatrix} \sqrt{1+e^{-\pi\epsilon^2}}e^{i\zeta_k} & ie^{-\frac{\pi}{2}\epsilon^2+2i\theta_k^j} \\ \\ -ie^{-\frac{\pi}{2}\epsilon^2-2i\theta_k^j} & \sqrt{1+e^{-\pi\epsilon^2}}e^{-i\zeta_k} \end{pmatrix} \begin{pmatrix} \alpha_k^j \\ \\ \beta_k^j \end{pmatrix} \tag{2.49}$$

where $\zeta_k = \arg\Gamma\left(\frac{1+i\epsilon^2}{2}\right) + \frac{\epsilon^2}{2}\left(1 + \ln\frac{2}{\epsilon^2}\right)$, and $\epsilon^2 = \sqrt{\frac{2\lambda}{g^2}}\kappa^2 = \frac{k^2}{\sqrt{\lambda/2}\tilde{\varphi}^2 g}$. The phase accumulated by the moment $x_j$ is $\theta_k^j = \int\limits_0^{x_j} dx\ \omega_k(x) = j\ \theta_k$,

where $\theta_k = 2\int\limits_0^{T/4} dx\ \sqrt{\kappa^2 + \frac{g^2}{\lambda}f^2(x)}$ is the phase accumulating with each half of a period of the inflaton oscillation.

In the regime when a large number of particles have been created, $n_k^j = |\beta_k^j|^2 \gg 1$, we have $|\alpha_k^j| \approx |\beta_k^j|$, so $\alpha_k^j$ and $\beta_k^j$ are distinguished by their phases only. In this case there is a simple solution of the matrix equation (2.49):

$$\alpha_k^j = \frac{1}{\sqrt{2}} \cdot e^{(\mu_k\frac{T}{2}+i\theta_k)\cdot j}, \beta_k^j = \frac{1}{\sqrt{2}}e^{i\vartheta} \cdot e^{(\mu_k\frac{T}{2}-i\theta_k)\cdot j} \ , \tag{2.50}$$

where $\vartheta$ is a constant phase and $\mu_k$ is the characteristic exponent. $T \approx 7.416$ is the period of oscillations of the inflaton field in the variable $x$, so the number of particles grows as $e^{2\mu_k x}$. Another solution is similar to (2.50) but with the substitution $\theta_k \to \theta_k + \pi$.

Substituting the solution (2.50) into equation (2.49), we get an equation for the parameters $\mu_k$ and $\theta_k$

$$\begin{aligned} e^{\mu_k \frac{T}{2}} &= |\cos(\theta_k - \zeta_k)|\sqrt{1+e^{-\pi\epsilon^2}} \\ &+ \sqrt{(1+e^{-\pi\epsilon^2})\cos^2(\theta_k-\zeta_k)-1}\ . \end{aligned} \tag{2.51}$$

In the instability zones, the parameter $\mu_k$ of equation (2.51) should be real. From this we obtain the condition

$$|\tan(\theta_k - \zeta_k)| \leq e^{-\frac{\pi}{2}\epsilon^2}\ . \tag{2.52}$$

for the momentum $k$ to be in a resonance band.

To further analyze the conditions for the strength (2.52) and width (2.51) of the resonance, one should calculate the phase $\theta_k - \zeta_k$. For $\frac{g^2}{\lambda} \gg 1$ we have

$$\begin{aligned} \theta_k - \zeta_k = 2\int_0^{T/4} dx\,\sqrt{\kappa^2 + \frac{g^2}{\lambda}f^2(x)} - \arg\Gamma\left(\frac{1+i\epsilon^2}{2}\right) \\ - \frac{\epsilon^2}{2}\left(1+\ln\frac{2}{\epsilon^2}\right) \approx \pi\sqrt{\frac{g^2}{2\lambda}} + \kappa^2\sqrt{\frac{\lambda}{8g^2}}\ln\frac{g^2}{\lambda}\ . \end{aligned} \tag{2.53}$$

Using equations (2.53), (2.52), and (2.51), we find the characteristics of the resonance in the regime $\frac{g^2}{\lambda} \gg 1$. From (2.52) it follows that the resonance is efficient for $\epsilon^2 \leq \pi^{-1}$, i.e for

$$\kappa^2 \leq \sqrt{\frac{g^2}{2\pi^2\lambda}}\ . \tag{2.54}$$

Equation (2.52) transparently shows that, for a given $\frac{g^2}{\lambda}$, there will be a sequence of stability/instability bands as a function of $\kappa$. The width of an instability band, where the resonance occurs, is $\Delta\kappa^2 \simeq \sqrt{\frac{g^2}{2\lambda}}$. Let the integer part of the large number $\sqrt{\frac{g^2}{2\lambda}}$ be $l$. From (2.53) it follows that if we vary $\kappa^2$ within the range $2\pi^2\sqrt{\frac{g^2}{2\pi^2\lambda}}(\ln\frac{g^2}{\lambda})^{-1}$, then within this interval of $\kappa^2$ the phase $\theta_k - \zeta_k$ reaches either $l\pi$ or $(l+1)\pi$.

Within this resonance band we get the maximum value $\mu_{max}$ defined by the equation (2.51) with $|\cos(\theta_k - \zeta_k)| = 1$:

$$e^{\frac{T}{2}\mu_{max}} = \sqrt{1+e^{-\pi\epsilon^2}} + e^{-\frac{\pi\epsilon^2}{2}}\ . \tag{2.55}$$

The characteristic exponent $\mu_{max}$ is a non-monotonic function of $\frac{g^2}{\lambda}$. If the value of the parameter $\frac{g^2}{\lambda}$ is exactly equal to $2l^2$ where $l$ is an integer, then the strongest resonance occurs at $\kappa^2 = 0$,[1] and from (2.55) we get

$$\mu_{\max} = \frac{2}{T} \ln(1+\sqrt{2}) \approx 0.2377 \; . \tag{2.56}$$

This is actually a general result for the upper limit of $\mu_{\max}$ for an arbitrary $\frac{g^2}{\lambda}$, see figure 2.6. One may compare it with a similar result for $\mu_{max}$ for the harmonic oscillations in the case of the Mathieu equation, where $T = 2\pi$ and $\mu_{max} = \frac{1}{\pi}\ln(1+\sqrt{2}) \approx 0.28$ [48]. If $\frac{g^2}{\lambda}$ is not exactly equal to $2l^2$, then $\mu_{max}$ occurs at a non-zero $\kappa^2$ and is smaller than 0.2377. It is interesting that in the formal limit $\frac{g^2}{\lambda} \to \infty$ the function $\mu_{\max}(\frac{g^2}{\lambda})$ asymptotically approaches the value 0.2377 for arbitrary $\frac{g^2}{\lambda}$. To see this, we have to check that a variation of $\kappa^2 \sim 2\pi^2\sqrt{\frac{g^2}{2\pi^2\lambda}}\,(\ln\frac{g^2}{\lambda})^{-1}$ is compatible with the condition for an efficient resonance, $\epsilon^2 \leq \pi^{-1}$. In figure 2.6 we see that the minimal value of $\mu$ as a function of $\frac{g^2}{\lambda}$ very slowly increases towards 0.2377. Therefore, although $\mu_{max}$ is not a monotonic function of $\frac{g^2}{\lambda}$, for $\frac{g^2}{\lambda} \gg 1$ the resonance is stronger both in terms of the characteristic exponent $\mu_{max}$ and the width $\kappa^2$.

## 2.5 The Role of Backreaction of Created Particles

Thus far we have considered the parametric resonance in the conformally invariant theory $\frac{1}{4}\lambda\phi^4 + \frac{1}{2}g^2\phi^2\chi^2$ in an expanding universe neglecting the backreaction of the amplified fluctuations of the fields $\phi$ and $\chi$. In this section we will study the effects related to the backreaction.

Let us consider the equation of motion for the inflaton field $\phi(t)$ including the effect of fluctuations through the one-loop Hartree diagrams:

$$\ddot{\phi} + 3H\dot{\phi} + \lambda\phi^3 + 3\lambda\langle\phi^2\rangle\phi + g^2\langle\chi^2\rangle\phi = 0 \, , \tag{2.57}$$

where $\langle\phi^2\rangle$ and $\langle\chi^2\rangle$ are due to the quantum fluctuations of the fields $\phi$ and $\chi$ respectively. Note that, in general, there are also higher-loop corrections such as $2g^2\langle\phi\chi^2\rangle$ and $6\lambda\langle\phi^3\rangle$, which are not necessarily negligible at the end of preheating

[1] It is easy to see from (2.53) that the mode $\kappa^2 = 0$ is within the resonance band if $2l^2 - l < \frac{g^2}{\lambda} < 2l^2 + l$.

when we may expect $n_\chi \sim 1/g^2$ and $n_\phi \sim 1/\lambda$ (or even higher, if one takes into account rescattering). Here we will work in the one-loop approximation.

If again we use the conformal transformation $\eta = \int \frac{dt}{a}$, $\chi_k = \frac{X_k}{a}$ and similarly $\phi_k = \varphi_k/a$, then the equation for the background field $\varphi(\eta)$ is

$$\varphi'' + \lambda\varphi^3 + 3\lambda\langle\varphi^2\rangle\varphi + g^2\langle X^2\rangle\varphi = 0 \, , \tag{2.58}$$

with the comoving vacuum expectation values for $X$ and $\varphi$ correspondingly

$$\langle X^2\rangle = \int \frac{d^3k}{(2\pi)^3}\,|X_k|^2, \quad \langle\varphi^2\rangle = \int \frac{d^3k}{(2\pi)^3}\,|\varphi_k|^2. \tag{2.59}$$

The first integral of equation (2.58) coincides with the energy density

$$\rho_{tot} = \frac{1}{2}\varphi'^2 + \frac{\lambda}{4}\varphi^4 + \rho_\varphi + \rho_X \ . \tag{2.60}$$

The first two terms describe the kinetic and potential energies of the classical field $\varphi$, while $\rho_\varphi$ and $\rho_X$ correspond to the energy density of $\varphi$-particles and $X$-particles respectively:

$$\rho_\varphi = \int \frac{d^3k}{(2\pi)^3}\,\sqrt{k^2 + 3\lambda\varphi^2}\; n_k^\varphi \, , \tag{2.61}$$

$$\rho_X = \int \frac{d^3k}{(2\pi)^3}\,\sqrt{k^2 + g^2\varphi^2}\; n_k^X \, . \tag{2.62}$$

Here $n_k^\varphi$ and $n_k^X$ correspond to the occupation numbers of the $\varphi$-particles and $X$-particles, respectively. It is easy to show that $\rho'_X = g^2\langle\chi^2\rangle\varphi\varphi'$ and $\rho'_\varphi = 3\lambda\langle\varphi^2\rangle\varphi\varphi'$, and hence, equation (2.60) is an integral of equation (2.58).

To close the set of self-consistent equations we need the equations for the modes $\varphi_k(x)$ and $X_k$:

$$\varphi_k'' + \Big(k^2 + \Pi_\varphi + 3\lambda\varphi^2\Big)\varphi_k = 0\,, \tag{2.63}$$

$$X_k'' + \Big(k^2 + \Pi_X + g^2\varphi^2\Big)X_k = 0\,. \tag{2.64}$$

The polarization operator $\Pi_\varphi$ consists of two parts: $\Pi^1_\varphi = 3\lambda\langle\varphi^2\rangle + g^2\langle X^2\rangle$ and the non-local term $\Pi^2_\varphi$ which emerges in the one-loop approximation beyond the Hartree diagram, see figure 2.8. The calculation of the polarization operator $\Pi^2_\varphi$ in the regime of parametric resonance is rather complicated. Estimates of $\Pi^2_\varphi$ performed in [15] indicate that it can be of the same order of magnitude as the standard Hartree polarization operator $\Pi^1_\varphi$. The polarization operator $\Pi^2_\varphi$ was not taken into account in other treatments of the self-consistent equations for the eigenmodes in the $\frac{1}{N}$ approximation [44, 45], but in fact it may survive in the limit

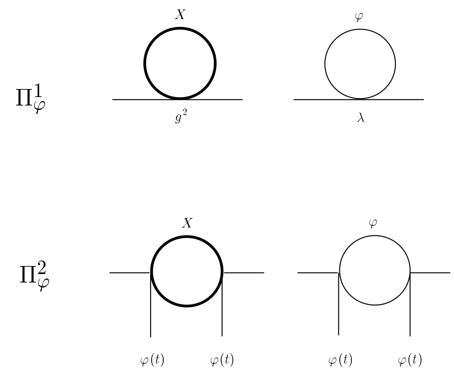


Figure 2.8: The diagrams for the polarization operator of the field $\varphi_k$. Thin and thick lines represent the fields $\phi$ and $\chi$ respectively. Vertical lines correspond to insertions the oscillating background field $\varphi(t)$. $\Pi^1_\varphi$ corresponds to the Hartree approximation which takes into account the contribution of $\langle X^2\rangle$ and $\langle\varphi^2\rangle$. The contributions of $\Pi^1_\varphi$ and $\Pi^2_\varphi$ to the effective mass of $\varphi$-particles can be comparable to each other.

$N \to \infty$ [15]. This may imply that in the context of the theory of preheating, the standard $1/N$ approximation breaks down.

Similarly, the polarization operator $\Pi_X$ is equal to $g^2\langle\varphi^2\rangle$, plus an additional non-local term $\Pi^2_X$. Nevertheless, we expect that $\Pi_\varphi \geq 0$, $\Pi_X \geq 0$, as suggested by the Hartree approximation.

A complete calculation of the polarization operators $\Pi_\varphi$ and $\Pi_X$ is outside the scope of this paper. Fortunately, we will see shortly that one need not really know exact expressions for $\Pi_\varphi$ and $\Pi_X$ in order to make an estimate of the density of produced particles at the time when the feedback of the amplified fluctuations terminates the parametric resonance.

### 2.5.1 Dynamical restructuring of the resonance

We have found that the structure of the parametric resonance in terms of its strength and width strongly depends on the parameters of the model. For example, the parametric resonance in the simplest conformally invariant theory $\frac{1}{4}\lambda\phi^4 + \frac{1}{2}g^2\phi^2\chi^2$ is very different from that in the theory $\frac{1}{2}m_\phi\phi^2 + \frac{1}{2}g^2\phi^2\chi^2$ [15]. In the simplest conformally invariant theories which we consider in this paper the structure of the resonance is determined by the combination $\frac{g^2}{\lambda}$.

How does the resonance develop if the backreaction of the accumulating fluctuations is taken into account? The answer to this question also strongly depends on the parameter $\frac{g^2}{\lambda}$.

For illustration, we consider the model of a self-interacting inflaton field $\frac{1}{4}\lambda\phi^4$, with no $\chi$ field involved. In this case we shall take $g^2 = 0$ in equations (2.58), (2.63), and (2.64). As already mentioned, if one neglects backreaction, the equations describing the resonance for the modes $\varphi_k$ in this theory coincide with the equations for the modes $\chi_k$ in the theory with $g^2 = 3\lambda$. Thus, we can use the results of the investigation of the theory with $g^2 = 3\lambda$ obtained in section 2.4 for our analysis.

Historically, the model $\frac{1}{4}\lambda\phi^4$ was one of the first models illustrating the general idea of preheating. The investigation of the stability/instability chart for the Lamé equation has shown that this model in a certain sense is the least favorable for the development of the resonance: it has only one resonance band, and the characteristic exponent $\mu_k$ for this theory is anomalously small, see figures 2.4 and 2.5. Originally it was expected that preheating in this model would rapidly transfer about half of the energy of the oscillating scalar field to $\phi$-particles, after which the decay of the field $\phi$ would continue at a much slower pace. However, the results of computer simulations of preheating in this theory indicated that the stage of efficient preheating ends as soon as the fluctuations of produced particles $\langle\varphi^2\rangle$ grow to $0.05\,\tilde{\phi}^2$ [37]. The interpretation of this result, however, was not quite clear. It was conjectured that the resonance terminates because of rescattering of the $\phi$-particles. Additionally, it was not clear whether the decay of the background $\phi$-field continues at a slower pace until this field completely decays, or if its decay eventually shuts down and is left incomplete.

A thorough investigation of this issue is rather difficult. First of all, the theory of rescattering is not fully developed: various approximations often break down near the end of preheating when the occupation numbers of particles are anomalously large ($n_k \sim \lambda^{-1}$) [48, 15]. Even in the Hartree approximation (or in the $1/N$-approximation) an investigation is very complicated [45, 46] because it is very difficult to work with the solutions of equations for the growing modes in terms of the transcendental functions. It might be easier to work with the solutions obtained in sections 2.4. We will not perform a full investigation of this issue here because, as argued above, one may need to calculate the polarization operator beyond the Hartree approximation, see [15]. Instead, we will make some simple estimates which will allow us to elucidate the mechanism which terminates the resonance in the theory $\frac{1}{4}\lambda\phi^4$.

As we will see, the main reason for the termination of the resonance in the theory $\frac{1}{4}\lambda\phi^4$ is the restructuring of the resonance band due to the backreaction of created particles. This process occurs at $\langle\varphi^2\rangle \ll \varphi^2$ because the resonance band is very narrow. At the start of preheating in the theory $\frac{1}{4}\lambda\phi^4$–before backreaction is important–the instability band is given by the condition $1.5\lambda\tilde{\varphi}_0^2 < k^2 < 1.73\lambda\tilde{\varphi}_0^2$, where $\tilde{\varphi}_0$ is the initial amplitude of the oscillations of the field $\varphi$ (2.41). It is sufficient to shift the position of the resonance band in momentum space by only a few percent, and the leading resonant modes $\chi_k$ which have been growing since the start of parametric resonance will not grow anymore. This will effectively shut down the resonance.

There are two different effects which lead to a restructuring of the resonance band, and these effects act in opposite directions. First of all, particle production reduces the energy of the scalar field, and therefore reduces the amplitude of its oscillations. This effect tends to reduce the frequency of the oscillations and to move the resonance band towards smaller $k$. On the other hand, the effective mass of the field $\varphi$ grows due to its interaction with the $\phi$-particles. This effect increases the frequency of oscillations and tends to shift the resonance band towards larger $k$. We will consider here both of these effects.

To investigate the decrease of the amplitude of the oscillations due to particle production, one should compare the total energy of the system before and after the appearance of $\langle\phi^2\rangle$:

$$\frac{\lambda}{4}\tilde{\varphi}_0^4 \approx \frac{\lambda}{4}\tilde{\varphi}^4(\eta) + \int \frac{d^3k}{(2\pi)^3}\sqrt{k^2 + 3\lambda\tilde{\varphi}^2}\; n_k \,. \tag{2.65}$$

Here we calculate the energy density at the moment when $\varphi' = 0$, when the oscillating field is equal to its amplitude $\tilde{\varphi}(\eta)$. This amplitude is smaller than $\tilde{\varphi}_0$ due to the transfer of energy to the created particles.

The resonance is most efficient in a small vicinity of $k^2 \approx 1.6\lambda\tilde{\varphi}^2$. Therefore, the leading contribution to $\rho_\phi$ is given by integration near $k^2 = 1.6\lambda\tilde{\varphi}^2$:

$$\rho_\phi \approx \int \frac{d^3k}{(2\pi)^3}\sqrt{4.6\lambda\tilde{\varphi}^2}\; n_k = \sqrt{4.6\lambda}\,\tilde{\varphi}\, n_\phi \,. \tag{2.66}$$

Equations (2.65) and (2.66) give

$$\tilde{\varphi}(\eta) \approx \tilde{\varphi}_0 - \frac{\sqrt{4.6\lambda}\, n_\phi}{\tilde{\varphi}^2} \,. \tag{2.67}$$

Thus, the creation of $\varphi$-particles diminishes the frequency of oscillations, because the frequency of oscillations of the field $\varphi$ in the theory $\lambda\phi^4$ is proportional to its amplitude. To evaluate the significance of this effect one may express it in terms of $\langle\phi^2\rangle$ calculated at $\varphi(\eta) = \tilde{\varphi}$:

$$\langle\phi^2\rangle \approx \int \frac{d^3k}{(2\pi)^3} \frac{n_k}{\sqrt{k^2 + 3\lambda\tilde{\varphi}^2}} \approx \frac{n_\phi}{\sqrt{4.6\lambda}\,\tilde{\varphi}} \,. \tag{2.68}$$

From the last two equations one obtains

$$\frac{\tilde{\varphi}^2(\eta)}{\tilde{\varphi}_0^2} \approx 1 - 9.2\frac{\langle\phi^2\rangle}{\tilde{\varphi}_0^2} \,, \tag{2.69}$$

which leads to a proportional shift of the resonance band towards smaller $k^2$. This indicates that even a very small amount of fluctuations $\langle\phi^2\rangle \sim 10^{-2}\tilde{\varphi}_0^2$ may shift the resonance band away from its original position, which may terminate the resonance for the leading modes $\varphi_k$.

This effect is partially compensated by the growth of the effective mass of the field $\varphi$. We will analyze this effect in the Hartree approximation, in which the field $\varphi$ acquires the effective mass squared $\Pi_\phi = 3\lambda\langle\varphi^2\rangle$. One may relate $\Pi_\phi = 3\lambda\langle\varphi^2\rangle$ to the number density of $\phi$-particles in the following way:

$$\begin{aligned} \Pi_\phi &\approx 3\lambda \int \frac{d^3k}{(2\pi)^3} \frac{n_k(\eta)}{\sqrt{k^2 + 3\lambda\varphi^2(\eta)}} \\ &\approx 3\lambda \int \frac{d^3k}{(2\pi)^3} \frac{n_k}{\sqrt{1.6\tilde{\varphi}^2 + 3\lambda\varphi^2}} = \frac{3\lambda n_\phi(\eta)}{\sqrt{1.6\tilde{\varphi}^2 + 3\lambda\varphi^2(\eta)}} \,. \end{aligned} \tag{2.70}$$

Note, that this quantity is time-dependent. It oscillates; its magnitude changes considerably several times within a single oscillation of the inflaton field, and it also grows exponentially during the resonance. The number density of $\varphi$-particles also oscillates and grows exponentially, but typically its oscillations are less wild than the oscillations of $\langle\varphi^2\rangle$. In the first approximation, we will neglect the oscillations of $n_\phi(\eta)$. Also, we are trying to find the time when the resonance terminates, and at that time the average number density of particles $n_\phi$ becomes nearly constant. It is still difficult to find an analytic solution for $\varphi_k$ with the time-dependent polarization operator (2.70), but one can easily find the solution numerically.

The result of the combined investigation of the two effects discussed above shows that the resonance on the leading modes effectively terminates as soon as $\langle\phi^2\rangle$ grows up to

$$\langle\phi^2\rangle \approx 0.05\,\tilde{\phi}^2 \,. \tag{2.71}$$

Note that even after this moment the resonance may continue for a while with new modes which can now be amplified by the restructured resonance band. However, this process is much less efficient. Thus, in pure $\lambda\phi^4$ theory the rapid development of the resonance ends when the dispersion of amplified fluctuations is about 20% of the amplitude of the inflaton field, which corresponds to only 0.2% of the total energy in fluctuations. This result is based on rather rough estimates neglecting rescattering. It is interesting, however, that it is in complete agreement with the results of the lattice simulation for parametric resonance in the pure $\lambda\phi^4$ theory done in [37].

We emphasize that there are several specific reasons why the resonance in the particular case of pure $\lambda\phi^4$ theory is relatively inefficient. First of all, the resonance band in this theory is quite narrow and the characteristic exponent $\mu_k$ is relatively small. This is no longer the case when one considers, for example, the theory describing a $\chi$-field with $g^2 = \lambda$ or with $g^2 = 2\lambda$. In these theories the characteristic exponent is much greater, the resonance band is rather broad, and it begins at $k = 0$. As a result, it is much more difficult to shut down the resonance in such theories.

In the theories with a massive inflaton field there is an additional effect which makes the resonance more stable. Broad parametric resonance in such theories is stochastic, which makes it more difficult to shut down [15]. Now we are going to study what happens to the resonance in the conformally invariant theories if this invariance is broken by a small mass term. As we will see, stochastic resonance may appear in such theories as well.

## 2.6 Preheating in the theory of a massive self-interacting inflaton field

In [15], Kofman, Linde, and Starobinsky investigated parametric resonance in the theory $\frac{1}{2}m_\phi^2\phi^2 + \frac{g^2}{2}\phi^2\chi^2$. They found that reheating can be efficient in that theory only if $g\Phi \gg m$, where $\Phi$ is the amplitude of oscillation of the inflaton field. As we saw in the introduction, this amplitude is extremely large immediately after inflation, $\phi \sim 0.1 M_p$. It then decreases as

$$\Phi \sim \frac{M_p}{3m_\phi t} \propto a^{-3/2}\,. \tag{2.72}$$

Due to this decrease, the resonance parameter in this model, $q = \frac{g^2\Phi^2}{m_\phi^2}$, changes rapidly. As a result, the broad parametric resonance regime in this theory is a stochastic process, which was called *stochastic resonance*.

Here we study the theory $\frac{1}{4}\lambda\phi^4 + \frac{1}{2}g^2\phi^2\chi^2$ for various relations between the coupling constants $g^2$ and $\lambda$. In this theory, the amplitude of the field $\phi$ also decreases in an expanding universe. Nevertheless, it does not make the resonance stochastic because all parameters of the resonance scale in the same way as $\Phi$ due to the conformal invariance and the resonance parameter is independent of the $\Phi$ field amplitude. One may wonder, what is the relation between these two theories? Indeed, neither of these two theories is completely general. In the theory of the massive scalar field one may expect terms $\sim \frac{\lambda}{4}\phi^4$ to appear because of radiative corrections. On the other hand, in many realistic theories the effective potential is quadratic with respect to $\phi$ near the minimum of the effective potential.

To address this question, let us study the theory $\frac{1}{2}m_\phi^2\phi^2 + \frac{1}{4}\lambda\phi^4 + \frac{1}{2}g^2\phi^2\chi^2$. One may expect that for $\phi \gg \frac{m}{\sqrt{\lambda}}$, parametric resonance in this theory occurs in the same way as in the model $\frac{1}{4}\lambda\phi^4 + \frac{1}{2}g^2\phi^2\chi^2$, whereas for $\phi \ll \frac{m}{\sqrt{\lambda}}$ the resonance develops as in the theory $\frac{1}{2}m^2\phi^2 + \frac{1}{2}g^2\phi^2\chi^2$. Let us check whether this is really the case, ignoring for simplicity the effects of backreaction of created particles, which is always possible in the beginning of the resonance regime.

First of all, one should remember that at the beginning of the stage of oscillations in this theory one has $\Phi \sim 0.1M_p$. Therefore, there are two basic possibilities. If $\frac{m_\phi}{\sqrt{\lambda}} \gg 0.1M_p$, then the term $\frac{1}{4}\lambda\phi^4$ never plays a role in determining the frequency of oscillations of the field $\phi$. Also, in this regime the particles $\phi$ are not produced by parametric resonance, because the condition $\sqrt{\lambda}\phi > m_\phi$ (analogous to the condition $g\phi > m_\phi$ for the production of $\chi$-particles [15]) is violated. In such a case $\chi$-particles can be produced if $0.1gM_p \gg m$. The theory of this process is described in [15]; we do not have anything new to add here.

Another possibility, which we are going to study here in more detail, is that $\frac{m_\phi}{\sqrt{\lambda}} \ll 0.1M_p$. Then in the beginning the mass term $\frac{1}{2}m_\phi^2\phi^2$ does not affect the frequency of the oscillating scalar field $\phi$. Therefore, one could expect that as the amplitude $\Phi$ decreases from $0.1M_p$ to $\frac{m_\phi}{\sqrt{\lambda}}$, the theory of parametric resonance coincides with the one described in this paper.

However, for large $\frac{g^2}{\lambda}$ the situation is more complicated. Even though the mass term for $0.1M_p > \Phi \gg \frac{m_\phi}{\sqrt{\lambda}}$ does not affect the frequency of oscillations, it may affect the nature of the broad parametric resonance by inducing an additional rotation of the phase $\theta$ of the modes $\chi_k$ (see section 2.4.3).

The reason why the broad resonance in the theory $\frac{1}{2}m_\phi^2\phi^2+\frac{1}{2}g^2\phi^2\chi^2$ was stochastic can be explained as follows. The $\chi$-particles are produced when the field $\phi(t)$ comes close to the point $\phi = 0$, which happens once during each time period $\Delta t = \frac{\pi}{m_\phi}$. During this time the phase of each mode $\chi_k$ grows approximately by $g\Phi(t)\pi m_\phi^{-1}$. During the next half of a period of an oscillation it changes by $g\Phi(t + \frac{\pi}{m_\phi})\,\pi m_\phi^{-1} \approx g\Phi(t)\pi m_\phi^{-1} + g\dot{\Phi}(t)\pi^2 m_\phi^{-2}$. This destroys the phase coherence required for the ordinary resonance and makes the resonance stochastic if $|g\dot{\Phi}(t)\pi^2 m_\phi^{-2}| \gtrsim 1$.

The condition for the stochastic resonance in the theory $\frac{1}{2}m_\phi^2\phi^2 + \frac{1}{2}g^2\phi^2\chi^2$ can be obtained from equation (2.72):

$$\Phi \gtrsim \sqrt{\frac{m_\phi M_p}{g}} \, . \tag{2.73}$$

In particular, for $\Phi = \frac{m_\phi}{\sqrt{\lambda}}$ it gives $\frac{g}{\sqrt{\lambda}} \gtrsim \frac{\sqrt{\lambda}M_p}{m_\phi}$. Note that by our assumption $\frac{\sqrt{\lambda}M_p}{m_\phi} \gg 1$.

The generalization of this result for the theory $\frac{1}{2}m_\phi^2\phi^2 + \frac{1}{4}\lambda\phi^4 + \frac{1}{2}g^2\phi^2\chi^2$ is straightforward, but the result is somewhat unexpected. As a rough estimate of the time $\Delta t$ one can take $\pi(2\lambda\Phi^2 + m_\phi^2)^{-1/2} = \pi(2\lambda\varphi^2 a^{-2}(t) + m_\phi^2)^{-1/2}$, where $\varphi \equiv \Phi a^{-1}(t)$ is the time-independent amplitude. The phase shift during this time is given by $g\varphi\pi(2\lambda\varphi^2 + m_\phi^2 a^2(t))^{-1/2}$. Thus, for $m_\phi = 0$ this quantity is time-independent, and one can have a regular stable resonance. In the limit $\Phi \gg \frac{m_\phi}{\sqrt{\lambda}}$ one can represent the phase shift as $\frac{g\pi}{\sqrt{2\lambda}}(1 - \frac{m_\phi^2 a^2(t)}{4\lambda\varphi^2})$. The change in this shift during one oscillation is $\frac{g\pi^2 m_\phi^2 H}{4\lambda^2\Phi^3}$, where $H = \frac{\dot{a}}{a} = \frac{\sqrt{2\pi\lambda}\Phi^2}{\sqrt{3}M_p}$. This gives the following condition for stochastic resonance:

$$\Phi \lesssim \frac{g}{\sqrt{\lambda}} \frac{\pi^2 m_\phi^2}{3\lambda M_p}. \tag{2.74}$$

Again, for $\Phi = \frac{m_\phi}{\sqrt{\lambda}}$ it gives $\frac{g}{\sqrt{\lambda}} \gtrsim \frac{\sqrt{\lambda}M_p}{m_\phi}$.

This conclusion is illustrated by figure 2.9, where we show the development of the resonance both for the massless theory with $\frac{g^2}{\lambda} \sim 5200$, and for the theory with a small mass $m_\phi$. As we see, in the purely massless theory the logarithm of the number density $n_k$ for the leading growing mode increases linearly in time $x$; whereas, in the presence of a small mass $m_\phi$, which we took to be much smaller than $\sqrt{\lambda}\phi$ during the whole process, the resonance becomes stochastic. In fact, the development of the resonance is rather complicated even for smaller $\frac{g^2}{\lambda}$. The resonance for a massive field with $m_\phi \ll \sqrt{\lambda}\phi$ in this case is not stochastic, but has a feature of intermittancy: it may consist of stages of regular resonance separated by the stages without any resonance, see figure 2.10. This is similar to what happens in the theory $\frac{1}{2}m_\phi^2\phi^2 + \frac{1}{2}g^2\phi^2\chi^2$ when the resonance parameter $q = \frac{g^2\phi^2}{m_\phi^2} \sim O(1)$ red-shifts, dragging modes into and out of different resonance bands [15].

Thus we see that the presence of the mass term $\frac{m^2}{2}\phi^2$ can modify the nature of the resonance even if this term is much smaller than $\frac{1}{4}\lambda\phi^4$. This is a rather un-

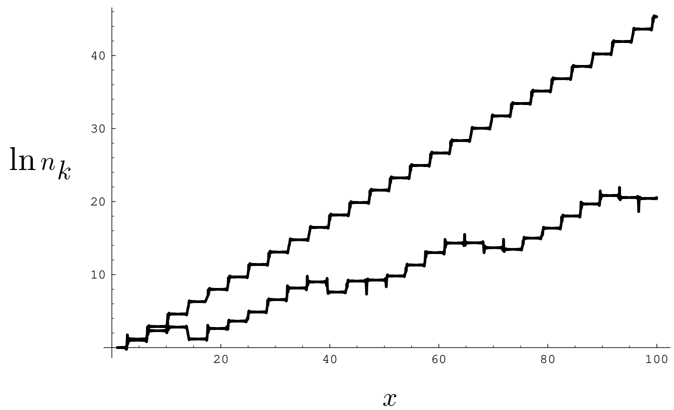


Figure 2.9: Development of the resonance in the theory $\frac{1}{2}m_\phi^2\phi^2 + \frac{1}{4}\lambda\phi^4 + \frac{1}{2}g^2\phi^2\chi^2$ for $\frac{g^2}{\lambda} = 5200$. The upper curve corresponds to the massless theory, the lower curve describes stochastic resonance with a theory with a mass $m_\phi$ which is chosen to be much smaller than $\sqrt{\lambda}\phi$ during the whole period shown. Nevertheless, the presence of this small mass term completely changes the development of the resonance.

expected conclusion, which is an additional manifestation of the non-perturbative nature of preheating.

Different regimes of parametric resonance in the theory $\frac{1}{2}m_\phi^2\phi^2+\frac{1}{4}\lambda\phi^4+\frac{1}{2}g^2\phi^2\chi^2$ are shown in figure 2.11. We suppose that immediately after inflation the amplitude $\Phi$ of the oscillating inflaton field is greater than $\frac{m_\phi}{\sqrt{\lambda}}$. If $\frac{g}{\sqrt{\lambda}} \lesssim \frac{\sqrt{\lambda}M_p}{m_\phi}$, the $\chi$-particles are produced in the regular, stable resonance regime until the amplitude $\Phi(t)$ decreases to $\frac{m_\phi}{\sqrt{\lambda}}$, after which the resonance occurs as in the theory $\frac{1}{2}m_\phi^2\phi^2 + \frac{1}{2}g^2\phi^2\chi^2$ [15]. The resonance never becomes stochastic.

If $\frac{g}{\sqrt{\lambda}} \gtrsim \frac{\sqrt{\lambda}M_p}{m_\phi}$, the resonance originally develops as in the conformally invariant theory $\frac{1}{4}\lambda\phi^4 + \frac{1}{2}g^2\phi^2\chi^2$, but with a decrease of $\Phi(t)$, the resonance becomes stochastic. Again, when $\Phi(t) \lesssim \frac{m_\phi}{\sqrt{\lambda}}$, the resonance occurs as in the theory $\frac{1}{2}m_\phi^2\phi^2 + \frac{1}{2}g^2\phi^2\chi^2$. In all cases, the resonance eventually disappears when the field $\Phi(t)$ becomes sufficiently small. As found in [48, 15], the complete decay of the inflaton in these models requires the addition of a three legs interaction. Thus, reheating in this class of models can be complete only if there is symmetry breaking in the theory, i.e. $m_\phi^2 < 0$, or if one adds interactions of the field $\phi$ with fermions. In both cases the last stages of reheating are described by perturbation theory, see section 1.2 and [53].

We will see in the next chapter how the addition of a Yukawa interaction alters parametric resonance in the conformal theory. Here, we note that the change of sign

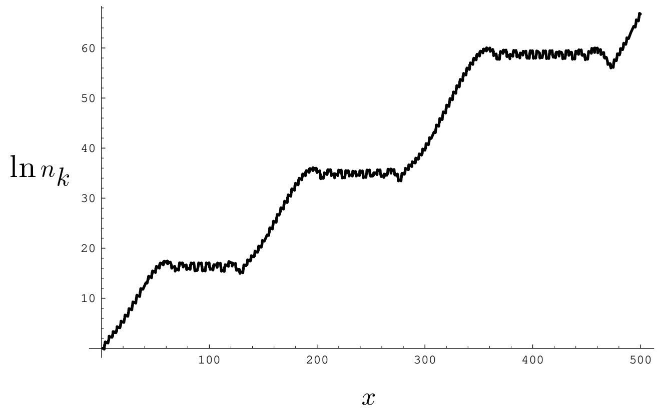


Figure 2.10: Development of the resonance in the theory $\frac{1}{2}m_\phi^2\phi^2 + \frac{1}{4}\lambda\phi^4 + \frac{1}{2}g^2\phi^2\chi^2$ with $m_\phi^2 \ll \lambda\phi^2$ for $\frac{g^2}{\lambda} = 240$. In this particular, case the resonance is not stochastic. As time $x$ grows, the relative contribution of the mass term to the equation describing the resonance also grows. This shifts the mode from one instability band to another.

of $m_\phi^2$ does lead to substantial changes in the theory of preheating, see figure 2.12. An investigation of preheating in the theory $-\frac{1}{2}m_\phi^2\phi^2 + \frac{1}{4}\lambda\phi^4 + \frac{1}{2}g^2\phi^2\chi^2$ appears in [40], where the issue of symmetry restoration through preheating is investigated. Here we will briefly describe the structure of the resonance for various $g^2$ and $\lambda$ neglecting effects of backreaction. This will give us a more general perspective on the theory of reheating.

First of all, at $\Phi \gg m_\phi/\sqrt{\lambda}$ the field $\phi$ oscillates in the same way as in the massless theory $\frac{1}{4}\lambda\phi^4 + \frac{1}{2}g^2\phi^2\chi^2$. Moreover, the condition for the resonance to be stochastic remains the same as before: $\Phi \lessapprox \frac{g}{\sqrt{\lambda}} \frac{\pi^2 m_\phi^2}{3\lambda M_p}$, see equation (2.74).

However, as soon as the amplitude $\Phi$ drops down to $\frac{m_\phi}{\sqrt{\lambda}}$, the situation changes dramatically. First of all, depending on the values of parameters, the field rolls to one of the minima of its effective potential at $\phi = \pm\frac{m_\phi}{\sqrt{\lambda}}$. The description of this process is rather complicated. Depending on the values of parameters and on the relation between $\sqrt{\langle\phi^2\rangle}$, $\sqrt{\langle\chi^2\rangle}$ and $\sigma \equiv \frac{m_\phi}{\sqrt{\lambda}}$, the universe may become divided into domains with $\phi = \pm\sigma$, or it may end up in a single state with a definite sign of $\phi$. This bifurcation period is described in [40]. After this transitional period the field $\phi$ oscillates near the minimum of the effective potential at $\phi = \pm\frac{m_\phi}{\sqrt{\lambda}}$ with an amplitude $\Phi \ll \sigma = \frac{m_\phi}{\sqrt{\lambda}}$. These oscillations lead to parametric resonance with $\chi$-particle production which can be (approximately) described as a narrow resonance in the first instability band of the Mathieu equation (2.45) with $A_k = 4\frac{k^2+g^2\sigma^2}{m_\phi^2}$

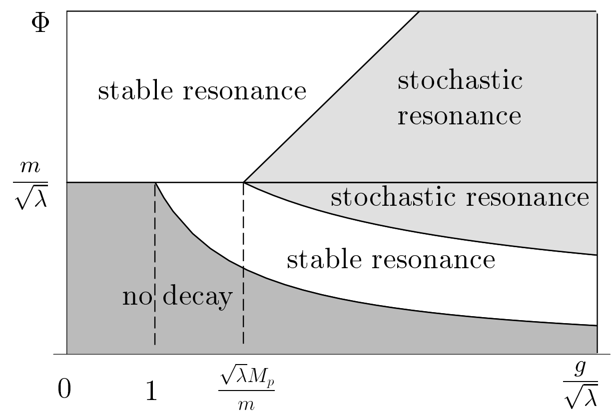


Figure 2.11: Schematic representation of different regimes which are possible in the theory $\frac{1}{2}m_\phi^2\phi^2 + \frac{1}{4}\lambda\phi^4 + \frac{1}{2}g^2\phi^2\chi^2$ for $\frac{m_\phi}{\sqrt{\lambda}} \ll 0.1M_p$ and for various relations between $g^2$ and $\lambda$ in an expanding universe. The theory developed in this paper describes the resonance in the white area above the line $\Phi = \frac{m_\phi}{\sqrt{\lambda}}$. The theory of preheating for $\Phi < \frac{m_\phi}{\sqrt{\lambda}}$ is given in [15]. A complete decay of the inflaton is possible only if additional interactions are present in the theory which allow one inflaton particle to decay to several other particles, for example, a Yukawa interaction with fermions: $\mathcal{L}_{\rm int} = h\phi\bar{\psi}\psi$.

and $q = \frac{4g^2\sigma\Phi}{m_\phi^2}$. For definiteness we will consider here the regime $\lambda^{3/2}M_p < m_\phi \ll \lambda^{1/2}M_p$. The resonance in this instability band is possible only if $\frac{g^2}{\lambda} < \frac{1}{2}$; the resonance in higher instability bands is very inefficient and rapidly shuts down due to the expansion of the universe. Using the results of [15] one can show that the resonance in the first band also terminates at $\Phi < \frac{\lambda m_\phi^2}{g^4 M_p}$. By taking the upper limit of this inequality at $\Phi \sim \frac{m_\phi}{\sqrt{\lambda}}$ one concludes that this resonance is possible only for $\frac{g}{\sqrt{\lambda}} \gtrsim (\frac{m_\phi}{\sqrt{\lambda}M_p})^{1/4}$. (The resonance may terminate somewhat earlier if the particles produced by the parametric resonance give a considerable contribution to the energy density of the universe.) However, this is not the end of reheating, because the perturbative decay of the inflaton field remains possible. It occurs with the decay rate $\Gamma(\phi \to \chi\chi) = \frac{g^4 m_\phi}{8\pi\lambda}$. This is the process which is responsible for the last stages of the decay of the inflaton field. It occurs only if one $\phi$-particle can decay into two $\chi$-particles, which implies that $\frac{g^2}{\lambda} < \frac{1}{2}$, see the introduction, section 1.2.

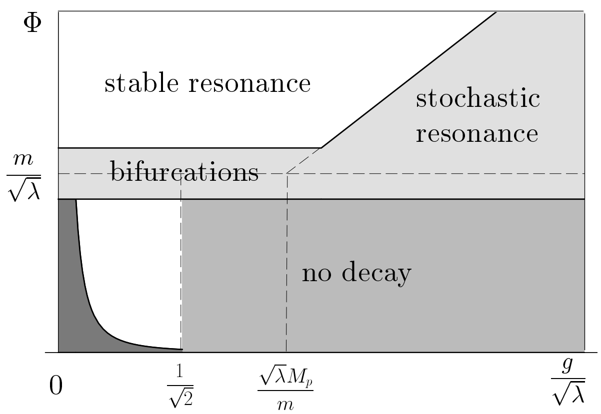


Figure 2.12: Schematic representation of different regimes which are possible in the theory $-\frac{1}{2}m_\phi^2\phi^2 + \frac{1}{4}\lambda\phi^4 + \frac{1}{2}g^2\phi^2\chi^2$. White regions correspond to the regime of a regular stable resonance, a small dark region in the left corner near the origin corresponds to the perturbative decay $\phi \to \chi\chi$. Unless additional interactions are included (see figure 2.11), a complete decay of the inflaton field is possible only in this small area.

## 2.7 Discussion

We have investigated the development of parametric resonance in the conformally invariant theories of the type of $\frac{1}{4}\lambda\phi^4 + \frac{1}{2}g^2\phi^2\chi^2$. We have found that the development of parametric resonance in these theories does not depend on the expansion of the universe, and can be classified in terms of the ratio $\frac{g^2}{\lambda}$. This ratio determines the structure of the stability/instability bands for the equations describing the resonance.

We have found that the behavior of the resonance with respect to $\chi$-particle production is a non-monotonic function of $\frac{g^2}{\lambda}$. For example, for $g^2 = \lambda$ and for $g^2 = 3\lambda$, the equation for the perturbations of the field $\chi$ has only one instability band. For $\frac{g^2}{\lambda} = \frac{n(n+1)}{2}$ there are only a finite number of instability bands, whereas for all other values of $\frac{g^2}{\lambda}$ the number of instability bands is infinite. Also, we have identified ranges of $\frac{g^2}{\lambda}$ for which the resonance band stretches down to $k^2 = 0$.

It is interesting that $\chi$-particle production is least efficient for $g^2 \ll \lambda$ and for $g^2 = 3\lambda$. For example, the characteristic exponent $\mu_{\max}$ for $g^2 = 2\lambda$ and for $g^2 = 8\lambda$ is almost 7 times greater than $\mu_{\max}$ for $g^2 = 3\lambda$, see figure 2.6. Meanwhile, the characteristic exponent for the production of $\phi$-particles in the pure $\frac{1}{4}\lambda\phi^4$ theory coincides with that of the field $\chi$ for $g^2 = 3\lambda$. Therefore, $\chi$-particle production is typically more efficient than the production of $\phi$-particles (unless $g^2 \ll \lambda$). The non-monotonic dependence of $\mu$ on the ratio $\frac{g^2}{\lambda}$ suggests that there exists an "unnatural selection" rule: The particles which are most intensively produced during preheating are not the ones which have the strongest coupling to the inflaton field, but those for which the characteristic exponent $\mu_{\max}(\frac{g^2}{\lambda})$ is the greatest.

In the conformally invariant theories, the expansion of the universe does not hamper the resonance, so it ends only due to the backreaction of the produced particles. There are several different mechanisms which may terminate the parametric resonance. First of all, creation of particles leads to a decrease in the amplitude of oscillation of the field $\varphi = a\phi$, which otherwise would remain constant. This leads to a proportional decrease in the frequency of oscillations in terms of the conformal time $\eta$, which may shift the position of the instability band towards smaller momenta. There is also an opposing effect which increases the frequency of oscillations due to the interaction of the homogeneous inflaton field with the produced particles. Finally, quantum fluctuations of the fields $\phi$ and $\chi$ acquire contributions to their masses, which changes their spectra. A combination of all these effects leads to restructuring of the instability bands. This terminates the amplification of the leading modes which have been growing from the very beginning of preheating. Additionally, one may envisage effects related to rescattering of produced particles, which may terminate the resonance even somewhat earlier. In this respect it is interesting that our estimates ignoring the process of rescattering give results which are in a very good numerical agreement with the results of computer simulations of reheating in the theory $\frac{1}{4}\lambda\phi^4$ performed in [37] where all of these effects, including rescattering, have been taken into account.

Rescattering may be more important for $g^2 \gg \lambda$ [54, 55, 47]. However, in this regime one may need to take into account possible small mass terms, $\frac{1}{2}m_\phi^2\phi^2$, which should be present in realistic versions of the theory. As we have found, for $g^2 \gg \lambda$ these mass terms lead to a radical change in the structure of the resonance not at $\Phi \lesssim m_\phi/\sqrt{\lambda}$, as one would naively expect, but much earlier, at $\Phi \lesssim \frac{g}{\sqrt{\lambda}}\frac{\pi^2 m_\phi^2}{3\lambda M_p}$. In this regime, the resonance becomes stochastic and the effective width of the resonance band increases, making it much more stable with respect to various backreaction effects including rescattering [15].

We should emphasize again that preheating is but the first stage of reheating, which does not lead to a complete decay of the inflaton field in any of these models. The last stages of preheating are always described by the perturbative theory. To illustrate this point, we described the development of the parametric resonance in the general class of models with an effective potential $V(\phi,\chi) = \pm\frac{1}{2}m_\phi^2\phi^2 + \frac{1}{4}\lambda\phi^4 + \frac{1}{2}g^2\phi^2\chi^2$. In these theories–with no other interactions accounted for–the inflaton field can completely decay only if the sign of the term $\frac{m_\phi^2}{2}\phi^2$ is negative, which corresponds to spontaneous symmetry breaking. Moreover, this process completes only for $\frac{g^2}{\lambda} < \frac{1}{2}$, see figures 2.11 and 2.12.

A complete perturbative decay is possible for $\frac{g^2}{\lambda} > \frac{1}{2}$ as well, even without spontaneous symmetry breaking, but only if the inflaton field has some other interactions, such as an interaction with fermions $h\phi\bar{\psi}\psi$ with mass $m_\psi < m_\phi/\sqrt{2}$ [53]. This conclusion implies that the decay of the inflaton field is by no means automatic even if it is heavy and strongly interacts with other fields. Generically, the inflaton field accumulates an enormously large energy density, which can be completely released only if it interacts with other particles in a very specific way [48]. We will see in the next two chapters how non-perturbative interactions with fermions affect the resonance.

To understand how these results may change our point of view on the thermal history of the universe, let us suppose for a moment that the inflaton field does not have any interactions with light fermions, and that it has an effective potential $-\frac{m_\phi^2}{2}\phi^2+\frac{1}{4}\lambda\phi^4+\frac{1}{2}g^2\phi^2\chi^2$ with $\lambda \sim g^2 \sim 10^{-13}$ and with a small mass $m_\phi \sim 10^2$GeV protected by supersymmetry. Then the final stage of reheating of the universe will begin only after the symmetry breaking in this theory, and the reheating temperature estimated in accordance with [15] will be smaller than $10^2 - 10^3$GeV. In such a theory, the electroweak phase transition may never happen, or it may occur in an entirely different way. From the end of inflation until the symmetry breaking and the final stage of reheating, the universe will remain far away from thermal equilibrium, and various non-thermal phase transitions and explosive processes of particle production may occur. In such a model one should reconsider all issues related to the primordial gravitino problem, moduli field problem, baryogenesis, etc.

The main conclusion of our investigation can be formulated as follows. The first stages of the process of the inflaton decay may occur much more efficiently than was previously thought, due to the effect of parametric resonance. The last stage of this process may be completely inefficient even if the coupling of the inflaton field to matter is very strong, or it may be efficient only in a very narrow range of parameters. As a result, the complete thermal (and non-thermal) history of the universe in the context of the inflationary universe scenario may be dramatically different from the standard lore of the hot Big Bang cosmology.

# Chapter 3

# Preheating of Fermions in the Conformal Theory

We begin our study of fermionic preheating by considering the conformally invariant theory specified by the Lagrangian

$$\mathcal{L}_{\text{int}} = -\frac{1}{4}\lambda\phi^4 - h\phi\bar{\psi}\psi\,, \tag{3.1}$$

where inflation is supported by the quartic inflaton potential, as in the last chapter. A yukawa term couples the inflaton to a massless spin-$\frac{1}{2}$ Dirac fermion, $\psi$, with dimensionless coupling constant, $h$. As we will see, much like the model considered in Chapter 2, this theory is reducible to a theory in Minkowski space-time for which there is no Hubble expansion. This simplifies the analysis and we shall present several analytic results for the particle production in these cases.

## 3.1 Evolution of the Background and Fluctuation Fields

Inflation due to the quartic term in (3.1) occurs exactly as in the conformal theory considered in chapter 2. Let us remind ourselves of the results we obtained there.

We consider flat FRW metrics $g_{\mu\nu} = \text{diag}\{1, -\text{a(t)}, -\text{a(t)}, -\text{a(t)}\}$ where $a(t)$is the scale factor of the universe. We assume that the homogeneous inflaton field gives the dominant contribution to the energy density during and at the end of inflation. The Friedmann equation (2.2) again determines the Hubble parameter:

$$H^2 = \left(\frac{\dot{a}}{a}\right)^2 = \frac{8\pi}{3M_{\text{pl}}^2}\left(\frac{1}{2}\dot{\phi}^2 + \frac{1}{4}\lambda\phi^4\right)\,. \tag{3.2}$$

The homogeneous inflaton field, $\phi(t)$ obeys the Klein-Gordon equation (2.4)

$$\ddot{\phi} + 3H\dot{\phi} + \lambda\phi^3 = 0\,, \tag{3.3}$$

which describes damped oscillations of the inflaton field, see figure 2.1. It is this stage of damped oscillations that will interest us here.

Recall that, for oscillations in a pure $\frac{1}{4}\lambda\phi^4$ potential, the equation of state averaged over an inflaton oscillation corresponds to that of a radiation dominated universe: $a(t) \sim \sqrt{t}$, $\langle\rho_\phi\rangle \propto a^{-4}$. Hence, the amplitude of the inflaton field decreases like $a^{-1}$. In chapter 2, we found that the explicit time-dependence of the coefficients in the Klein-Gordon equation (3.3) could be removed by working in new, "conformal" field and time variables: $\eta = \int \frac{dt}{a}$ and $\varphi = a\phi$. In terms of these variables, and neglecting a small term proportional to the scalar curvature $R$ (see the discussion following equation (2.9)), the Klein-Gordon equation (3.3) becomes simply: $\varphi'' + \lambda\varphi^3 = 0$, where $'$ denotes differentiation with respect to the conformal time. The oscillations of $\varphi(\eta)$ are undamped. (We are neglecting the backreaction of produced particles, which is valid at the start of the inflaton's oscillations.) In fact, this equation is easily solved in terms of Jacobi elliptic functions. This solution is equation (2.14), which we will need below.

We now turn to the solution of the fermion equation in the background provided by this inflaton field.

### 3.1.1 Dirac equation for fermions in a time dependent background

The evolution of the field $\psi$ is governed by the general relativistic generalization of the Dirac equation

$$\left[i\bar{\gamma}^\mu D_\mu - h\phi(t)\right]\psi(x) = 0\,, \tag{3.4}$$

where $D_\mu = \partial_\mu + \frac{1}{4}\gamma_{\alpha\beta}\omega_\mu^{\alpha\beta}$ is the spin-$\frac{1}{2}$ covariant derivative with vierbein dependent spin-connection, $\omega_\mu^{\alpha\beta}$. Barred gammas are the time dependent Dirac matrices which, for our FRW space-time, reduce simply to $\bar{\gamma}^0 = \gamma^0$ and $\bar{\gamma}^i = \frac{1}{a(t)}\gamma^i$, where the unbarred gammas are standard, Minkowski space-time Dirac matrices. Refer to Appendix A for our notational conventions.

In Appendix A the spin connection is shown to reduce to

$$\frac{1}{4}\bar{\gamma}^\mu\gamma_{\alpha\beta}\omega_\mu^{\alpha\beta} = \frac{3}{2}\left(\frac{\dot{a}}{a}\right)\gamma^0\ . \tag{3.5}$$

Thus, in our case, the Dirac equation becomes

$$\left[i\gamma^0\partial_0 + i\frac{1}{a}\vec{\gamma}\cdot\vec{\nabla} + i\frac{3}{2}\left(\frac{\dot{a}}{a}\right)\gamma^0 - h\phi(t)\right]\psi(x) = 0\,. \tag{3.6}$$

Only standard gamma matrices now appear. Similarly, variation of the full action with respect to the $\psi$-field leads to an equation for $\bar{\psi} = \psi^\dagger\gamma^0$. This equation is just the Hermitian conjugate of equation (3.6).

Following the example of the conformal bosonic theory, let us seek new, conformal field and time variables for the Dirac equation (3.6). From the Klein-Gordon equation for the background field, we already know that we want to work in conformal time, $\eta$. For our field variable, inspection of the "damping" term in the Dirac equation (3.6), the first order character of this equation, suggest that we should use a new field variable: $\Psi = a^{3/2}\psi$. Changing variables to these leads to the equation

$$\left[i\gamma^0\partial_\eta + i\vec{\gamma}\cdot\vec{\nabla} - h\varphi(\eta)\right]\Psi(\eta,\mathbf{x}) = 0\,, \tag{3.7}$$

where $\varphi = a\phi$ is the conformal background field variable introduced above. As the gamma matrices in (3.7)are still the usual flat-space ones, we have again transformed an expanding space problem into a flat space one.

Let us now try to find eigenmode solutions to this equation. In the Heisenberg representation of QFT, the Dirac equation (3.7) becomes the equation of motion for the $\hat{\Psi}(x)$ field operator. $\hat{\Psi}(x)$ may be decomposed into eigenspinors

$$\hat{\Psi}(\eta,\mathbf{x}) = \sum_{s=\pm}\int\frac{d^3k}{(2\pi)^3}\left(\hat{a}_{k,s}\mathbf{u}_{k,s}(\eta)\,e^{+i\mathbf{k}\cdot\mathbf{x}} + \hat{b}^\dagger_{k,s}\mathbf{v}_{k,s}(\eta)\,e^{-i\mathbf{k}\cdot\mathbf{x}}\right), \tag{3.8}$$

where $\mathbf{u}_{k,\pm}(\eta)$ is a positive-frequency eigenspinor of the Dirac equation (3.7) with helicity $\pm\frac{1}{2}$ and $\mathbf{v}_{k,\pm}(\eta) = \mathcal{C}\bar{\mathbf{u}}^T_{k,\pm}(\eta)$ is its charge conjugate. Here $\mathcal{C} = i\gamma_0\gamma_2$ is the standard charge conjugation matrix.

To construct these eigenspinors we use the ansatz

$$\mathbf{u}_{k,\pm}(\eta)\,e^{+i\mathbf{k}\cdot\mathbf{x}} = \left[-i\gamma^0\partial_\eta - i\vec{\gamma}\cdot\vec{\nabla} - h\varphi(\eta)\right]X_k(\eta)R_\pm(\mathbf{k})e^{+i\mathbf{k}\cdot\mathbf{x}}\,, \tag{3.9}$$

where $R_\pm(\mathbf{k})$ are eigenvectors of the helicity operator $\hat{\mathbf{k}}\cdot\Sigma$ such that $\hat{\mathbf{k}}\cdot\Sigma R_\pm(\mathbf{k}) = \pm 1$ and $\gamma^0 R_\pm(\mathbf{k}) = +1$. The time dependence of the eigenspinor is contained entirely in the scalar mode function $X_k(\eta)$. Substituting this ansatz into equation (3.7) leads to the mode equation

$$X_k'' + \left[k^2 + h^2\varphi^2 - ih\varphi'\right]X_k = 0\,. \tag{3.10}$$

By construction, equation (3.10) contains no dependence on the expansion of the universe, but depends only on the, undamped oscillations of the rescaled inflaton field, $\varphi$.[1]

For reference, we can now express the eigenspinors in terms of the scalar function $X_k(\eta)$. Using the mode equation and ansatz, we find

$$\mathbf{u}_{k,\pm}(\eta) = \left[-iX'_k + (\gamma \cdot \mathbf{k} - h\varphi)X_k\right] R_\pm(\mathbf{k}) \ . \tag{3.11}$$

Taking the charge conjugate of $\mathbf{u}_{k,\pm}$, we find

$$\mathbf{v}_{k,\pm}(\eta) = \left[iX'^*_k - (\gamma \cdot \mathbf{k} + h\varphi)X^*_k\right] \bar{R}_\pm(\mathbf{k}) \ , \tag{3.12}$$

where $\bar{R}_\pm(\mathbf{k}) \equiv -i\gamma^2 R^*_\pm(\mathbf{k})$ is an eigenvector of helicity such that $\hat{\mathbf{k}} \cdot \Sigma \bar{R}_\pm(\mathbf{k}) = \pm 1$ and $\gamma^0 \bar{R}_\pm(\mathbf{k}) = -1$.

We now turn to the interpretation of the mode function $X_k$. As in the last chapter, it will be convenient to develop the particle interpretation of the Dirac field and to find the number density of produced particles.

### 3.1.2 Interpretation of the mode functions $X_k$.

The energy-momentum tensor is obtained from the ($\psi$ and $\bar{\psi}$ symmetrized) matter action by variation with respect to the vierbein

$$T^{\mu\nu} = \frac{i}{2} g^{\mu\alpha} g^{\nu\beta} \left[\bar{\psi}\bar{\gamma}_{(\alpha}\ \overrightarrow{D}_{\beta)}\ \psi - \bar{\psi}\ \overleftarrow{D}_{(\alpha}\ \bar{\gamma}_{\beta)}\psi\right] . \tag{3.13}$$

Transforming to conformal field and space-time variables we obtain the Hamiltonian

$$\mathbf{H}_D = a^{-3} \int d^3x \left[i\hat{\Psi}^\dagger \partial_\eta \hat{\Psi}\right] . \tag{3.14}$$

In general, if this Hamiltonian is diagonal in the annihilation and creation operators $\hat{a}_{k,s}$, $\hat{a}^\dagger_{k,s}$ and $\hat{b}_{k,s}$ , $\hat{b}^\dagger_{k,s}$ at $t = 0$, it will not be for later times. This is the signature of particle creation due to the time dependent background. In order to determine the number of particles produced, we perform a Bogliubov transformation on the creation and annihilation operators so as to diagonalize the Hamiltonian at time $t$. The result of this procedure is that the expectation value of the Hamiltonian

[1] If we transform our initial Lagrangian to conformal variables, there is a faster and more elegant way to obtain this result which relies on the fact that $\gamma^\mu\gamma^\nu D_\mu D_\nu \psi = \gamma^\mu\gamma^\nu \left(D_{(\mu}D_{\nu)}\psi + D_{[\mu}D_{\nu]}\right)\psi$. As always, the commutator of two vectors is just proportional to the curvature, $\gamma^\mu\gamma^\nu D_{[\mu}D_{\nu]}\psi \propto R\psi$, which vanishes in this case. The first term is simplified because $\gamma^\mu\gamma^\nu D_{(\mu}D_{\nu)}\psi = g^{\mu\nu} D_\mu D_\nu \psi = \Box^2\psi$.

density in the "in" state may be written, at any time:

$$\rho_\psi(\eta) = a^3 \langle \mathcal{H}_D \rangle = \frac{2}{\pi^2} \int dk\, k^2\, \Omega_k\, n_k(\eta)\,, \tag{3.15}$$

where $\Omega_k = \sqrt{k^2 + h^2\varphi^2}$ is the energy per particle and $n_k$ is the comoving number density of fermions with momentum $k$. $\rho_\psi$ is the comoving energy density of produced fermions. A factor of 4 for the degeneracy of the Dirac fermion (particle and anti-particle, spin up and down) has been included in (3.15).

Using our operator expansion (3.8) and our expressions for the eigenspinors (3.11) and (3.12), we can write an explicit expression for the comoving number density of created fermions per spin state in terms of the mode functions $X_k(\eta)$. The result of a short calculation gives

$$n_k(\eta) = \left(\frac{\Omega_k - h\varphi}{2\Omega_k}\right) \left[|X_k'|^2 + \Omega_k^2 |X_k|^2 - 2\Omega_k Im(X_k X_k'^*)\right]\,. \tag{3.16}$$

This result can be understood in a manner similar to the bosonic equivalent (2.24). If we look for adiabatic (aka WKB or semi-classical) approximations to the mode equation (3.10), we find

$$X_k(\eta) = \alpha_k N_+\, e^{-i\int_0^\eta d\eta'\, \Omega_k(\eta')} + \beta_k N_-\, e^{+i\int_0^\eta d\eta'\, \Omega_k(\eta')}\,, \tag{3.17}$$

where $N_\pm = (2\Omega_k(\Omega_k \mp h\varphi))^{-1/2}$ and the coefficients $\alpha_k$ and $\beta_k$ correspond to the coefficients of the Bogliubov transformation. Our expression for the particle number is exactly the square of Bogliubov's "beta" coefficient: $n_k(t) = |\beta_k|^2$, just as in the bosonic case. An added benefit of the adiabatic expansion is that it tells us how to normalize our mode functions for an initial "positive frequency vacuum" state: the initial vacuum should contain no particles so that $\alpha_0 = 1$, $\beta_0 = 0$. Thus, we chose $X_k(t \to 0^+) = N_+ e^{-i\Omega_k\eta}$ to insure $n_k(0) = 0$. Substituting this back into the adiabatic approximation confirms that $N_+ = (2\Omega_k(\Omega_k - h\varphi))^{-1/2}$ there, as expected. It also follows from the adiabatic approximation that whenever (3.17) is valid *and* the coefficients are constant, then both $n_k$ and $\rho_\psi$ will be conserved.

It is important to understand that, while expression (3.16) for $n_k$ is only meaningful during those periods of time when the adiabatic approximation is good (i.e. we have slowly varying Bogliubov coefficients), our expression (3.10) for the mode functions is always valid. They contain all the information obtainable about the quantum state of the fermions–neglecting backreaction, of course. Thus, if we observe the number of particles to be changing rapidly, we should understand that this only means that particle number is not a good quantum number to be considering. It does not mean that our calculation of $X_k$ has gone awry.

A comment about the regularization of fermion vevs. In principle, fermionic vevs like $\langle T^{\mu\nu}\rangle$ require regularization, which in the presence of the background metric and scalars is rather non-trivial, see e.g. [24, 56] and references therein. We will consider only the processes of particle creation, ignoring vacuum polarization. The creation of particles, which corresponds to the imaginary part of the effective action, has no formal divergences and does not require regularization. Assuming the particle creation process dominates over vacuum polarization, we will not consider the issues of regularization.

## 3.2 Solution to the Master Equation for Fermions

Let us rescale our field and time variables to make them dimensionless. In Chapter 2, we found the time evolution for the conformal field $\varphi$ in terms of the Jacobi elliptic function $cn$. There we found it convenient to introduce the rescaled background field variable

$$f(x) = \varphi_0^{-1}\varphi = cn(x - x_0\,,\, \frac{1}{\sqrt{2}})\,, \tag{3.18}$$

where $\varphi_0 \sim O(0.1\mathrm{M_p})$ is the amplitude of $\varphi$'s oscillations, $x = (\sqrt{\lambda}\varphi_0)^{-1}\eta$ is the rescaled conformal time, and $x_0 \approx 2.44$ is the start of oscillations. $x$ here should not be confused with the spatial coordinates to which we will no longer have need to refer. Recall that the period of an inflaton oscillation in $x$ units is just $T = 7.416$. The rescaled field $f(x)$ has unit amplitude.

In terms of these new variables, we may write the fermionic mode equation (3.10) in the form

$$X_k'' + \left[\kappa^2 + qf^2 - i\sqrt{q}f'\right] X_k = 0\ , \tag{3.19}$$

where $'$ is differentiation with respect to $x$. This will be our master equation for the investigation of fermion production during preheating. The parameters $\kappa^2$ and $q$ are dimensionless momentum and resonance strength parameters, respectively. Specifically, we have

$$\kappa^2 = \frac{k^2}{\lambda\varphi_0^2} \qquad , \qquad q = \frac{h^2}{\lambda}\,. \tag{3.20}$$

We see that the typical (comoving) momentum scale for produced fermions will be $k \sim O(\sqrt{\lambda}\varphi_0) \sim 10^{11}$ GeV and the resonance parameter $q \sim h^2\,10^{13}$. Here we

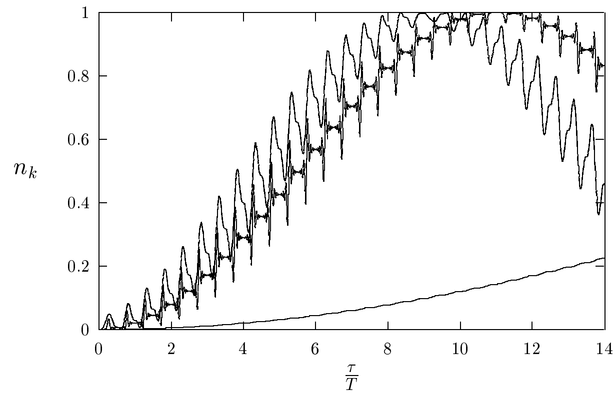


Figure 3.1: The occupation number $n_k$ as a function of time, measured in inflaton oscillations, for $q \equiv \frac{h^2}{\lambda} = 10^{-4}$ (lower), 1 (middle on right), and 100 (upper on right) and $\kappa^2 = 0.18, 1.11$, and 11.9, respectively. The period of the modulation $\frac{\pi}{\nu_k}$ (see equation (3.21)) is about 88, 20 and 22, respectively.

have again taken $\lambda \approx 10^{-13}$ as follows from the CMB constraints on inflationary density perturbations.

It is a simple matter to obtain numerical solutions to the master equation (3.19) for given values of $\kappa^2$ and $q$ and to plot the occupation number (3.16) from these. Note that, we can easily effect our change of variables in expressions (3.15) and (3.16) by taking $k \to \kappa$, $h\varphi \to qf$ and inserting a factor of $\sqrt{\lambda}\varphi_0$ for each mass dimension. Perturbation theory gives some intuition as to what we should expect: if individual, *massive* inflatons at rest are decaying into light fermions in a process $\phi \to \bar{\psi}\psi$, perturbative calculations give the rate of decay $\Gamma_{\phi\to\psi\psi} \simeq \frac{h^2 m_\phi}{8\pi}$. Furthermore, we expect each fermion to carry away half of the inflaton's energy. Thus, we expect the spectrum of created fermions to be sharply peaked around $k = m_\phi/2$ with a width $\Gamma^{-1}_{\phi\to\psi\psi}$. Translating this into our case, we note that the mass, $m_\phi$, corresponds to the effective frequency of inflaton oscillations, which is just $(\frac{2\pi}{T})\sqrt{\lambda}\varphi_0$ in our case. Recall that $T \approx 7.416$. Thus, perturbation theory leads us to expect particle creation at a rate $\Gamma \propto h^2\sqrt{\lambda}\varphi_0$ and sharply peaked around $\kappa^2 = (\frac{\pi}{T})^2 \approx 0.18$.

In figure 3.1, we plot the time-dependence of the occupation number, $n_k$, for several values of $\kappa^2$ and $q$, as follows from the numerical solution of the master equation (3.19). Time here is measured in units of inflaton oscillations, $\frac{\tau}{T} = \frac{x}{T}$. We find that, for all $\kappa$ and $q$, the occupation number exhibits high frequency (period $< \frac{T}{2}$) oscillations which are modulated by a longer period behavior. If we average the occupation number over these high frequency oscillations, $\bar{n}_k(x) = \frac{1}{T}\int_x^{(x+T)} dx n_k(x)$, we can write the smoothed occupation number of fermions in a factorized form

$$\bar{n}_k(x) = F_k \sin^2(\nu_k x) \ . \tag{3.21}$$

One can show analytically that, for all $\kappa$ and $q$, the occupation number of fermions evolves *periodically* with time [21, 23, 22]. The spectrum (or envelope) function $F_k$ and the period $\frac{\pi}{\nu_k}$ depend on the parameter the parameters $\kappa$ and $q$. Typically $\frac{\pi}{\nu_k} \sim 10-100$, see figure 3.2. Therefore, the fermionic modes get fully exited around their time-average value $\frac{F_k}{2}$ within just tens of inflaton oscillations! This is very different from the result of the perturbative approximation which gives the timing for excitation $\sim \Gamma^{-1}_{\phi\to\psi\psi}\sqrt{\lambda}\varphi_0 \sim h^{-2}$ inflaton oscillations. In the cases shown, this corresponds to–in order of decreasing $q$–from $10^{12}$ to $10^{18}$ inflaton oscillations; whereas, we actually find between 20 and 88 oscillations is all that's necessary! One would naively expect that perturbation theory should work well for $h \ll 1$. Here, however, we see that it is totally inadequate even for $q = 10^{-4} \to h = 10^{-9}$. It is important to realize that this is not due to the large, $O(0.1M_p)$ amplitude of the inflaton fields initial oscillations. The $q$ parameter is independent of $\varphi_0$ in this model and is also independent of time.

Notice also in figure 3.1 that, for $q \gg 1$, the number of fermions is almost constant between two successive zeros of the inflaton field. It jumps in a step-like manner at instances when $\phi(t)$ crosses zero. This is a familiar picture for the creation of bosons that we saw in the last chapter. We expect the adiabatic approximation to be good most of the time when $q \gg 1$. In the next chapter, we will develop the method of parabolic scatterings for fermions, as was first done in [14]. We will find that, contrary to the bosonic resonance which is unbounded, the fermionic resonance reaches its peak value $F_k \leq 1$ after a time $\frac{\pi}{2\nu_k}$ and then falls back to zero, where it begins the cycle again.

In figure 3.2 we plot the envelope function $F_k$ and modulation period $\frac{\pi}{\nu_k T}$ for several values of the resonance parameter $q = \frac{h^2}{\lambda}$. To obtain these plots, we have used a semi-analytic method for finding $F_k$ and $\nu_k$ that requires us to numerically integrate the master equation (3.19) over only a single period of the inflaton field. We will explain these equations in the next section. The spectrum, $F_k$, of $n_k$ is very different from what is expected from the perturbative calculations. While, for $q \lesssim 10^4$, the spectrum is peaked around $\kappa^2 = 0.18$, we find that the width is not proportional to $h^2$, as perturbation theory would suggest. For larger values of $q$, the perturbative result is completely wrong. We also see that there are higher order bands of excitation. We find that, for any $q$, the first (and broadest) band has the width $\Delta\kappa \sim q^{1/4}$. This can be understood from the condition for non-adiabatic excitation of particles, $\dot{\Omega}_k \geq \Omega_k^2$, which gives us $\Delta k \leq q^{1/4}\sqrt{\lambda}\tilde{\varphi}$. This same scaling is seen in the bosonic theory and can be explained similarly [15].

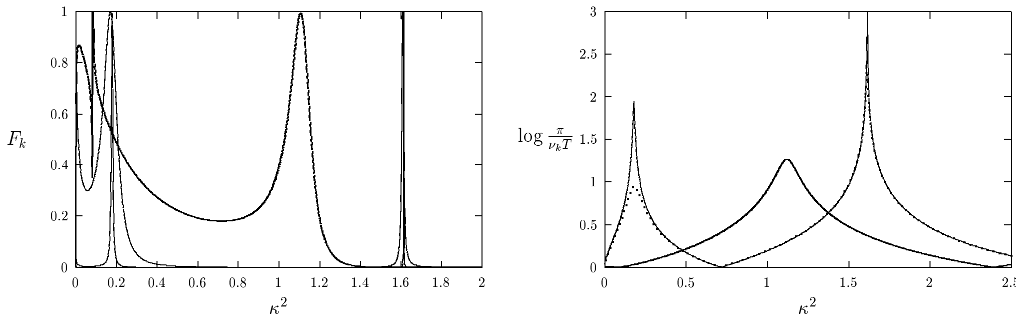


Figure 3.2: In the left panel we plot the envelope functions $F_k$ showing the bands of fermion parametric excitation for $q \equiv \frac{h^2}{\lambda} = 10^{-4}, 10^{-2}$, and 1.0 (the narrowest to broadest bands, respectively). The band in the case $q = 10^{-4}$ is peaked where one would expect from perturbation theory, but differs in width. Note that $q = 10^{-2}$ corresponds to $h = 10^{-8}$, and yet it differs considerably from the perturbative expectation. The right panel shows the log of the period of modulation $\frac{\pi}{\nu_k}$ (in units of $T$) as a function of $\kappa^2$ for $q \equiv \frac{h^2}{\lambda} = 10^{-4}, 10^{-2}$, and 1.0 (light, dotted, and heavy curves respectively). For $q \gtrsim 1$ the band fills in only tens of inflaton oscillations.

The function $\nu_k$, plotted in figure 3.2, gives us the time scale for fermion excitation. This function is peaked where $F_k$ is peaked, i.e. the peaks of the resonance curve are the last to fill. For $q \gtrsim 1$, the period for modes in the principle peak is about $20T$. When $q \ll 1$, modes in the principle peak grow more slowly, with a period of approximately $\frac{T}{\sqrt{q}}$. Interestingly, the period of modes out of the $F_k$-peaks is significantly *shorter*. For this reason, the integrated number of fermions is quickly saturated to its time-average value.

In figure 3.3 we show how the fermionic resonance bands are filled after 10 background oscillations. We also plot the envelope function $F_k$ for comparison. In general, after a few dozen inflaton oscillations, the spectrum will saturate with $n_k \approx \frac{1}{2} F_k$.

The huge differences in the spectrum and rate of excitation of fermions produced by the coherently oscillating background field vs. those in the naive perturbative calculations are due to the interference of the fermion fluctuations. In this respect we can talk about *the parametric excitation of fermions*, where $q$ plays the role of the resonance parameter, and the frequency $\nu_k$ can be viewed as the fermionic counterpart of the bosonic characteristic exponent $\mu_k$. The amplitude of $n_k$ shows a distinct sequence of "resonance bands" whose widths sharply narrow with increasing zone number. This is again reminiscent of the usual bosonic

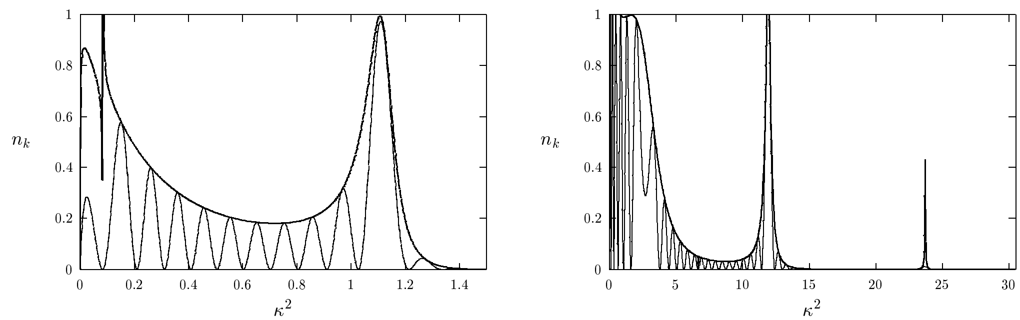


Figure 3.3: The left panel shows the resonance excitation band of fermions for $q \equiv \frac{h^2}{\lambda} = 1.0$. The heavy line shows the envelope $F_k$ of maximum occupation number. The light curve is the actual occupation number $n_k$ of each mode, calculated from equation (3.21), after 10 background oscillations. The right panel is similar, but for $q \equiv \frac{h^2}{\lambda} = 100.0$ this time. The heavy line shows the envelope function $F_k$. The light curve is the actual occupation number of each mode $n_k$ after 10 background oscillations.

resonance. For $q \ll 1$, the resonance bands are located at $\kappa = \frac{\pi}{T}(2l+1)$, where $l = 0, 1, 2, \ldots$.

It is instructive to compare the spectrum and evolution of fermionic occupation numbers with those of bosonic occupation numbers. We saw in the last chapter that the mode function of a quantum bose scalar field $\chi$ with a $\frac{1}{2}g^2\phi^2\chi^2$ interaction with the $\frac{1}{4}\lambda\phi^4$ theory inflaton obeys the bosonic oscillator-like equation

$$X''_{b,k} + \left[\kappa_b^2 + q_b f^2\right] X_{b,k} = 0 \ , \tag{3.22}$$

where $q_b = \frac{g^2}{\lambda}$, $\kappa_b^2 = \frac{k^2}{\lambda\varphi_0^2}$, and $f(x)$ is the same function we consider here. In figure 3.4 we plot the spectrum and time evolution of bosonic occupation number calculated from the bosonic oscillator-like equation (3.22) and the number density (2.24). We use the familiar model of bosonic resonance due to the self-interaction in $\frac{1}{4}\lambda\phi^4$ inflation, which corresponds to $q = \frac{g^2}{\lambda} = 3$.

In the bosonic case, there are distinct resonance bands in which bosonic modes are exponentially unstable, $n_k(t) \sim \sinh^2(\mu_k x) \sim e^{2\mu_k x}$. Particle creation takes place outside of the resonance bands as well, although there the occupation number is bounded and oscillates periodically. In the fermionic case, $n_k \leq 1$ always because of Pauli blocking. The occupation number in both cases is changing in time.

Comparison of bosonic and fermionic parametric excitations is useful to understand some features of bosonic preheating. As we have seen, there is production of bosons outside of the resonance band. If we take into account the expansion of the

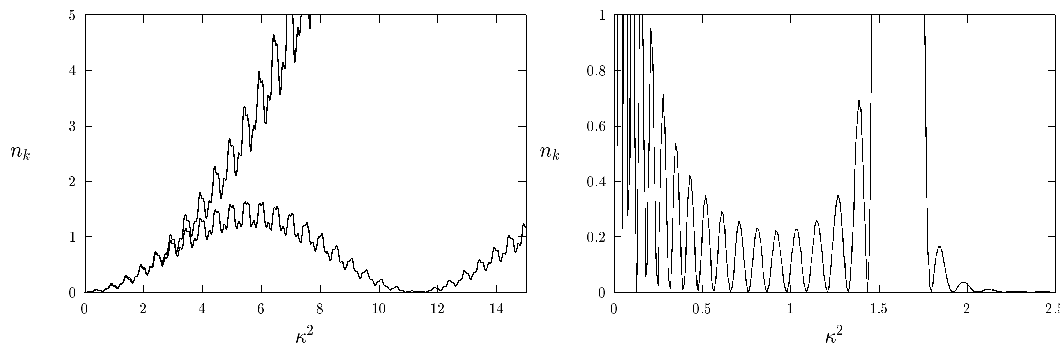


Figure 3.4: The left panel shows the time dependence of the occupation number in $\frac{1}{4}\lambda\phi^4 + \frac{1}{2}g^2\phi^2\chi^2$-theory for $q = \frac{g^2}{\lambda} = 3$ (aka pure $\frac{1}{4}\lambda\phi^4$ theory with self interaction) for two different modes: one is just inside the resonance band which grows like $\sinh^2(\mu_k x) \sim e^{2\mu_k x}$ and another just outside of the resonance band which oscillates like $\sin^2(\nu_k t)$. The right panel shows the bosonic occupation number after 10 background oscillations for the same theory. A stripe with sharp edges with $\frac{3}{2} < \kappa^2 < \sqrt{3}$ corresponds to the $\sinh^2(\mu_k x)$ instability.

universe, in the most interesting case of large $q_b$, the difference between resonant and non-resonant excitations of bosons will be erased, and the regime of stochastic resonant production of bosons will be settled down [15].

## 3.3 Some General Analytic Results

The dynamics of the Dirac field coupled to the background homogeneous scalar can be understood by considering some general properties of the master equation (3.19) for the mode functions $X_k(x)$. This a second-order, oscillator-like equation with complex, periodic coefficients. For periodic background oscillations $f(x) = f(x + T)$, the fermionic master equation has the same form at time $x + T$ as at $x$. Some generic analytic results were derived a long time ago [22] for this equation in the context of particle creation in a periodic external electromagnetic field. In particular, the occupation number of created particles at instances $x = N_s T$, i.e. exactly after $N_s$ background oscillations, is given by the expression [22]

$$n_k(N_s T) = \frac{k^2}{2\Omega_k^2} \frac{\sin^2(N_s d_k)}{\sin^2(d_k)} \left( Im X_k^{(1)}(T) \right)^2 , \tag{3.23}$$

where $\cos d_k = Re X_k^{(1)}(T)$. To derive this result, one introduces two fundamental solutions of the master equation (3.19), $X_k^{(1)}(x)$ and $X_k^{(2)}(x)$; such that initially

$X_k^{(1)} = 1$, $\dot{X}_k^{(1)} = 0$ and $X_k^{(2)} = 0$, $\dot{X}_k^{(2)} = 1$. Expression (3.23) involves only the value of the first fundamental solution $X_k^{(1)}(T)$ exactly after the first oscillation. This is the basis of our formula (3.21). It says that the occupation number of created particles after $N_s$ background oscillations is modulated with a certain frequency $\nu_k$ (which, as we will see, does not coincide with $\frac{d_k}{2}$). However, the practical application of the generic formula (3.23) is rather limited, because it does not address the full time evolution of $n_k(t)$, and cannot strictly determine a period of modulation $\frac{\pi}{\nu_k}$. This is basically a sampling problem: equation (3.23) tells us what the occupation number is after exactly an integer number of background field oscillation, but it doesn't tells us how the occupation number changes between these times.

To get an idea of how the occupation number of created particles $n_k(t)$ evolves with time, again let us look at figure 3.1. For small and moderate $q$ (but not too small $\kappa$) the occupation number exhibits high frequency (period $< \frac{T}{2}$) oscillations which are modulated by a long period behavior. For large $q$, the number of fermions jumps in a step-like manner at instances when the effective mass of the fermi field crosses zero, superposed by very high frequency oscillations around almost constant values. These jumps are modulated with a frequency $\frac{\nu_k}{2}$: steps in the first half of the cycle up are accumulated until $n_k(t)$ reaches its maximum $F_k$, and then steps down to zero in the second half of the cycle.

However, this picture of high frequency features superimposed over long-period modulation is not universal and can be misleading. For small $\kappa$, or for one of the most interesting cases of $q \gg 1$ and moderate $\kappa$, the occupation number of fermions jumps between zero and one within a time interval shorter than the period of background oscillations. There are interesting situations when fermions are created in an instant (single kick) process, where formula (3.23) is not applicable. Therefore, for different ranges of parameters we will shall develop different approaches.

In the next section we will develop the theory leading to equation (3.21). We will reserve a discussion of the step-like production of fermions for $q \gg 1$ for the next chapter.

## 3.4 Semi-Analytic Theory for the Averaged Occupation Number

Numerical curves for the mode functions suggest a splitting of the time evolution into higher frequency features with the time-scale comparable or less than the period of background oscillations $\leq T$, and low-frequency modulations with the period $\frac{\pi}{\nu_k}$ greater than $T$. In this case we can utilize the generic result (3.23).

However, it is convenient to use not the values $n_k(N_sT)$, but rather the smoothed occupation number $\bar{n}_k(x)$ which is $n_k(x)$ averaged over high frequency oscillations, $\bar{n}_k(x) = \frac{1}{T}\int_x^{(x+T)} dx n_k(x)$. Then we can write the smoothed occupation number of fermions in the factorized form (3.21)

$$\bar{n}_k(x) = F_k \sin^2(\nu_k x) \ , \tag{3.24}$$

The average occupation number of fermions evolves *periodically* with time. The spectrum of $\bar{n}_k$ can be characterized by the envelope function $F_k$ and the period of modulation $\frac{\pi}{\nu_k}$ which depend also on the parameter $q$, as we have seen.

Now we will utilize the result (3.23). We found that the envelope function can be extrapolated from the factor in front of $\sin^2 N_s d_k$ in (3.23) and given by the expression

$$F_k = \frac{1}{\sin^2 \nu_k T} \frac{\kappa^2}{2\Omega_k^2} \left(Im X_k^{(1)}(T)\right)^2 \ . \tag{3.25}$$

Next we need to determine the frequency $\nu_k$ of the $\bar{n}_k$ modulations. The value $d_k$ defined after (3.23) cannot be the right answer because it would incorrectly predict that the peaks of $F_k$ are filled up first, while actually they are filled last. We tried the combination $\nu_k = \pi/2 - d_k$, because it corresponds to the correct order of saturation of $F_k$. From our numerical results, it appears to work well. Therefore, the modulation frequency $\nu_k$ is given by the relation $\cos(\nu_k T) = -Re X_k^{(1)}(T)$. Thus, to find $F_k$ and $\nu_k$, one need only calculate the complex value $X_k^{(1)}(T)$ after a single background oscillation, instead of performing a full numerical integration of the master equation (3.19). We used these formulae for $F_k$ and $\nu_k$ to construct figures 3.2 and 3.3 and checked them against longer integrations of the master equation past one inflaton oscillation.

## 3.5 Discussion

We have seen that the production of fermions is far from perturbative. Let us now estimate the energy that will be accumulated in created fermions in the theory $\frac{1}{4}\lambda\phi^4 + h\bar{\psi}\psi$. Averaging over short-period oscillations, we can express the comoving energy density in fermions as

$$\bar{\rho}_\psi = \frac{2\lambda^2\varphi_0^4}{\pi^2} \int d\kappa\, \kappa^2\, \Omega_k\, F_k\, \sin^2(\nu_k x)\,, \tag{3.26}$$

which follows from (3.15) and (3.21). In the broad resonance case, $q \gg 1$, we can approximate $\left\langle F_k \sin^2(\nu_k x)\right\rangle \approx \frac{1}{2}$ for $\kappa \leq q^{1/4}$ and cut the integral off there.

This will be accurate after only a few inflaton oscillations. Taking the value of the inflaton field at the peak of an oscillation, we have $\Omega_k \approx q$. Thus we find

$$\bar{\rho}_\psi \approx h^{7/2}\, 10^9\, \rho_\phi \tag{3.27}$$

where $\rho_\phi = \frac{1}{4}\lambda\varphi_0^4$ is the comoving energy density in the inflaton field, neglecting backreaction. We see that for $h \gtrsim 10^{-3}$ it is possible for a large quantity of the inflaton's energy to be deposited in fermions. For comparison, recall that, in the pure $\frac{1}{4}\lambda\phi^4$ theory with preheating of $\varphi_k$-particles, the resonance terminates do to backreaction when 0.2% of the inflaton's energy has been converted into fluctuations. Here, we see that fermions can achieve this shift in inflaton energy (and thus amplitude) in only a few oscillations, if $h \gtrsim 5 \times 10^{-4}$.

It seems possible that, if we push the parameters to $h \gtrsim 10^{-2}$, the inflaton energy might be completely transferred into fermions before a bosonic resonance develops. This conclusion is tentative for a number of reasons. For one thing, we have to be careful that radiative corrections $\sim h^4\phi^4$ don't ruin the flatness of the inflaton potential. This restricts the magnitude of $h$. Also, it is not clear how the backreaction of created fermions will influence the parametric excitation of fermions. We will see in the next chapter, when we apply the method of parabolic scattering to the problem of fermion production in the broad resonance regime, that fermion production in massive, non-conformal theories is stochastic. In this case, it is likely that the stochastic production of fermions is robust, just as happens for bosons.

These issues have not yet been thoroughly investigated. There is some numerical evidence that fermion production might catalyze the bosonic resonance [13]. In that study, however, the effects of rescattering were not taken into account. In general, however, we know that rescattering can be very important for the late time development of preheating [37, 15]. Thermalization occurs through the collisional rescattering of the large amplitude bosonic fluctuations created by parameteric resonance, in conjunction with the continual and eventual perturbative decay of the inflaton field. There has been some investigation into how thermalization comes about [39]. This is achieved through lattice simulations for classical scalar field interactions.

Unfortunately, fermions cannot be treated so easily and their ultimate role in the preheating to thermalization transition is not well understood. Most of the work on fermions has concentrated on the non-thermal production of dangerous or useful relics. The most important example being the spin-$\frac{3}{2}$ gravitino. The primordial abundance of gravitinos is tightly constrained by nucleo-synthesis, c.f. [35]. It has been found that the fermionic master equation (3.19) is the prototype to understanding the parametric excitation of gravitinos as well [57], as anticipated by Greene and Kofman [12].

# Chapter 4

# Preheating of Massive Fermions

In this chapter we will study fermionic preheating in the theory

$$-\mathcal{L}_{\rm int} = \frac{1}{2}m_\phi^2\phi^2 + (m_\psi + h\phi)\bar{\psi}\psi\,. \tag{4.1}$$

Inflation in this model will be supported by the quadratic inflaton potential $\frac{1}{2}m_\phi^2\phi^2$. We studied inflation and the stage of oscillations for this potential in the introduction. We will see that this theory does not reduce to a similar problem in flat space-time. We will find that fermion modes in this theory obey an equation similar to the master equation for fermions in the conformal theory (3.19), but with time dependent momentum and resonance parameters: $\kappa(t)\,,\, q(t)$. This leads to the stochastic production of fermions, rather than the nice periodic oscillations we found in the conformal case. We also find that the well defined spectra, $F_k$, shown in the last chapter turn into a fermi-sphere with $\langle n_k\rangle \sim \frac{1}{2}$ which grows in momentum space like $q^{1/4}$ while the fermion bare mass $m_\psi$ can be considered small [16]. Eventually, the resonance parameter decreases to a point where the parametric excitation of fermions no longer occurs and we are left after this "freeze out" with a non-degenerate fermi-sphere of heavy fermions.

The time dependence of the parameters occurring in the master equation makes the general analytic results we found in the last chapter inapplicable to this non-conformal case. In the interesting case of a large (initial) resonance parameter, we will see that the method of parabolic scatterings–so useful in the bosonic case [15, 11]– can be generalized to fermions [14]. This will allow us to determine the final spectrum of produced fermions. We will also study the production of supermassive fermions. It turns out that, due to the linear relationship between $m_\psi$ and $h\phi$ in the Lagrangian (4.1), fermions with masses as large as $h\phi_0 \sim h\times 10^{18}\,\mathrm{GeV}$ can be produced during inflation. This was noticed in [16] and investigated numerically in [17]. This result should be compared with that for supermassive bosons in the theory $\frac{1}{2}m_\phi^2\phi^2 + \frac{1}{2}(m_\chi^2 + g^2\phi^2)\chi^2$, where the maximum mass of produced $\chi$-particles is $\sqrt{h\phi_0 m_\phi} \sim h \times 10^{15}\,\mathrm{GeV}$, see [15]. While in both cases, inflatons can decay into more massive particles, $m_\psi > m_\phi$, due to their coherent oscillations, in the fermionic case this mass can even be as large as the SUSY GUT scale for $h \gtrsim 10^{-2}$.

Another application of our large $q$ results will be to the theory of "instant" particle creation. In this case, a single zero of the fermion's effective mass, $m_\psi + h\phi$, gives an exponential spectrum of particles. We confirm results found previously [58].

We begin the study of preheating in this model with the equations governing the inflaton and femionic fields. We solve these in a manner similar to the conformal case, but we will not be able to eliminate the effects of expansion. Nevertheless, we will next study the solutions of our new master equation in the limit that there is no expansion. This can be relevant for other theories of preheating, such as in hybrid inflation models where $m_\phi \gg H$ immediately after inflation.

Next, the method of parabolic scatterings will be developed in this Minkowski space-time limit. The most important result here will be an expression for the change in the number density of fermions between each zero of the fermion's effective mass. Because the occupation number never becomes large in the fermionic case, we will not be able to use the same trick as was used in the bosonic case to find the growth rate explicitly. We will, nevertheless, be able to understand general features of the particle production. The effect of expansion can then be incorporated and understood. This will lead to the desired results for the spectrum of massive fermions after "freeze out" and after just a single kick.

## 4.1 Evolution of the Background and Fluctuation Fields

We have already mentioned that inflation due to the quadratic term $\frac{1}{2}m_\phi^2\phi^2$ in (4.1) occurs as we discussed in the introduction. Let us remind ourselves of the results we obtained there.

We consider flat FRW metrics $g_{\mu\nu} = \mathrm{diag}\{1, -\mathrm{a(t)}, -\mathrm{a(t)}, -\mathrm{a(t)}\}$ where $a(t)$is the scale factor of the universe. We assume that the homogeneous inflaton field gives the dominant contribution to the energy density during and at the end of inflation. The Friedmann equation (1.3) again determines the Hubble parameter:

$$H^2 = \left(\frac{\dot{a}}{a}\right)^2 = \frac{8\pi}{3M_{\mathrm{pl}}^2}\left(\frac{1}{2}\dot{\phi}^2 + \frac{1}{2}m_\phi^2\phi^2\right) . \tag{4.2}$$

The homogeneous inflaton field, $\phi(t)$ obeys the Klein-Gordon equation (1.2)

$$\ddot{\phi} + 3H\dot{\phi} + m_\phi^2\phi = 0\,, \tag{4.3}$$

which describes damped oscillations of the inflaton field, see figure 1.2. It is this stage of damped oscillations that will interest us here.

Recall that, for oscillations in a pure $\frac{1}{2}m_\phi^2\phi^2$ potential, the equation of state averaged over an inflaton oscillation corresponds to that of a pressureless, or matter dominated, universe: $a(t) \sim t^{2/3}$ , $\langle\rho_\phi\rangle \propto a^{-3}$. Hence, the amplitude of the inflaton field decreases like $a^{-3/2} \sim t^{-1}$. Thus, the damping term in the Klein-Gordon equation (4.3) can be removed by working with a new field variable: $\varphi = a^{3/2}\phi$. The evolution equations for this new field is very simple: $\ddot{\varphi} + m_\phi^2\varphi = 0$. The oscillations of $\varphi(t)$ are undamped: $\varphi = \phi_0\cos(m_\phi(t-t_0))$. As usual, we are neglecting the backreaction of produced particles, which is valid at the start of the inflaton's oscillations. We are also ignoring the slight difference from harmonic oscillations during the first couple of oscillation of the inflaton, while the equation of state is still transitioning to that of pressureless matter.

We will now turn to the Dirac equation obeyed by the fermionic fluctuations. Our development will be similar to the conformal case section 3.1.1, but we will have to carry around extra factors of $a(t)$.

### 4.1.1 Dirac Equation for Massive Fermions

Variation of the action with respect to $\bar{\psi}$ leads to the general relativistic generalization of the Dirac equation

$$\left[i\bar{\gamma}^\mu D_\mu - (m_\psi + h\phi(t))\right]\psi(x) = 0\,, \tag{4.4}$$

as in the last chapter. Again, for an FRW space-time, we have $\bar{\gamma}^0 = \gamma^0$ and $\bar{\gamma}^i = \frac{1}{a(t)}\gamma^i$, with $\gamma^\alpha$ the standard, Minkowski space-time Dirac matrices. The spin connection,

$$\frac{1}{4}\bar{\gamma}^\mu\gamma_{\alpha\beta}\omega_\mu^{\alpha\beta} = \frac{3}{2}\left(\frac{\dot{a}}{a}\right)\gamma^0 \tag{4.5}$$

as derived in Appendix A, occurs in the covariant derivative: $D_\mu = \partial_\mu + \frac{1}{4}\gamma_{\alpha\beta}\omega_\mu^{\alpha\beta}$. Substituting this expression into (4.4), the Dirac equation becomes

$$\left[i\gamma^0\partial_0 + i\frac{1}{a}\vec{\gamma}\cdot\vec{\nabla} + i\frac{3}{2}\left(\frac{\dot{a}}{a}\right)\gamma^0 - (m_\psi + h\phi)\right]\psi(x) = 0\ . \tag{4.6}$$

Only standard gamma matrices now appear. Again, variation of the action with respect to $\psi$ leads to an equation for $\bar{\psi} = \psi^\dagger \gamma^0$ that is just the Hermitian conjugate of (4.6).

In the Heisenberg representation of QFT, the Dirac equation (4.4) or (4.6) becomes the equation of motion for the $\hat{\psi}(x)$ field operator. $\hat{\psi}(x)$ may be decomposed into eigenspinors just like in the conformal theory:

$$\psi(\mathbf{x}, t) = \sum_{s=\pm} \int \frac{d^3k}{(2\pi)^3} \left( \hat{a}_{k,s} \mathbf{u}_{k,s}(t)\, e^{+i\mathbf{k}\cdot\mathbf{x}} + \hat{b}^\dagger_{k,s} \mathbf{v}_{k,s}(t)\, e^{-i\mathbf{k}\cdot\mathbf{x}} \right), \tag{4.7}$$

where $\mathbf{u}_{k,\pm}(t)$ is a positive-frequency eigenspinor of the Dirac equation (4.6) with helicity $\pm\frac{1}{2}$ and $\mathbf{v}_{k,\pm}(t) = \mathcal{C}\bar{\mathbf{u}}^T_{k,\pm}(t)$ is its charge conjugate. Here $\mathcal{C} = i\gamma_0\gamma_2$ is the standard charge conjugation matrix. Unlike in the conformal case, these eigenspinors will have a time dependence due to the expansion of the universe, even when no particle creation is occurring.

To construct the new eigenspinors, we again use an ansatz:

$$\mathbf{u}_{k,\pm}(t)\, e^{+i\mathbf{k}\cdot\mathbf{x}} = a \left[ -i\gamma^0 \partial_0 - i\frac{1}{a}\vec{\gamma}\cdot\vec{\nabla} - i\frac{3}{2}\left(\frac{\dot{a}}{a}\right)\gamma^0 - (m_\psi + h\phi) \right] \chi_k(t) R_\pm(\mathbf{k}) e^{+i\mathbf{k}\cdot\mathbf{x}}\ , \tag{4.8}$$

where $R_\pm(\mathbf{k})$ are eigenvectors of the helicity operator $\mathbf{k}\cdot\mathbf{\Sigma}$ such that $\mathbf{k}\cdot\mathbf{\Sigma}R_\pm(\mathbf{k}) = \pm 1$ and $\gamma^0 R_\pm(\mathbf{k}) = +1$. The time dependence of the eigenspinor is contained entirely in the scalar mode function $\chi_k(t)$. Substituting this ansatz into equation (4.6) leads to the mode equation

$$\ddot{\chi}_k + 4\frac{\dot{a}}{a}\dot{\chi}_k + \left[ \frac{k^2}{a^2} + M_{\text{eff}}^2 - i\frac{(a\, M_{\text{eff}})^{\cdot}}{a} + \frac{9}{4}\left(\frac{\dot{a}}{a}\right)^2 + \frac{3}{2}\frac{\ddot{a}}{a} \right] \chi_k = 0\ , \tag{4.9}$$

where $k = |\mathbf{k}|$ is the comoving momentum of the fermion mode and the effective mass of the fermions is

$$M_{\text{eff}} \equiv (m_\psi + h\phi(t))\ . \tag{4.10}$$

The damping term in this equation may be removed by defining a new mode function $X_k(t) = a^2 \chi_k(t)$. The mode equation becomes

$$\ddot{X}_k + \left[ \frac{k^2}{a^2} + M_{\text{eff}}^2 - i\frac{(a\, M_{\text{eff}})^{\cdot}}{a} + \Xi(a) \right] X_k = 0\ , \tag{4.11}$$

where $\Xi(a) \equiv [\frac{1}{4}\left(\frac{\dot{a}}{a}\right)^2 - \frac{1}{2}\left(\frac{\ddot{a}}{a}\right)]$. When $a \propto t^n$ such as in a matter or radiation dominated universe, $\Xi(a) \sim t^{-2}$ and can be neglected soon after inflation. We will make this approximation here, but notice that this does not eliminate the time dependence of the coefficients in (4.11).

It is useful to have the explicit expressions for the eigenspinors when one calculates the expectation value of the Hamiltonian for the fermions. For reference, we will give them here: using the mode equation and ansatz, one finds

$$\mathbf{u}_{k,\pm}(t) = a^{-1}\left[-i\dot{X}_k - i\frac{1}{2}\left(\frac{\dot{a}}{a}\right)X_k + (\gamma\cdot\mathbf{k} - M_{\rm eff})X_k\right]R_\pm(\mathbf{k}) \ . \tag{4.12}$$

Taking the charge conjugate of $\mathbf{u}_{k,\pm}$, one finds

$$\mathbf{v}_{k,\pm}(t) = a^{-1}\left[i\dot{X}_k^* + i\frac{1}{2}\left(\frac{\dot{a}}{a}\right)X_k^* - (\gamma\cdot\mathbf{k} + M_{\rm eff})X_k^*\right]\bar{R}_\pm(\mathbf{k}) \ , \tag{4.13}$$

where $\bar{R}_\pm(\mathbf{k}) \equiv -i\gamma^2 R_\pm^*(\mathbf{k})$ is an eigenvector of helicity such that $\mathbf{k}\cdot\mathbf{\Sigma}\bar{R}_\pm(\mathbf{k}) = \pm 1$ and $\gamma^0\bar{R}_\pm(\mathbf{k}) = -1$.

### 4.1.2 Interpretation of the mode functions $X_k$.

The energy-momentum tensor is obtained from the ($\psi$ and $\bar{\psi}$ symmetrized) matter action by variation with respect to the vierbein

$$T^{\mu\nu} = \frac{i}{2}g^{\mu\alpha}g^{\nu\beta}\left[\bar{\psi}\bar{\gamma}_{(\alpha}\overrightarrow{D}_{\beta)}\,\psi - \bar{\psi}\,\overleftarrow{D}_{(\alpha}\,\bar{\gamma}_{\beta)}\psi\right] \ . \tag{4.14}$$

The Hamiltonian is thus ($\mathbf{x}$ is a comoving coordinate)

$$\mathbf{H}_D = \int d^3x\left[i\hat{\psi}^\dagger\partial_t\hat{\psi}\right] \ . \tag{4.15}$$

In general, if this Hamiltonian is diagonal in the annihilation and creation operators $\hat{a}_{k,s}$, $\hat{a}^\dagger_{k,s}$ and $\hat{b}_{k,s}$ , $\hat{b}^\dagger_{k,s}$ at $t = 0$, it will not be for later times. As before, this is the signature of particle creation due to the time dependent background. In order to determine the number of particles produced, we perform a Bogliubov transformation on the creation and annihilation operators so as to diagonalize the Hamiltonian at time $t$. The result of this procedure is that the expectation value of the Hamiltonian density in the "in" state may be written, at any time:

$$\rho_\psi(t) = \langle\mathcal{H}_D\rangle = \frac{2}{\pi^2}\int dk\,k^2\,\Omega_k\,\frac{n_k(t)}{a^3} \ , \tag{4.16}$$

where $n_k$ is the *comoving* number density of fermions with momentum $k$ and we have defined the effective frequency

$$\Omega_k = \sqrt{\frac{k^2}{a^2} + M_{\rm eff}^2} \tag{4.17}$$

is a useful definition. A factor of 4 for the degeneracy of the Dirac fermion (particle and anti-particle, spin up and down) has been included in (4.16).

$\rho_\psi$ in (4.16) is the energy density of produced fermions. If no particle production is occurring, we expect $n_k$ to be conserved. Moreover, when no particle production occurs, and if the fermions are relativistic, we expect their energy density to red-shift like that of radiation: $\rho_{\rm rad} \sim a^{-4}$. Similarly, if they are non-relativistic, their energy density will red-shift like pressureless matter: $\rho_{\rm rad} \sim a^{-3}$. In general, particle production will occur and $n_k$ will be time dependent. Using the operator expansion (4.7) and the expressions for the eigenspinors (4.12) and (4.13), we can write an explicit expression for the comoving number density of created fermions per spin state in terms of the mode functions $X_k(t)$. The result is

$$n_k(t) = a\left(\frac{\Omega_k - M_{\rm eff}}{2\Omega_k}\right)\left[|\dot{X}_k|^2 + \Omega_k^2|X_k|^2 - 2\Omega_k Im(X_k\dot{X}_k^*)\right] , \tag{4.18}$$

This result can be understood in a manner similar to the bosonic equivalent (2.24). As in the conformal case, we can look for adiabatic (aka WKB or semi-classical) approximations to the mode equation (4.11). They take the form

$$X_k(t) = \alpha_k N_+ \, e^{-i\int_0^t dt' \, \Omega_k(t')} + \beta_k N_- \, e^{+i\int_0^t dt' \, \Omega_k(t')} , \tag{4.19}$$

where $N_\pm = (2\Omega_k(\Omega_k \mp M_{\rm eff}))^{-1/2}$ and the coefficients $\alpha_k$ and $\beta_k$ correspond to the coefficients of the Bogliubov transformation. Our expression for the particle number is exactly the square of Bogliubov's "beta" coefficient: $n_k(t) = |\beta_k|^2$, just as in the bosonic case. An added benefit of the adiabatic expansion is that it tells us how to normalize our mode functions for an initial "positive frequency vacuum" state: the initial vacuum should contain no particles so that $\alpha_0 = 1$ , $\beta_0 = 0$. Thus, we chose $X_k(t \to 0^+) = N_+ e^{-i\Omega_k t}$ to insure $n_k(0) = 0$. Substituting this back into the adiabatic approximation confirms that $N_+ = (2\Omega_k(\Omega_k - h\varphi))^{-1/2}$ there, as expected. It also follows from the adiabatic approximation that whenever (4.19) is valid with constant coefficients, $n_k$ will be conserved.

## 4.2 Fermionic Preheating without Expansion of the Universe

It is convenient to begin the investigation of fermionic preheating due to an oscillating scalar field with potential $\frac{1}{2}m_\phi^2\phi^2$ with a simplified setting neglecting the expansion of the universe. This setting may have not only methodological advantages. Indeed, whenever the frequency of $\phi$ oscillations is much greater than the rate of cosmic expansion $H$, it is sensible to neglect the time dependence of the scale factor in solving the mode equation (4.11). This can be the case, for example, when spontaneous symmetry breaking occurs rapidly leaving the $\phi$-field oscillating about a new minimum where the effective mass $m_\phi$ happens to be much larger than the Hubble parameter at the time of the transition. One such example is hybrid inflation scenarios which end with TeV scale energy densities. We have already seen that this approximation is exact for the conformal theory of chapter 3.

If we make the replacement $a = 1$ in all the formulas of section 4.1, all the effects of expansion will be removed. Background oscillations take the form of harmonic oscillations $\phi(t) = \phi_0 f(t)$ with $f(t) = \cos(m_\phi t)$ and $\phi_0$ the time independent amplitude. It is convenient to define a new, dimensionless time variable $\tau \equiv m_\phi t$. With this change of variables, the mode equation (4.11) may be written

$$X_k'' + \left[\kappa^2 + (\tilde{m} + \sqrt{q}f)^2 - i\sqrt{q}f'\right] X_k = 0 \ , \tag{4.20}$$

where we have introduced the dimensionless momentum $\kappa^2 \equiv \frac{k^2}{m_\phi^2}$, the dimensionless fermion mass $\tilde{m} \equiv \frac{m_\psi}{m_\phi}$, and the resonance parameter $q \equiv \frac{h^2\phi_0^2}{m_\phi^2}$. These three parameters completely determine the strength of the effect. This is the generalization of the master equation (3.19) for fermions in the conformal theory. In fact, this form of the mode equation is valid not only for harmonic background oscillations, but for generic $\phi$ oscillations in a general potential, when expansion can be neglected. For a general potential, we identify $m_\phi$ with the frequency of oscillation, $\phi_o$ with its amplitude, and $f(\tau)$ with the periodic background oscillations normalized to unit amplitude. Note that the frequency will be amplitude-dependent for a general, non-quadratic potential. In the $\frac{1}{4}\lambda\phi^4$ case, we have simply $m_\phi \to \sqrt{\lambda}\phi_0$. Note that, when there is no expansion, the distinction between $\phi$ and $\varphi$ or $t$ and $\eta$ disappears.

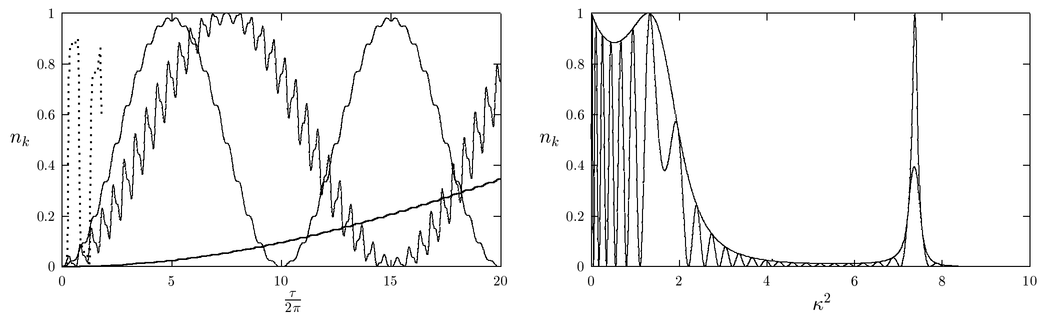


Figure 4.1: The left panel shows the occupation number $n_k$ of fermions in $\frac{1}{2}m_\phi^2\phi^2$ theory (neglecting expansion) as a function of time measured in inflaton oscillations $\frac{\tau}{2\pi}$. The values of $(q;\kappa)$ are: dotted curve $\rightarrow (1.0; 0.05)$, bold curve $\rightarrow (10^{-4}; 0.5)$, smooth sine-like curve $\rightarrow (10^{-2}; 0.5)$, and jagged sine-like curve $\rightarrow (1; 1.3)$. The right panel is for the same model. It shows the occupation number, $n_k$, of fermions as a function of $\kappa^2$ after 10 inflaton oscillations for resonance parameter $q = 10$. Also shown is the envelope function $F_k$ defined by equation (3.25).

### 4.2.1 Parametric Excitation of Fermions

If individual inflatons at rest are decaying into light fermions in a process $\phi \rightarrow \bar{\psi}\psi$, perturbative calculations give the rate of decay $\Gamma_{\phi\rightarrow\psi\psi} \simeq \frac{h^2 m_\phi}{8\pi}$ and the spectrum of created fermions is sharply peaked around $m_\phi/2$ with the a width $\Gamma^{-1}_{\phi\rightarrow\psi\psi}$. In figure 4.1, however, we plot the time-dependence and spectrum of occupation number for fermions created from the coherently oscillating inflaton field, as follows from the numerical solution of the master equation (4.20) and (4.18). The spectrum and time evolution are drastically different from what is expected from the perturbative calculations, just as we found in the last chapter.

The analytic results we found in the last chapter are valid for this theory as well, as expansion has been neglected. In particular, we can find envelope functions, $F_k$, for the spectrum of created fermions. We can also find the period of the occupation number's oscillation. We calculated $X_k^{(1)}(T)$ numerically for $\frac{1}{2}m^2\phi^2$-theory and constructed the envelope functions $F_k$ plotted in the left panel of figure 4.2. The right panel of figure 4.1 shows how the fermionic resonance bands are filled after 10 background oscillations. The function $\nu_k$ gives us the time scale for fermion excitation. The right panel of figure 4.2 shows the period of modulation $\frac{\pi}{\nu_k}$ as a function of $k$. This function is peaked where $F_k$ is peaked, i.e. the peaks of the resonance curve are the last to fill.

Just as in the conformal case, we can now find the energy density of created fermions. Again, the width of the bands goes like $q^{1/4}$, just as in the conformal

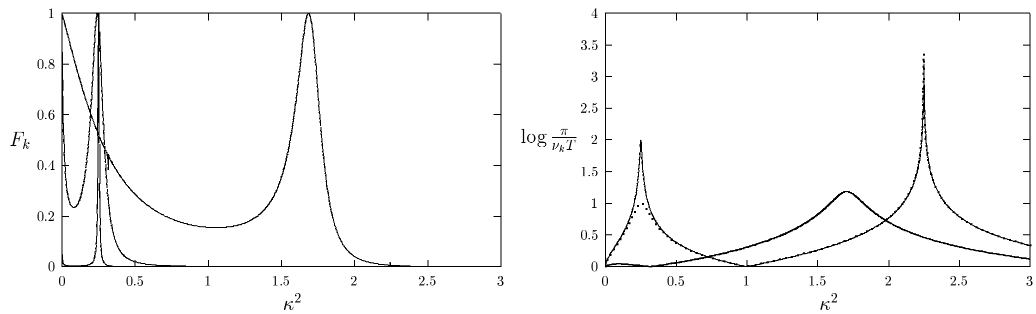


Figure 4.2: The left panel shows the envelope function $F_k$ for the amplitude of occupation number oscillations in $m_\phi^2\phi^2$-theory. Values for $q = 10^{-4}, 10^{-2}$ and 1 are shown, from narrowest to broadest, respectively. The right panel shows the log of the modulation period (in units of the inflaton period $T$) in $m_\phi^2\phi^2$-theory, where $q = 1$ corresponds to the middle curve, $q = 10^{-2}$ corresponds to the dotted curve, and $q = 10^{-4}$ corresponds to the low, solid.

case. We will not develop this here as we are most interested in the case with expansion.

## 4.3 Method of Successive Parabolic Scatterings for Fermions

It turns out that for large values of the parameter $q$ we can significantly advance calculations of $n_k(t)$ beyond the results of the last chapter. One can expect that $q = \frac{h^2\phi_0^2}{m_\phi^2}$ may be much greater that one. Indeed, in the context of chaotic inflation with the potential $V(\phi) = \frac{1}{2}m_\phi^2\phi^2$, it follows from the theory of cosmological perturbations that $\frac{\phi_0^2}{m_\phi^2} \simeq 10^{12}$. On the other hand, one should certainly admit that the Yukawa coupling can be $h \gg 10^{-6}$, which would result in $q \gg 1$.

In this section, we will generalize for fermions the method of parabolic scatterings introduced for the bosonic resonance in reference [15]. The method is based on the observation that, for $q \gg 1$, change of the particle number occurs only during a short time interval near the zeros of the effective mass of the particles. This occurs because equation (4.18) for the number of particles in terms of the mode functions is an adiabatic invariant of the mode equation.

For large $q$, the adiabaticity condition $\Omega_k' < \Omega_k^2$ is violated only near the times $\tau_*$ when the effective mass vanishes. This leads to a step-like evolution in the number

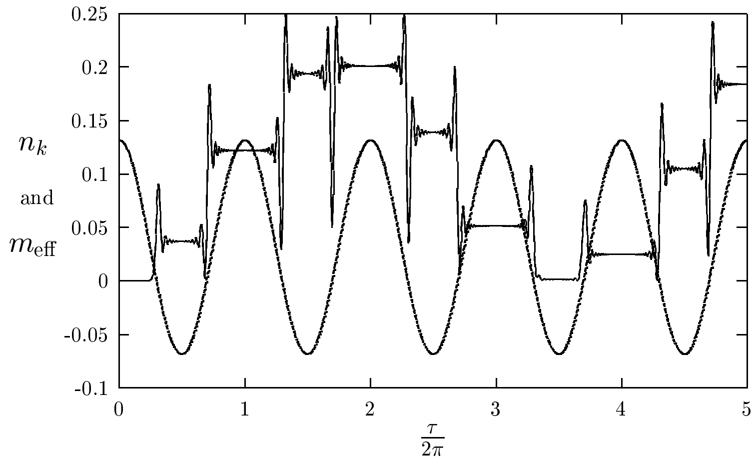


Figure 4.3: $n_k$ and $M_{\text{eff}}(\tau) = m_\psi + h\phi(\tau)$ for $q = 10^3$, $\kappa = \sqrt{q} \approx 31.6$, and $m_\psi = 10\, m_\phi$.

of fermions as illustrated in figure 4.3 which shows the evolution of $n_k(\tau)$ and $M_{\text{eff}}(\tau) = m_\psi + h\phi(\tau)$ Near the times $\tau_*$, we may approximate the effective mass in equation (4.20) by $(\tilde{m} + \sqrt{q} f) = \frac{1}{m_\phi}(m_\psi + h\phi(\tau)) \approx \frac{h}{m_\phi}\phi'(\tau_*)\cdot(\tau - \tau_*) + O((\tau-\tau_*)^2)$. We may also write this as

$$(\tilde{m} + \sqrt{q} f) \approx \sqrt{q} f'(\tau_*)(\tau - \tau_*) = \pm\sqrt{q - \tilde{m}^2} \cdot (\tau - \tau_*) \ , \qquad (4.21)$$

where the sign on the left hand side depends on whether $f(\tau)$ is increasing (+) or decreasing (−) at $\tau_*$. Thus, in the neighborhood of $\tau_*$, the mode equation becomes

$$X_k'' + \left[\kappa^2 + (q - \tilde{m}^2)\cdot(\tau - \tau_*)^2 - i\,\text{sgn}(f'(\tau_*)) \cdot \sqrt{q - \tilde{m}^2}\right] X_k = 0 \ , \qquad (4.22)$$

which is a Schrödinger-like equation for scattering off a negative parabolic potential centered at $\tau_*$ and with a *complex* effective frequency. In the bosonic case [15], the effective frequency is real. Here, the absorptive character of this term will ensure that the Pauli principle is respected.

The method of parabolic scattering uses the exact solution of equation (4.22) to provide a connection formula between the adiabatic approximations of the full mode equation on either side of $\tau_*$. Suppose the $j$-th zero of $M_{\text{eff}}$ occurs at time $\tau_j$. For times between $\tau_{j-1} < \tau < \tau_j$, the general solution of the mode equation (4.20) takes the adiabatic form

$$X_k^j(\tau) = \alpha_k^j N_+ \, e^{-i\int_0^\tau d\tau\,\Omega_k(\tau)} + \beta_k^j N_- \, e^{+i\int_0^\tau d\tau\,\Omega_k(\tau)} \;, \qquad (4.23)$$

where the coefficients $\alpha_k^j$ and $\beta_k^j$ are constant for $\tau_{j-1} < \tau < \tau_j$. After the scattering at $\tau_j$, $X_k(t)$, within the interval $\tau_j < \tau < \tau_{j+1}$, again has the adiabatic form

$$X_k^{j+1}(\tau) = \alpha_k^{j+1} N_+ \, e^{-i\int_0^\tau d\tau\,\Omega_k(\tau)} + \beta_k^{j+1} N_- \, e^{+i\int_0^\tau d\tau\,\Omega_k(\tau)} \;, \qquad (4.24)$$

with new coefficients $\alpha_k^{j+1}$ and $\beta_k^{j+1}$ that are constant for $\tau_j < \tau < \tau_{j+1}$. At $\tau = 0$, our vacuum positive frequency condition requires $\alpha_k^1 = 1$ and $\beta_k^1 = 0$. Particle creation occurs when, after scattering at the times $\tau_j$, the initial positive frequency wave acquires a negative frequency part. The number density of produced particles with momentum $k$ is $n_k^{j+1} = |\beta_k^{j+1}|^2$ for times $\tau_j < \tau < \tau_{j+1}$. Furthermore, normalization requires $|\alpha_k^j|^2 + |\beta_k^j|^2 = 1$ for all $j$.

The important observation is that the outgoing amplitudes $(\alpha_k^{j+1},\ \beta_k^{j+1})$ can be expressed through the incoming amplitudes $(\alpha_k^j,\ \beta_k^j)$ by means of a scattering matrix:

$$\begin{pmatrix} \alpha_k^{j+1} e^{-i\theta_k^j} \\ \beta_k^{j+1} e^{+i\theta_k^j} \end{pmatrix} = \begin{pmatrix} \sqrt{1-\Delta_k^2}\; e^{+i\varphi_k} & i\Delta_k \\ i\Delta_k & \sqrt{1-\Delta_k^2}\; e^{-i\varphi_k} \end{pmatrix} \begin{pmatrix} \alpha_k^j e^{-i\theta_k^j} \\ \beta_k^j e^{+i\theta_k^j} \end{pmatrix} \;. \qquad (4.25)$$

Here $\theta_k^j = \int\limits_0^{\tau_j} d\tau\,\Omega_k(\tau)$ is the phase accumulated by the moment $\tau_j$. The form of the scattering matrix follows from the symmetries of equation (4.22) and the (conserved) normalization of the $\alpha_k$ and $\beta_k$ coefficients. In particular, the scattering matrix is symmetric and unimodular. It therefore depends on only two, real, k-dependent functions: $\Delta_k$ and $\varphi_k$. We will determine $\Delta_k$ below.

If we let $x = (q - \tilde{m}^2)^{1/4}\tau$, equation (4.22) may be written

$$\frac{d^2 X_k}{dx^2} + \left[\Lambda_k^2 - i(-1)^j + x^2\right] X_k = 0 \;, \qquad (4.26)$$

where the parameter

$$\Lambda_k^2 \equiv \frac{\kappa^2}{|\sqrt{q}\cdot f'(\tau_*)|} = \frac{\kappa^2}{\sqrt{q-\tilde{m}^2}} \;. \qquad (4.27)$$

A general analytic solution of equation (4.26) is a linear combination of the parabolic cylinder functions $W\left(-\frac{(\Lambda_k^2 - i(-1)^j)}{2}; \pm\sqrt{2}x\right)$. The scattering functions $\Delta_k$ and $\varphi_k$ can be found from the asymptotic forms of these analytic solutions. In particular,

$$\Delta_k = (-1)^j e^{-\frac{\pi}{2}\Lambda_k^2} \, . \tag{4.28}$$

The momentum dependent phase $\varphi_k$ is similar to that derived in [15] for the bosonic case. As we will not need this phase, we don't write its form here. Substituting (4.28) into (4.25), we can determine the change induced in the $\alpha_k$ and $\beta_k$ coefficients by a single parabolic scattering in terms of the parameters of the parabolic potential and the phase $\theta_k^j$. Specifically, we find

$$\begin{pmatrix} \alpha_k^{j+1} \\ \beta_k^{j+1} \end{pmatrix} = \begin{pmatrix} \sqrt{1-e^{-\pi\Lambda_k^2}}e^{i\varphi_k} & -(-1)^j e^{-\frac{\pi}{2}\Lambda_k^2+2i\theta_k^j} \\ (-1)^j e^{-\frac{\pi}{2}\Lambda_k^2-2i\theta_k^j} & \sqrt{1-e^{-\pi\Lambda_k^2}}e^{-i\varphi_k} \end{pmatrix} \begin{pmatrix} \alpha_k^j \\ \beta_k^j \end{pmatrix} \, . \tag{4.29}$$

It is now a simple matter to find the change in particle number after one scattering. From the normalization of $\alpha_k$ and $\beta_k$ we have the relation

$$\begin{pmatrix} \alpha^{*j+1}_k & \beta^{*j+1}_k \end{pmatrix} \begin{pmatrix} 1 & 0 \\ 0 & -1 \end{pmatrix} \begin{pmatrix} \alpha_k^{j+1} \\ \beta_k^{j+1} \end{pmatrix} = |\alpha_k|^2 - |\beta_k|^2 = 1 - 2n_k^{j+1} \, , \tag{4.30}$$

which, when applied to equation (4.29), gives the desired result

$$\begin{aligned} n_k^{j+1} &= e^{-\pi\Lambda_k^2} + \left(1 - 2e^{-\pi\Lambda_k^2}\right) n_k^j \\ &+ 2(-1)^j e^{-\frac{\pi}{2}\Lambda_k^2}\sqrt{1-e^{-\pi\Lambda_k^2}}\sqrt{n_k^j(1-n_k^j)}\sin\theta_{tot}^j \, , \end{aligned} \tag{4.31}$$

where the phase $\theta_{tot}^j = 2\theta_k^j - \varphi_k + \arg\beta_k^j - \arg\alpha_k^j$. Let us discuss this formula, which is the main result of our paper. If fermions are light, $m_\psi \ll m_\phi$, their occupation number is changing with time only when the background field crosses zero. Without expansion of the universe, the phases $\theta$ accumulated between successive zeros are equal. In this case one can try to proceed to find the solution of the matrix equation (4.25), as was done for bosons [15]. However, for bosons that was needed to find the stability/instability bands, which is not so interesting for fermions. In the case of massive fermions, the time intervals between successive zeros of $M_{\text{eff}}$ are not equal, and the problem of finding a matrix solution of equation (4.25) becomes even more complicated. However, in the most interesting case of an expanding universe, the phases between successive zeros of $M_{\text{eff}}$ will become random (see [15] for details). Then we can just treat $\theta_{tot}$ as a random phase and use formula (4.31) as it is.

## 4.4 Parametric Excitation of Fermions with Expansion of the Universe

To address the problem of fermionic preheating after $\frac{1}{2}m_\phi^2\phi^2$ chaotic inflation, we must now deal with the full mode equation (4.11), which no longer has a periodic time dependence in the complex frequency. Nevertheless, it is still convenient to work with the form (4.20) in the time variable $\tau = m_\phi t$ where the parameter $q$ is now understood to be time dependent:

$$X_k'' + \left[\frac{\kappa^2}{a^2} + \frac{M_{\text{eff}}^2}{m_\phi^2} - i\frac{(a\,M_{\text{eff}})'}{am_\phi} + \frac{\Delta(a)}{m_\phi^2}\right] X_k = 0 \ , \tag{4.32}$$

where $'$ stands for the derivative with respect to $\tau$ and $\kappa$ is a comoving momentum scaled in units of $m_\phi$. Often, another form of the fermionic mode equation (4.9), written in terms of conformal time $\eta = \int dt/a$ and mode function $Y_k = a^{-3/2}\chi_k$, is used

$$\partial_\eta^2 Y_k + \left[k^2 + M_{\text{eff}}^2 - i\partial_\eta(a\,M_{\text{eff}})\right] Y_k = 0 \ . \tag{4.33}$$

As in the last chapter, this form is useful, for instance, in the conformal theory $V(\phi) = \frac{1}{4}\lambda\phi^4$ when the problem can be reduced to a problem in Minkowski spacetime [12]. In this case, background field oscillations are periodic with respect to the conformal time, $\eta$. However, in the case of a quadratic inflaton potential, the background field oscillates with a constant period in physical time $t$ (or $\tau$). Thus, the use of the mode equation (4.32) is preferable. In this equation, $M_{\text{eff}} = (m_\psi + \sqrt{q} f(\tau))$ but the parameter $q$ is now understood to be time dependent. Specifically, we have $q(\tau) \equiv \frac{h^2\Phi^2(\tau)}{m_\phi^2}$ and the scaled physical momentum $p \equiv \frac{\kappa}{a} \equiv \frac{1}{a}\frac{k}{m_\phi}$ Here, $\Phi(\tau)$ is the time dependent amplitude of inflaton oscillations. As is well known (c.f. [15]), oscillations of $\phi$ in this model quickly approach the asymptotic solution $\phi(\tau) = \Phi(\tau)\,\cos(\tau)$, $\Phi(\tau) \approx \frac{\phi_0}{a^{3/2}} \sim \frac{M_{\text{pl}}}{\sqrt{3\pi}(1+\tau)}$ where time is measured from the start of inflaton oscillations, $\phi_0 \approx \frac{M_{\text{pl}}}{\sqrt{3\pi}}$, and the scale factor averaged over several oscillations behaves as in a matter dominated universe: $a(\tau) = (1+\tau)^{2/3}$.

### 4.4.1 Stochastic Parametric Excitation of Fermions

Let us first consider the case of light fermions with a large initial resonance parameter: $h\phi_0 \gg m_\phi \gg m_\psi$. The left panel of figure (4.4) shows a numerical solution of equation (4.32) in the absence of expansion with a resonance parameter $q = 10^6$. As expected for such a large $q$ parameter, we see a step-like change in occupation number with periodic modulation. In the right panel of figure (4.4), we show a

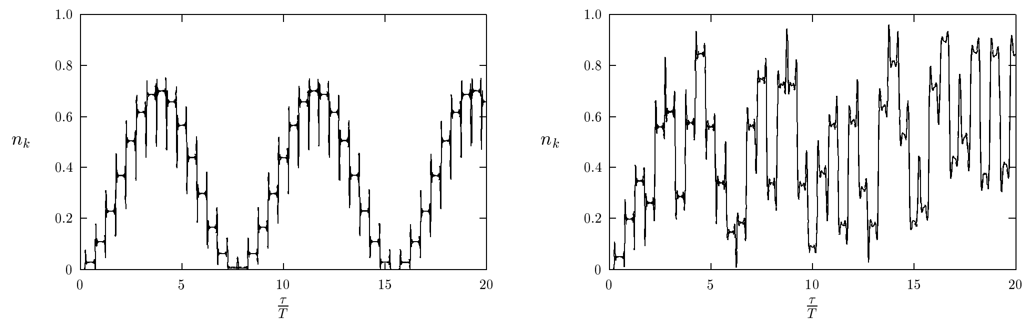


Figure 4.4: The left panel shows the occupation number $n_k$ of fermions in $m_\phi^2\phi^2$-theory in the broad resonance case, $q \gg 1$, without expansion. Here $q = 10^6$ and the particular mode is $\kappa^2 \approx \sqrt{q}$. In the right panel we show the occupation number $n_k$ of fermions in $m_\phi^2\phi^2$-theory with expansion taken into account. Here, the *initial* resonance parameter is $q_0 = 10^6$ and the comoving mode is $\kappa^2 \approx \sqrt{q}$.

numerical solution to equation (4.32) in the presence of expansion with the *initial* parameter $q_0 = 10^6$. Here, the *comoving* number density of particles (4.18) is plotted. We see that, as for the non-expanding case, the evolution between zeros of the effective mass (or, equivalently in this approximation, the inflaton field), $M_{\text{eff}} \approx m_\phi \sqrt{q(\tau)}\cos(\tau)$, is adiabatic. We can thus apply the results of the last section, and in particular, the analytic formula (4.31), mutatis mutandis. The Pauli principle is obviously still obeyed and the typical step in particle number is still suppressed by a factor $e^{-\pi\Lambda_k^2}$, which is now time dependent. The most important qualitative change is that the accumulated phase $\theta_{\text{tot}}$ is now uncorrelated between successive zeros of the effective mass (inflaton field). This occurs because the effective frequency $\Omega_k = \sqrt{p^2 + q^2(\tau)\cos^2\tau}$ is no longer periodic and the accumulated phase $\theta = \int_j^{j+1}\Omega_k \approx \frac{2h\Phi(\tau)}{m} + O(k^2)$ changes substantially in magnitude within one inflaton oscillation, $\delta\theta_k \simeq \frac{\sqrt{q}}{2N_s^2}$, after the $N_s$-th oscillation [15]. The result is that the $\sin(\theta_{\text{tot}})$ term in (4.31) becomes a random variable. As is readily apparent in figure (4.4), this destroys the periodic modulation of $n_k$ and the parametric excitation of fermions becomes stochastic, as anticipated in [12] and reported in [16, 14].

Once the periodic modulation of $n_k$ is destroyed, the construction of the last chapter in terms of envelope function and period is no longer valid: the occupation number cannot be characterized by an amplitude and period. In fact, the spectrum of created particles is even simpler. Stochastic excitation allows a given comoving mode $\kappa$ to obtain any amplitude in the range $0 \leq n_k \leq 1$ if there are a sufficient number of parabolic scatterings, $N_s$. This gives us the picture of stochastically

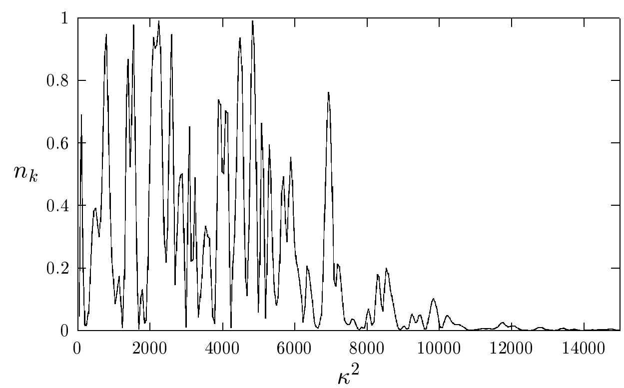


Figure 4.5: The comoving occupation number of fermions in $m_\phi^2\phi^2$-inflation after 20 inflaton oscillations for initial resonance parameter $q_o = 10^6$ and $m_\psi = 0.1\, m_\phi$. Expansion destroys the details of the resonance band and leads to a Fermi-sphere of width $q^{1/4}$ which grows like $a^{1/4}$ while $q(\tau) > 1$.

filling a sphere in momentum space. One might call this a non-degenerate Fermi-sphere. Numerical calculations confirm this picture, see figure 4.5. Let us find the radius, $\kappa_s$, of this sphere. A comoving mode will be excited if $\Lambda_k^2(\tau) \leq \frac{1}{\pi}$. Since $\Lambda_k^2(\tau) = \frac{\kappa^2}{a^2\sqrt{q(\tau)}}$, we have

$$\frac{\kappa_s^2}{a^2\sqrt{q(\tau)}} = \frac{\kappa_s^2}{\sqrt{a\, q_0}} \leq \frac{1}{\pi}\ . \tag{4.34}$$

Therefore, for light fermions, the comoving radius of excited modes increases with time as $\kappa_s \sim a^{1/4}$ and scales as $\kappa_s \sim q_0^{1/4} a^{1/4}$. Due to the expansion, the amplitude $\Phi(\tau)$, and thus the parameter $q(\tau)$, decreases. Once $q(\tau)$ is of order unity, the excitation is no longer strong, and red-shifting of fermion modes will be fast enough to prevent parametric excitation. By this moment, the Fermi-sphere will have quit expanding. Eventually, fermions will be produced in the perturbative regime; but, if the fermionic mass is non-zero, the perturbative decay can only occur for $2m_\psi < m_\phi$.

### 4.4.2 Analytic Results for the Production of Supermassive Fermions

One of the most significant differences between bosonic and fermionic parametric amplification is the possibility to create superheavy fermions from much lighter inflatons, if the inflatons are oscillating coherently. As we have seen, for large $q$, massive fermions are created not when the inflaton field itself crosses zero, but when the combination $M_{\rm eff} = m_\psi + h\phi(\tau)$ crosses zero. This is because, at those instances, even very heavy fermions are effectively massless; their bare mass is "compensated" by the large value $h\phi$, if $\phi$ can have such a large amplitude. This is exactly the case when $\phi$ is the inflaton field. For example, in the chaotic inflationary scenario, the amplitude of its oscillations immediately after inflation can be as large as $0.1M_p$.

In this case, we again have a situation where the mode function, now for heavy fermions, has the adiabatic form between zeros of $M_{\rm eff}$. It can be described with parabolic scattering around these instants. Therefore, our general formula (4.31) works for superheavy fermions as well. The only modification is that the phase between successive scatterings will be defined by the integral over the time intervals between them. In formula (4.31), the parameter $\Lambda_k(\tau)$ will be

$$\Lambda_k^2(\tau) = \frac{\kappa^2}{a^2\sqrt{\frac{q_0}{a^3} - \tilde{m}^2}} \tag{4.35}$$

In the case of massive fermions, the criteria for excitation will be

$$\frac{\kappa_s^2}{a^2\sqrt{\frac{q_0}{a^3} - \tilde{m}^2}} \leq \frac{1}{\pi}\,, \tag{4.36}$$

instead of (4.34). For large $q_0$, the fermion mass term $\tilde{m}^2$ will be negligible at the start of background oscillations. Thus, as in the last section, we expect a Fermi-sphere to fill with a radius $\kappa_s = q_0^{1/4}\, a^{1/4}$. It is easy to see from the denominator in (4.35), that as the scale factor increases and $q$ drops, $\kappa_s^2$ will reach a maximum, $\kappa_m$. This maximum occurs when the scale factor is $a_m = \left(\frac{q_0}{4\tilde{m}^2}\right)^{1/3}$. This gives $\kappa_m^2 = \frac{\sqrt{3}}{\pi}\left(\frac{q_0}{4\sqrt{\tilde{m}}}\right)^{2/3}$. Notice that $\kappa_m$ scales as $q_0^{1/3}$.

It is tempting to say that $\kappa_m$ will be the final width of the band in comoving momentum space. Numerical solution shows, however, that this is not the case. Particle creation continues to occur for $\kappa > \kappa_m$ because there are a number of background oscillations for which $q(\tau) \gg 1$ remaining after the time corresponding to $a = a_m$. Let, $a_f$, denote the scale factor when the denominator in (4.35) goes to zero. It is easy to show that $a_f = 4^{1/3} a_m$. Now let the number of inflaton oscillations that occur between $a = 1$ and $a = a_m$ be $N_m$. Then, one can also show that the number of oscillations that occur between $a_m$ and $a_f$ will be approximately $4N_m$. In this time, even modes suppressed exponentially as $e^{-\pi\Lambda_k}$ can achieve significant occupation numbers due to the pre-exponential factor which accumulates

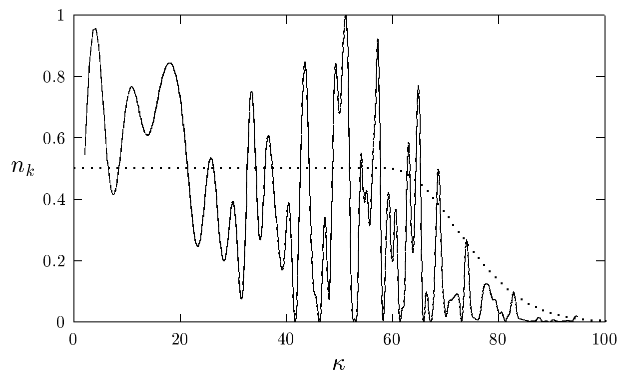


Figure 4.6: Final spectrum of heavy fermions with mass $m_\psi = 10\, m_\phi$ when $q_0 = 10^6$. Also shown is the analytic estimate (4.38).

as $N$. For $n_k \ll 1$, the general result (4.31) tells us that the change in particle number after each kick is given approximately by just the first, spontaneous emission, term. That is, for large momentum, $\delta n_k^j = n_k^{j+1} - n_k^j \approx +e^{-\pi\Lambda_k} \ll 1$ for each kick. Thus, we can estimate the range of appreciable particle creation by summing the contribution from all the kicks between $a_m$ and $a_f$ and requiring that this be $O(1)$:

$$\sum_j \delta n_k^j \approx 4N_m \exp\left(-\pi \frac{\kappa^2}{\kappa_m^2}\right) \sim O(1)\ , \tag{4.37}$$

where, in the second step, we have approximated the denominator of $\Lambda_k$ by its maximum value: $\kappa_m^2$. Note that, contrary to the light fermion case, there is no perturbative end of the particle creation process. The excitation of superheavy fermions is abruptly terminated near $a_f$ when $\frac{q_0}{a^3} - \tilde{m}^2$ approaches zero.

Using (4.37) with the multiplicative factor and taking the rhs to be exactly 1, we estimate that the spectrum of created supermassive particles after the creation process terminates is given by the formula

$$\langle n_k \rangle = \begin{cases} \frac{1}{2} & ,\ \text{for } \kappa < \kappa_m \\ \frac{1}{2} \exp\left(-\pi \frac{(\kappa - \gamma\kappa_m)^2}{\kappa_m^2}\right) & ,\ \text{for } \kappa \geq \kappa_m \end{cases} \tag{4.38}$$

where $2\gamma^2 = \ln\left(\frac{q_0}{\pi^2 \tilde{m}^2}\right)$. This formula is valid for $N_m$ greater than a few. In figure 4.6 we plot the numerically calculated final spectrum of supermassive fermions for $q_0 = 10^6$ and $m_\psi = 10\, m_\phi$ and the analytic formula (4.38), which are in a good agreement. We verified this for several values of $q_0$ and $\tilde{m}$ and found that,

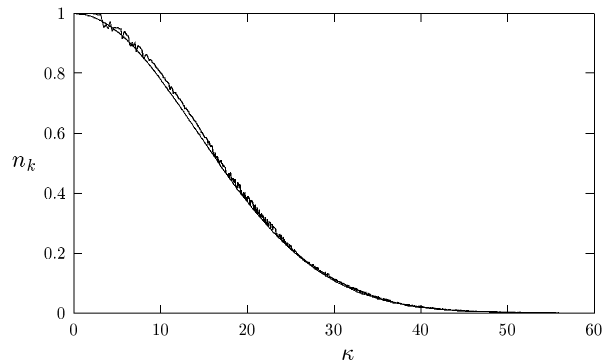


Figure 4.7: The comoving occupation number $n_k$ of fermions after $M_{\text{eff}}$ crosses its first zero for $q = 10^6$ and $m_\psi = 50\,m_\phi$. Also shown is the analytic formula (4.39) which fits perfectly.

as expected, the formula works well as long as $4\tilde{m}^2$ is not too close to $q_0$. This result shows that, for superheavy particles in an expanding universe, the maximum radius of the k-sphere scales with $q_0$ as $\gamma k_m \sim q_0^{1/3}(\ln q_0)^{1/2}$, which, up to the log factor, is in agreement with [17]. However, one should also check that at the moment when the excitation of superheavy fermions terminates, their back reaction $h\langle\bar{\psi}\psi\rangle$ to the dynamics of the inflaton oscillations is still negligible.

### 4.4.3 Fermionic Production from a Single Kick

As we have seen, formula (4.31) can be extended to the case of an expanding universe. Consider the very first term in that formula. This term describes 'spontaneous emission': the creation of fermions by the inflaton field in the fermionic vacuum state. This is the case when the effective mass $M_{\text{eff}}(t)$ crosses zero for the first time. Thus, after a single kick we have

$$n_k = e^{-\pi\Lambda_k^2}\,, \tag{4.39}$$

where $\Lambda_k$ is as in equation (4.35) with the scale factor in the denominator evaluated at the time of the first kick. The occupation number of fermions generated from such a single kick is plotted in figure 4.7. The two curves corresponding to formula (4.39) and to the numerical solution are shown and are practically indistinguishable. One can use this formula to estimate the final occupation number of superheavy fermions when $4\,m_\psi^2$ is not much smaller than $q_0$; that is, when $N_m$

is only $O(1)$ and the cumulative effect of kicks after $a_m$, as described in the last section, is insignificant.

## 4.5 Discussion

In this chapter we developed the non-perturbative theory for fermion production by an oscillating inflaton field. As we have seen, the production of fermions can be characterized as parametric excitation. Even in the simple model of a Yukawa coupling between fermions and a background scalar field in an expanding universe oscillating around the minimum of its quadratic potential, the theory of fermionic parametric excitation is rich and leads to important results. Fermions are created very quickly, within about ten(s) oscillations, in an out-of-equilibrium state. For large values of the resonance parameter $q = \frac{h^2\phi_0^2}{m_\phi^2}$, the occupation number of light fermions ($m_\psi < m_\phi \ll h\phi_0$) changes in a step-like manner at instances $t_j$ when the inflaton amplitude $\phi(t_j)$ passes through zero, $j = 1, 2, 3, \ldots$ . We have developed the method of parabolic scattering for fermions, based closely on a similar approach for the bosonic resonance [15]. It is possible to derive a unified recursive formula, which relates the occupation number of fermions or bosons $n_k^{j+1}$ at the moment $t_{j+1}$ to the earlier value $n_k^j$ :

$$\begin{aligned} n_k^{j+1} &= e^{-\pi\Lambda_k^2} + \left(1 \pm 2e^{-\pi\Lambda_k^2}\right) n_k^j \\ &- 2(-1)^j e^{-\frac{\pi}{2}\Lambda_k^2}\sqrt{1 \pm e^{-\pi\Lambda_k^2}}\sqrt{n_k^j(1 \pm n_k^j)}\,\sin\theta_{tot}^j \ , \end{aligned} \tag{4.40}$$

For bosons, one should use the upper sign and neglect the factor $(-1)^j$ in the third term [15]; while for fermions, one should use the lower sign. For light fermions and bosons $\Lambda_k^2 = \frac{k^2}{\sqrt{q}m_\phi^2}$. For large $q$ the angle $\theta_{tot}^j$ can be treated as a random phase. As a result, formula (4.40) predicts the stochastic character of parametric excitation of both bosons and fermions. In the fermionic case it leads to the conclusion that in the momentum space, fermions chaotically fill a broad sphere of radius $k_s \sim q^{1/4}m_\phi$. This formula clearly shows several interesting features of particle creation. For both bosons and fermions, the first term corresponds to spontaneous emission and leads after the first half inflaton oscillation to the spectrum $n_k = e^{-\pi\Lambda_k}$. For bosons with $n_k \gg 1$, we see that $(n_k^{j+1} - n_k^j) \propto n_k^j$ corresponding to stimulated emission. Finally, for fermions, we find that if $n_k^j = 1$, the next value will always be $n_k^{j+1} = 1 - e^{-\pi\Lambda_k} < 1$ even in the stochastic case. This prevents the occupation number of fermions from exceeding 1 and protects the Pauli principle.

Formula (4.40) can be extended to the case of massive bosons and fermions. However, here important differences emerge. For bosons we have $\Lambda_k^2 = \frac{k^2+m_b^2}{\sqrt{q}m_\phi^2}$, where $m_b$ is the $\chi$-boson mass. This leads to the conclusion that the creation of superheavy, $m_b > q^{1/4}\, m_\phi$, bosons is exponentially suppressed. However, for fermions we have $\Lambda_k^2 = \frac{k^2}{m_\phi\sqrt{q\, m_\phi^2 - m_\psi^2}}$. Therefore, even superheavy fermions with a mass as large as $\sqrt{q}\, m_\phi = h\phi_0$ can be created in abundance from the coherent inflaton oscillations [16, 17]. This occurs because the effective mass of fermions is given by the algebraic combination $m_\psi + h\phi(t)$ and the creation of fermions occurs when this effective mass goes to zero. The method of parabolic scatterings, applied to instances when this happens, leads to both formulae (4.40) with the appropriate $\Lambda_k$. The maximum radius in comoving momentum space is found to scale as $q_0^{1/3}(\ln q_0)^{1/2}$ for massive fermions.

There are situations where a single instance (single kick) of particle creation may lead to interesting effects. An example is the scenario of instant preheating, which is especially important for inflationary models without minima of the inflaton potential [30]. Another example is the interaction of the inflaton with superheavy fermions during the inflationary stage when the combination $m_\psi + h\phi(t)$ can go through zero only once. The generic formula (4.40) embraces the case where bosons and fermions are created by such a single kick as well. One takes $j = 1$, $n_k^1 = 0$, and then $n_k^2 = e^{-\pi\Lambda_k^2}$. Rather than just the parameter $q$, the effect is described by another combination of the coupling constants, $\phi_0$, and $m_\phi$. In this case the effect is defined by the velocity $\dot{\phi}_*$ at the moment of creation $t_*$, which is different for bosons and fermions. For bosons, a single instance of creation gives the spectrum [15, 30]

$$n_k = e^{-\frac{\pi(k^2+m_\chi^2)}{g\dot{\phi}_*}} \tag{4.41}$$

where $t_*$ corresponds to $\phi(t_*) = 0$. For fermions, a single instance of creation gives [58, 14]

$$n_k = e^{-\frac{\pi k^2}{h\dot{\phi}_*}} \tag{4.42}$$

where $\phi(t_*) + m_\psi/h = 0$.

We believe that the theory of fermionic preheating will be an important ingredient of realistic scenarios describing the process of reheating after inflation.

# Chapter 5

# Tachyonic Preheating and Hybrid Inflation

In this chapter we consider p/reheating in theories of inflation that involve more than one field shifted away from its vev. These fields make up the *inflaton sector* of the theory. Inflation in these *hybrid* models ends when the slow-rolling of one field, called the inflaton, triggers spontaneous symmetry breaking (SSB) in another inflaton sector field, which we will call the Higgs [59, 60]. This latter field should not be confused with the Standard Model Higgs, which would be in the matter sector of the theory[1]. As we will see, the increased multiplicity of fields in the inflaton sector means that a wide range of parameters can lead to successful inflation. This is particularly important when one tries to find a supersymmetric model of inflation. The simple power-law chaotic models that we have been using thus far all require field amplitudes larger than $M_p$ during inflation. In supersymmetric theories, we expect strong supergravity corrections in this regime. These corrections typically spoil the flatness of the inflaton's potential. Rather than the slow-roll of the inflaton, hybrid models can use the false vacuum energy of the Higgs field in its symmetric state to support inflation. Thus, while the amplitude of density perturbations created during the slow-roll of the inflaton depends on the Hubble parameter during inflation, the Hubble parameter in hybrid models no longer depends strongly on the form of the slow-roll potential itself. Supersymmetric realizations of inflation exploit this possibility to circumvent, in a natural way, the problem of supergravity corrections to the slow-roll potential.

[1]In supergravity theories there can be an additional sector, the *hidden* sector. In general, the inflaton sector should couple relatively strongly with the matter sector–which contains the Standard Model fields–and may or may not couple strongly to the hidden sector. By definition, hidden sector fields couple only weakly with matter sector fields.

Reheating in hybrid models begins with SSB in the Higgs field. Originally, it was thought that the reheating stage for hybrid models would look similar to that for the power-law models we've considered. SSB would divide the universe into many domains of some characteristic size $l_c$, determined by the details of the SSB process. In each of these domains, the Higgs and inflaton fields would be quasi-homogeneous and would roll towards their true vevs in a classical manner. The fields would oscillate around their vevs and interactions with other fields would lead to their eventual decay. With the discovery of preheating, several authors analyzed the possibility of bosonic and later fermionic preheating due to the coherent oscillations of the Higgs and inflaton fields in hybrid inflation [61, 62, 63].

However, the present author and his collaborators have recently found that, contrary to original expectations, the early stages of reheating in many hybrid models does not occur at all in the way it was described in the last paragraph [18, 19]. In fact, we find that a stage of quasi-homogeneous oscillations never occurs. Tachyonic (or spinoidal) instabilities in the SSB potentials used in hybrid models lead to the rapid growth of fluctuations in the Higgs and inflaton fields. Frequently, the quasi-homogeneous character of the Higgs and inflaton fields is destroyed within one or two oscillations of the mean background field. The result is that the energy that would have gone into oscillations is distributed into large amplitude, long wavelength semi-classical fluctuations in the fields. Thus, SSB and the end of inflation in hybrid models leads to a state very similar to that of the simple power-law models, only without the amplification of fluctuations by parametric (or stochastic) resonance. This occurs after the initial stages of SSB. We have termed this new effect *tachyonic preheating*.

The process of SSB is fundamental to modern theories of elementary particle physics and to cosmology. In the simplest models, an instability appears because of the presence of tachyonic mass terms such as $-\frac{1}{2}m_\phi^2\phi^2$ in the effective potential. As a result, the Klein-Gordon equation for fluctuations is unstable. Long wavelength quantum fluctuations $\phi_k$ of the field $\phi$ with momenta $k < m_\phi$ grow exponentially, $\phi_k \sim \exp(t\sqrt{m_\phi^2 - k^2})$. The growth of these fluctuations leads to spontaneous symmetry breaking. Note that, unlike the case of parametric resonance, the tachyonic instability is not due to a non-adiabatically changing effective mass.

SSB through the growth of fluctuations may occur gradually, as in the theory of second order phase transitions, when the parameter $m_\phi^2$ slowly changes from positive to negative and the degree of symmetry breaking gradually increases in time [64]. Sometimes the symmetry breaking occurs discontinuously, due to a first order phase transition [65]. But there is also another possibility, which will concern us here: The tachyonic mass term may appear suddenly, on a time scale that is much shorter than the time required for symmetry breaking to occur. This is what happens in the hybrid inflation scenario as the motion of the inflaton field "suddenly" triggers the instability of the Higgs field. In condensed matter physics, such phase transitions are called "quenches". Aside from hybrid inflation, the theory of tachyonic preheating will be relevant to many quenched systems. In particular, super-cooling during the expansion of the universe can lead to non-inflation related *cosmic quenches* which might lead to tachyonic preheating.

The process of symmetry breaking has been studied before by advanced methods of perturbation theory, see e.g. [44, 45, 66] and references therein. However, spontaneous symmetry breaking is a strongly nonlinear and non-perturbative effect. It usually leads to the production of particles with large occupation numbers inversely proportional to the coupling constants. As a result, the perturbative description, including the Hartree and $1/N$ approximations, has limited applicability. It does not properly describe rescattering of created particles and other important features such as production of topological defects [15, 40, 41].

For further theoretical understanding of the issue one should go beyond perturbation theory. Fortunately, during the last few years new methods of lattice simulations have been developed. They are based on the observation that quantum states of bose fields with large occupation numbers can be interpreted as classical waves and their dynamics can be fully analyzed by solving relativistic wave equations on a lattice [37, 67]. In [18, 19], we have further developed these methods and applied them to the investigation of tachyonic preheating. A significant advantage of these methods as compared to other lattice simulations of quantum processes is that the semi-classical nature of the effects under investigation allows us to have a clear visual picture of all the processes involved.

The layout of this chapter is as follows. We first will describe the simplest model of hybrid inflation with just two real scalar fields. We use this model to elaborate the well known constraints that can be imposed on it. We further analyze the two field model by considering the stage of SSB. We find that symmetry breaking can occur through two distinct mechanisms. For some ranges of parameters, the swift motion of the inflaton field leads to a large tachyonic mass for the Higgs field, triggering SSB. In other models, SSB occurs due to the quantum diffusion of the Higgs and inflaton fields. Though the effective mass for Higgs fluctuations vanishes near the critical point, it is still possible for random quantum fluctuations to push the Higgs field into the tachyonic regime, triggering SSB. For the parameter choices we consider, this diffusion process will actually dominate.

With a simple model in hand, we next present two supersymmetric models from the literature that lead to hybrid inflation. These models are characterized as F-term or D-term according to which of these terms in the SUSY scalar potential supports inflation. As is well known, both of these models reduce to the simple two field model during inflation and at the initial stage of SSB. We show this correspondence and identify parameters in each model.

With our models in hand, we next analyze preheating for the F- and D-term models. First, we present a linearized analysis, separating the Higgs and inflaton fields into classical background plus fluctuations, as we did in previous chapters. In each case, however, we find that the fluctuations grow so strongly that backreaction should be incorporated within just one oscillation of the background fields. We then put these models on the lattice and find that, indeed, the tachyonic instabilities make any attempt at identifying a useful mean field hopeless within just one or two oscillations.

## 5.1 Hybrid Inflation and Cosmic Quenches

In this section we describe the class of hybrid inflationary models. We will begin with the simplest model involving two real scalar fields [59, 60]. Inflation in this model is supported by a field $\phi$ whose slow-roll is interrupted by spontaneous symmetry breaking for a field $\sigma$ that we will refer to as the Higgs field. As we are mostly interested in the p/reheating stage, we will only briefly review the inflationary stage for this model. In particular, we will develop the well known constraints that can be applied to this model.

While discussing the two-field model, we will also analyze spontaneous symmetry breaking in this theory. We find that the process can occur through two distinct channels: growth of a tachyonic mass for the Higgs field due to the initial inflaton velocity as it crosses the critical point or an effective tachyonic mass due to the initial quantum dispersion of the inflaton and Higgs fields. Which effect will dominate depends on the particular parameters of the theory. We will, however, get useful estimates for initial conditions to be used in a mean field analysis of preheating in these models.

Next, we introduce two supersymmetric models. These are classified as F-term or D-term depending on whether inflation is supported by the vev of the F- or D-term contributions to the scalar potential. The F- and D-term models we consider reduce to the simple two field model during the inflationary stage and around the moment of SSB.

### 5.1.1 The basic two-field hybrid model

The simplest form of two-field hybrid inflation is described by the potential [59, 60]

$$V(\phi, \sigma) = \frac{\lambda}{4}(\sigma^2 - v^2)^2 + \frac{g^2}{2}\phi^2\sigma^2 + V_{\rm sr}(\phi)\,, \tag{5.1}$$

where $\phi$ and $\sigma$ are two real scaler fields that we will call the inflaton and Higgs, respectively. $V_{\rm sr}(\phi)$ is a strictly concave function of the inflaton field alone, such as a mass term $\frac{1}{2}m_\phi^2\phi^2$. The potential (5.1), then has two global minima at $\phi = 0$, $\sigma = \pm v$. The non-zero vev of the Higgs field at one of these minima spontaneously breaks the discrete $Z_2$ symmetry of (5.1). During inflation, we need to consider values of the inflaton and Higgs fields away from their true minima. We see that, for $\sqrt{\langle\phi^2\rangle} \gg \frac{\sqrt{\lambda}}{g}v$, the effective mass-squared of the Higgs field

$$m_\sigma^2(\phi) = -\lambda v^2 + g^2\left\langle\phi^2\right\rangle , \tag{5.2}$$

is large and positive. Meanwhile, if $\sqrt{\langle\phi^2\rangle} \le \frac{\sqrt{\lambda}}{g}v$, the Higgs field develops a tachyonic mass and is unstable near $\sqrt{\langle\sigma^2\rangle} = 0$. The inflaton value $\phi_c = \frac{\sqrt{\lambda}}{g}v$ is seen to be a critical point.

Let us see how inflation can occur in this model. We imagine that chaotic initial conditions lead to a patch of the early universe over which the inflaton is approximately homogeneous and for which $\phi > \phi_c$. As usual, we use $\phi$ to represent the vev, $\langle\phi\rangle$. When this occurs, the large vev of the inflaton field will drive the Higgs field to zero, because the effective mass-squared (5.2) becomes large and positive. In this case, the potential (5.1) will have only two contributions: $V \sim V_0 + V_{\rm sr}$, where $V_0 = \frac{1}{4}\lambda v^4$ is the false vacuum energy of the symmetric state.

The role of $V_{\rm sr}$ is to allow the inflaton to evolve towards its true vev. Let us assume, for simplicity, that the false vacuum energy dominates $V_{\rm sr}(\phi)$ during the time of interest to us. Then, the Friedmann equation (1.3) tells us that inflation is truly exponential in this model:

$$H^2 \approx H_0^2 = \frac{2\pi}{3M_p^2}\lambda v^4 \ \ , \ \ a(t) = a_0 e^{H_0 t}\,. \tag{5.3}$$

For potentials that are not too steep, and field values that are not too large, the Klein-Gordon equation for the inflaton will be over-damped; the inflaton will slowly evolve towards $\phi = 0$ under the influence of $V_{\rm sr}$ and the Hubble friction. Thus, $V_{\rm sr}$ describes the *slow-roll* of the inflaton towards its true vev, but does not support inflation.

As the inflaton field rolls towards zero, it will cross the bifurcation point, $\phi_c$. After this, the effective mass-squared of the Higgs field (5.2) becomes negative. This leads to the exponential growth of $\sigma$ fluctuations, with some typical time scale, $\mu^{-1}$. As discussed in [59, 60], inflation should end fairly abruptly (in a "waterfall" manner) after the bifurcation point so as to avoid the overproduction of isocurvature fluctuations in the Higgs field. In the language of condensed matter physics, we require that symmetry breaking in the Higgs field be quenched by the rapid motion of $\phi$ into the region of tachyonic (or spinoidal) instability. Thus, we require the $\sigma$ field to grow substantially within one Hubble time, $H_0^{-1}$, after $\phi$ reaches the bifurcation point.

We have intentionally left the exact character of the slow-roll potential somewhat nebulous. In the original versions of hybrid inflation, $V_{\rm sr}$ was simply a mass term. It was later pointed out that, even if one doesn't include a slow-roll potential in the bare Lagrangian, one would expect radiative corrections around the non-zero inflaton vev to induce a potential for the inflaton field, c.f. [68]. To one loop, and taking into account only the massive Higgs field, the correction to the inflaton potential takes the form

$$V_{1-\rm loop} \sim \frac{g^4\phi^4}{32\pi^2}\left[\log\left(\frac{\phi^2}{\phi_c^2}\right)+C\right], \tag{5.4}$$

for $\phi \gg \phi_c$. $C$ here is a numerical coefficient of $O(1)$. The $\phi^4$ dependence of this potential is rather extreme. In the supersymmetric models, the coefficient of the log can be independent of $\phi$ due to cancellation between the bosonic and fermionic contributions to $V_{1-\rm loop}$. As we will be most interested in supersymmetric theories, it is most natural to take the SUSY form of (5.4)

$$V_{1-\rm loop}^{\rm SUSY} \sim \frac{\lambda^2 v^4}{16\pi^2}\left[\log\left(\frac{\phi^2}{\phi_c^2}\right)+C\right], \tag{5.5}$$

which is valid when $\phi \gg \phi_c$. Only the numerical factor $C$ would differ between the F-term and D-term models we consider in this paper [69].

Here, however, we will take the slow-roll potential to be simply a mass term as in the original theory:

$$V_{\rm sr} = \frac{1}{2}m_\phi^2\phi^2\,. \tag{5.6}$$

With a definite form for $V_{\rm sr}$ in hand, we can constrain the parameters occurring in the hybrid model from the spectrum of adiabatic density perturbations generated during inflation. The COBE normalization may be expressed as [7]

$$\left(\frac{8\pi}{M_p^2}\right)^{3/2}\left(\frac{V_0^{3/2}}{V_{{\rm sr},\phi}}\right) = (2\pi\lambda)^{3/2}\left(\frac{v}{M_p}\right)^6\left(\frac{M_p^3}{m_\phi^2\phi}\right) \approx 5.3\times 10^{-4}\,, \tag{5.7}$$

where $\phi$ is to be evaluated at the moment when fluctuations that today are galaxy sized left the Hubble radius during inflation. To estimate the value of $\phi$ at this time, let us solve the Klein-Gordon equation for the amplitude of the inflaton as a function of time during inflation. The Klein-Gordon equation takes the form: $3H_0\dot{\phi} \approx -V_{\mathrm{sr},\phi}$. Using the potential (5.6), we find that

$$\phi_N = \phi_c \exp\left(\frac{m_\phi^2}{3H_0^2}N\right), \tag{5.8}$$

where $\phi_N$ is the amplitude of the inflaton field $N$ e-foldings prior to the end of inflation. (We assume inflation ends abruptly when $\phi \approx \phi_c$.) If we assume that the scales of interest left the Hubble radius while $\phi \approx \phi_c$, we have the constraint

$$m_\phi \ll H_0 \quad \Leftrightarrow \quad \left(\frac{m_\phi}{M_p}\right) \ll \sqrt{2\pi\lambda}\left(\frac{v}{M_p}\right)^2 . \tag{5.9}$$

and taking $\phi \approx \phi_c$ in (5.7), we can write the COBE constraint as

$$\lambda g \left(\frac{v}{M_p}\right)^5 \approx 3.4 \times 10^{-5} \left(\frac{m_\phi}{M_p}\right)^2 . \tag{5.10}$$

For completeness, let us right the vacuum domination constraint here as well

$$V_{\mathrm{sr}}(\phi_c) \ll V_0 \quad \Leftrightarrow \quad m_\phi \ll \frac{g}{\sqrt{2}}v\,. \tag{5.11}$$

The three constraints (5.9)-(5.11) still allow considerable freedom in the choice of parameters. In particular, the ratio $\frac{g^2}{\lambda}$ can take both large and small values. We will now consider the end of inflation to see how the waterfall constraint can be added to this set.

### 5.1.2 SSB: growth of tachyonic mass vs. quantum diffusion

Let us now turn to the process of SSB itself. This is important for two reasons. The first is that it will provide us with an understanding of the initial conditions at the start of reheating. Second, it will lead to an additional constraint from the waterfall condition: $\mu > H_0$, where $\mu^{-1}$ is the characteristic time scale for SSB to occur. In order to implement this constraint, we must estimate $\mu$ for our theory, and in order to do that, we must understand how SSB occurs.

According to the classical equations of motion, the Higgs field cannot evolve away from zero, even after the inflaton drops below the critical point, because the first derivative of the effective potential at $\sigma = 0$ vanishes. The process of spontaneous symmetry breaking in this case occurs due to the exponential growth of quantum fluctuations. Indeed, the field $\sigma$ has a (negative) effective mass squared (5.2) which vanishes at the critical point, but becomes large and grows up to $|m_\sigma(0)| = \sqrt{\lambda}v$ as the field $\phi$ rolls towards $\phi = 0$. Quantum fluctuations of the scalar field $\sigma$ with momentum $\mathbf{k}$ grow as $\exp(w_k t)$, where $w_k = \sqrt{-m_\sigma^2 - k^2}$ and $k = |\mathbf{k}|$. Symmetry breaking occurs due to the growth of fluctuations with $k < |m_\sigma|$. Note that even the quantum evolution will maintain $\langle\sigma\rangle = 0$ when averaged over all space. However, $\sqrt{\langle\sigma^2\rangle} = \sigma_{\rm rms}$ will grow exponentially (at first).

This process produces an inhomogeneous distribution of the Higgs field. The resulting distribution is relatively homogeneous on a scale $l_c \sim \mu^{-1}$ or even somewhat greater, because the rate of exponential growth is maximal at $k = 0$, and the fluctuations with $k > |m_\sigma|$ do not grow at all. However, in our case we have an additional complication: the effective mass-squared (5.2) changes with time. In order to estimate the typical scale over which the growth of the Higgs field will remain relatively homogeneous, we will do the following. We find $m_\sigma^2$ as a function of time, $\Delta t$, from the moment when $\phi = \phi_c$. The exponential growth becomes efficient when $|m_\sigma| \sim \Delta t^{-1}$. After this time, $|m_\sigma(t)|$ will continue to grow, and all modes $\sigma_k$ which began growing by the moment $\Delta t$, will continue growing exponentially with approximately equal speed. This growth eventually triggers a more rapid motion of the Higgs field. This motion will preserve the initial homogeneity on a scale smaller than $\mu^{-1} \sim \Delta t$, which we now determine.

The time evolution of the Higgs' effective mass can be determined from the motion of the inflaton field. Considering (5.2) around the critical point

$$m_\sigma^2 = -g^2\left(\phi_c^2 - \phi^2(\Delta t)\right) \approx -2g^2\phi_c|\dot{\phi}_c|\Delta t\,, \tag{5.12}$$

where $|\dot{\phi}_c|$ is the speed of the inflaton field at the critical point. We can approximate this by its slow-roll value, which follows from the over-damped Klein-Gordon equation. $\mu$ will be the magnitude of this effective mass after a time $\mu^{-1}$. We conclude that

$$\mu_{\rm vel}^3 \approx 2g^2\phi_c|\dot{\phi}_c| \approx \sqrt{\frac{2\lambda}{3\pi}}m_\phi^2 M_p\,, \tag{5.13}$$

where we have denoted this by a subscript referring to the *velocity* of the inflaton field for later convenience. The waterfall constraint, $\mu \gg H_0$ leads to the condition

$$\sqrt{\lambda}\left(\frac{v}{M_p}\right)^3 \ll 10^{-1}\left(\frac{m_\phi}{M_p}\right)\,. \tag{5.14}$$

The waterfall constraint, combined with the COBE constraint (5.10) gives

$$\left(\frac{v}{M_p}\right) \ll 3 \times 10^2 g \,, \tag{5.15}$$

which is not particularly restrictive.

There is another channel through which the Higgs field can move to its true vev. Imagine for a moment that the inflaton field had no initial velocity at the critical point. Then, our argument above suggests that the lifetime of the symmetric state is infinite. This is clearly incorrect. The solution lies in the fact that the Higgs field has quantum dispersion around the false vacuum vev. In effect, it is possible for the Higgs field to diffuse away from the critical point due only to the effects of quantum noise. As we will see, it is possible for this process to give the dominant contribution to the SSB in this model.

Let us expand the potential (5.1) around the critical point to determine the paths along which a field, localized at the critical point but with finite dispersion, would most easily diffuse. Letting $\sigma = r\sin(\theta)$ and $\phi = \phi_c - r\cos(\theta)$, the potential reduces to

$$V(r,\theta) \approx V_0 - g\sqrt{\lambda} v r^3 \cos(\theta)\sin^2(\theta) \,, \tag{5.16}$$

for small $r$. Differentiation with respect to $\theta$ reveals two minima of this potential at fixed $r$: $\theta = \pm\arctan(\sqrt{2})$. Along these directions, and near the critical point, the potential looks like

$$V(r) \approx V_0 - \frac{2\sqrt{\lambda} g v}{3\sqrt{3}} r^3 + O(r^4) \,. \tag{5.17}$$

The quantum diffusion problem for such a potential was original investigated for this problem in [18] and subsequently more thoroughly in [70]. We now summarize the results of this investigation.

Let us consider the evolution of quantum fluctuations of the (canonically normalized) field $r$. For the moment, we will neglect the role of expansion. At the critical point, $r$ is a massless, real scalar field. We know that the variance of such a field due to its quantum fluctuations formally diverges. To regulate this divergence, we can imagine that the field is divided into hard modes with $k > k_*$ and soft modes with $k < k_*$ for some arbitrary cut-off $k_*$. The amplitude of vacuum fluctuations is just $\delta r_k \sim 1/\sqrt{2k}$. Thus, the contribution of the soft modes to the mean-square fluctuation is just

$$\left\langle r^2(k_*) \right\rangle = \frac{1}{2\pi^2}\int_0^{k_*} dk\, k^2 |\delta r_k|^2 = \frac{k_*^2}{8\pi^2} \,. \tag{5.18}$$

The Klein-Gordon equation for the hard modes can then be written

$$\delta\ddot{r}_k + \left(k^2 - 4\sqrt{\frac{\lambda}{3}}gv\sqrt{\langle r^2(k_*)\rangle}\right)\delta r_k = 0\,. \tag{5.19}$$

We see that hard modes with $k^2 < 4\sqrt{\frac{\lambda}{3}}gv\sqrt{\langle r^2(k_*)\rangle} = \sqrt{\frac{2\lambda}{3\pi^2}}gvk_*$ will have a tachyonic mass and will grow exponentially.

It is reasonable to guess that, taking $k \sim k_*$, we will get a self-consistent tachyonic growth for all modes $k < \mu$ where

$$\mu_{\rm diff} \sim \sqrt{\frac{2\lambda}{3\pi^2}}gv\,. \tag{5.20}$$

A more careful analysis based on the stochastic approach to quantum diffusion suggests that this result is indeed correct [70, 71]. We can associate (5.20) with the diffusion time scale for SSB[2].

This time scale should be compared with that for SSB via the initial velocity of the inflaton field (5.13). Their ratio is

$$\frac{\mu_{\rm diff}}{\mu_{\rm vel}} \sim 10^{-1}\, g^{2/3}\left(\frac{v}{M_p}\right)^{-2/3}, \tag{5.21}$$

where we have used the COBE constraint (5.10) to eliminate $m_\phi$. Thus, we see that, for different choices of parameters, either quantum diffusion or the growth of the tachyonic mass will dominate.

To see what scales these constraints lead to, let us take a few examples and apply the constraints. Table 5.1 lists several possibilities. Even requiring that both $g^2$ and $\lambda$ be less than $10^{-1}$, we can have a broad range for the ratio $\frac{g^2}{\lambda}$. The values of $\lambda$ in the table suggest we consider at least a range $10^5 \gtrsim \frac{g^2}{\lambda} \gtrsim 10^{-5}$. The value of $v$ can be associated with the SUSY GUT scale $O(10^{16}\,\text{GeV})$. However, the first two rows are marginal with respect to constraint (5.9). This constraint can be relaxed somewhat and rewritten in terms of a constraint on the spectral index $n$ of perturbations generated during inflation [72]. This analysis shows that these values really are acceptable.

Here, we will stick with values of $v$ below $10^{15}$ GeV. The reason for this is two-fold. First, from Table 5.1 we see that that larger values of $v$ tend to have marginal

[2]In fact, one finds that SSB in this model resembles bubble formation in a first order phase transition. This is because the few regions of space with fluctuations somewhat larger than (5.18) will evolve towards their true vev much faster than regions with the amplitude (5.18), see [70].

| $v$( GeV) | $\lambda$ | $g^2$ | $\phi_c$( GeV) | $m_\phi$( GeV) | $\mu_{\mathrm{vel}}/\mu_{\mathrm{diff}}$ | $H_0$( GeV) |
|---|---|---|---|---|---|---|
| $10^{16}$ | $10^{-01}$ | $2 \cdot 10^{-01}$ | $7.1 \cdot 10^{15}$ | $8.5 \cdot 10^{12}$ | $1.4 \cdot 10^{00}$ | $3.8 \cdot 10^{12}$ |
| $10^{16}$ | $10^{-04}$ | $1 \cdot 10^{-01}$ | $3.2 \cdot 10^{14}$ | $2.3 \cdot 10^{11}$ | $1.7 \cdot 10^{00}$ | $1.2 \cdot 10^{11}$ |
| $10^{16}$ | $10^{-01}$ | $1 \cdot 10^{-04}$ | $3.2 \cdot 10^{17}$ | $1.3 \cdot 10^{12}$ | $1.7 \cdot 10^{01}$ | $3.8 \cdot 10^{12}$ |
| $10^{16}$ | $10^{-02}$ | $2 \cdot 10^{-02}$ | $7.1 \cdot 10^{15}$ | $1.5 \cdot 10^{12}$ | $3.0 \cdot 10^{00}$ | $1.2 \cdot 10^{12}$ |
| $10^{14}$ | $10^{-01}$ | $2 \cdot 10^{-01}$ | $7.1 \cdot 10^{13}$ | $8.5 \cdot 10^{07}$ | $6.4 \cdot 10^{-02}$ | $3.8 \cdot 10^{08}$ |
| $10^{14}$ | $10^{-04}$ | $1 \cdot 10^{-01}$ | $3.2 \cdot 10^{12}$ | $2.3 \cdot 10^{06}$ | $8.0 \cdot 10^{-02}$ | $1.2 \cdot 10^{07}$ |
| $10^{14}$ | $10^{-01}$ | $1 \cdot 10^{-04}$ | $3.2 \cdot 10^{15}$ | $1.3 \cdot 10^{07}$ | $8.0 \cdot 10^{-01}$ | $3.8 \cdot 10^{08}$ |
| $10^{14}$ | $10^{-02}$ | $2 \cdot 10^{-02}$ | $7.1 \cdot 10^{13}$ | $1.5 \cdot 10^{07}$ | $1.4 \cdot 10^{-01}$ | $1.2 \cdot 10^{08}$ |
| $10^{12}$ | $10^{-01}$ | $2 \cdot 10^{-01}$ | $7.1 \cdot 10^{11}$ | $8.5 \cdot 10^{02}$ | $3.0 \cdot 10^{-03}$ | $3.8 \cdot 10^{04}$ |
| $10^{12}$ | $10^{-04}$ | $1 \cdot 10^{-01}$ | $3.2 \cdot 10^{10}$ | $2.3 \cdot 10^{01}$ | $3.7 \cdot 10^{-03}$ | $1.2 \cdot 10^{03}$ |
| $10^{12}$ | $10^{-01}$ | $1 \cdot 10^{-04}$ | $3.2 \cdot 10^{13}$ | $1.3 \cdot 10^{02}$ | $3.7 \cdot 10^{-02}$ | $3.8 \cdot 10^{04}$ |
| $10^{12}$ | $10^{-02}$ | $2 \cdot 10^{-02}$ | $7.1 \cdot 10^{11}$ | $1.5 \cdot 10^{02}$ | $6.4 \cdot 10^{-03}$ | $1.2 \cdot 10^{04}$ |

Table 5.1: Some sample parameter values for a simple hybrid model. All meet the constraints (5.10) and (5.11) and easily meet the waterfall constraint $\max\{\mu_{\mathrm{diff}}, \mu_{\mathrm{vel}}\} \gg H_0$. The first two rows are marginal for constraint (5.9), but are, in fact, acceptable.

SSB. That is, in these cases both the initial inflaton velocity and quantum diffusion must be considered together. This is not a difficulty for lattice simulations, but it makes a linearized mean field analysis less straight forward. As we will see, one of our conclusions is that the mean field analysis is not very good even in optimal cases and that the lattice simulation should be used. Lattice simulations suggest that this is true even for the other cases [19].

A second point is that, for large field amplitudes $(\phi, \sigma) \gtrsim O(10^{17})\,\mathrm{GeV}$, we expect supergravity corrections to become important. From the table, we see that situations in which $\lambda \ll g^2$ and $v \gtrsim 10^{15}\,\mathrm{GeV}$ are then suspect. Though we will not pursue it here, in principal one should be careful that supergravity corrections do not invalidate the use of our simple $\frac{1}{2}m_\phi^2\phi^2$ slow-roll potential.

Having restricted ourselves to models in which SSB occurs due to quantum diffusion, we know that $\mu_{\mathrm{diff}}^{-1}$ will give us the typical time and length scale for the start of domain formation. Equation (5.18) tells us that, after a time $\mu_{\mathrm{diff}}^{-1}$, the $r$ field will have a r.m.s. amplitude

$$r_0 = \sqrt{\langle r^2 \rangle} \approx \frac{\mu_{\mathrm{diff}}}{\sqrt{8\pi^2}} = \sqrt{\frac{\lambda}{12}}\left(\frac{gv}{\pi^2}\right) . \tag{5.22}$$

The Higgs and inflaton fields are most likely to diffuse along the line $\theta = \pm\arctan(\sqrt{2})$. A given domain will correspond to one of these values. Taking the positive one, we may write $\phi_c - \phi_0 \approx \sqrt{2}\sigma_0 \approx \sqrt{3}r_0$. We will use these values for our linearized mean field calculations.

Several criticisms can be lodged against the analysis above. One is the one dimensional treatment of the radial potential near the critical point. Another is the assumption that the fields will tunnel exactly along the channels $\theta = \pm\arctan(\sqrt{2})$. The first objection is not likely to change our estimate (5.22) by more than an order of magnitude. The second is also not very important as the field is most likely to tunnel along the channel and, in those regions of space where it does not, the fields will tend to roll into the channels $\theta = \pm\arctan(\sqrt{2})$ as part of their classical motion away from the critical point. Our lattice simulations support these views.

### 5.1.3 The F-term Model

The simplest F-term hybrid inflation model is based on a superpotential with two left-chiral superfields: $W = \frac{\sqrt{\lambda}}{2}\Phi\left(2\Sigma^2 - v^2\right)$. Parametric resonance in this model was considered in [62]. However, spontaneous breaking of the discrete $Z_2$ symmetry in this model leads to domain wall production which would be cosmologically unacceptable. Therefore, we will consider a three field F-term model [73] based on the superpotential

$$W = \frac{\sqrt{\lambda}}{2}\Phi\left(4\bar{\Sigma}\Sigma - v^2\right), \tag{5.23}$$

where $\Phi$, $\Sigma$ and $\bar{\Sigma}$ are left-chiral superfields. In this case, the spontaneous breaking of the local (global) $U(1)$ symmetry between the $\Sigma$ and $\bar{\Sigma}$ fields will lead to gauge (global) string formation[3].

In global SUSY, using the same notation for superfields and their complex scalar components, this superpotential contributes

$$V_{\mathrm{F}} = \frac{\lambda}{4}|4\bar{\Sigma}\Sigma - v^2|^2 + 4\lambda|\Phi|^2\left(|\Sigma|^2 + |\bar{\Sigma}|^2\right) \tag{5.24}$$

to the scalar potential. In general, $\Sigma$ and $\bar{\Sigma}$ could be (oppositely) charged under a local $U(1)$ symmetry, in which case we should include a D-term, $V_{\mathrm{D}}$, in the complete potential. However, for our purposes, we will consider either that the $U(1)$ is global or that the charges of these fields, and any possible Fayet-Illiopolous term are small.

[3] These strings can contribute isocurvature perturbations in addition to the adiabatic ones generated during inflation. Because these two mechanisms are independent, their contributions and can be added separately. This will alter the COBE constraint (5.10), but we do not pursue it here [74]

Hence, we take $V_{\rm D} \simeq 0$. As discussed in the last section, there should also be a slow roll potential for the inflaton. We take this to be a soft SUSY-breaking mass term. The value of the mass term will be important for determining the scale of SSB, however, we expect this term to contribute negligible to the dynamics after symmetry breaking. Our numerical simulations confirm that this is indeed the case.

In this model, inflation occurs when chaotic initial conditions lead to $\langle|\Phi|\rangle \gg v$. When this happens, the two $\Sigma$ fields acquire large effective masses and roll to their local minimum at $\langle\bar{\Sigma}\rangle = \langle\Sigma\rangle = 0$. In this limit, the potential (5.24) becomes $V \approx \frac{\lambda v^4}{4}$, which gives rise to a non-vanishing effective cosmological constant. However, this is a false vacuum state; the true vacuum corresponds to $\langle\bar{\Sigma}\Sigma\rangle = \frac{v^2}{4}$ and $\langle\Phi\rangle = 0$. The slow-roll potential drives the evolution of the inflaton towards its true vev. When its magnitude reaches the value $\langle|\Phi_{\rm c}|\rangle = \frac{v}{2}$ spontaneous symmetry breaking occurs.

As discussed in the last section, this leads to domains of size $l_c \approx \mu^{-1} > v^{-1}$ over which the $\Sigma$, $\bar{\Sigma}$, and $\Phi$ fields are all approximately homogeneous.

For further discussion of symmetry breaking in this model, let us rewrite (5.24) in terms of polar fields: $\Sigma = |\Sigma|e^{i\theta}$, $\bar{\Sigma} = |\bar{\Sigma}|e^{i\bar{\theta}}$. The potential becomes

$$V_{\rm F} = \frac{\lambda}{4}\left(16|\bar{\Sigma}|^2|\Sigma|^2 - 8v^2|\bar{\Sigma}||\Sigma|\cos(\theta+\bar{\theta}) + v^4\right) + 4\lambda|\Phi|^2\left(|\Sigma|^2 + |\bar{\Sigma}|^2\right) . \quad (5.25)$$

At the stage of symmetry breaking, when $\langle|\bar{\Sigma}\Sigma|\rangle$ begins to move away from zero, the absolute phase $\mathrm{Arg}(\bar{\Sigma}\Sigma) = \theta + \bar{\theta}$ acquires a mass and is forced to zero. Note, however, that the potential is independent of the relative phase, $\theta - \bar{\theta}$, reflecting the $U(1)$ symmetry. Thus, in a quasi-homogeneous patch, the $U(1)$ symmetry allows us to choose the relative phase of the $\Sigma$ fields to be zero without any loss of generality. This choice, combined with the vanishing of the absolute phase, is equivalent to choosing the two complex $\Sigma$ fields to be real. In order to leave canonical kinetic terms, we define $\sigma_\pm \equiv |\Sigma| \pm |\bar{\Sigma}|$. Furthermore, as inflation has left the inflaton homogeneous across all the patches, we may choose it to be real: $\phi \equiv \sqrt{2}|\Phi|$.

In terms of these three real fields, the potential now becomes

$$V_{\rm F} = \frac{\lambda}{4}\left(\sigma_+^2 - \sigma_-^2 - v^2\right)^2 + \lambda\phi^2\left(\sigma_+^2 + \sigma_-^2\right) . \quad (5.26)$$

In the symmetric phase, when $\sigma_\pm = 0$, the $\sigma$ fields have an effective mass-squared: $m_\pm^2(\phi) = \lambda\left(2\phi^2 \mp v^2\right)$. We can now see that spontaneous symmetry breaking occurs in this model exactly as in the two field model of the last section. For $\phi < \phi_c = \frac{v}{\sqrt{2}}$, the $\sigma_+$ field has a tachyonic mass that triggers symmetry breaking and the end of inflation. On the other hand, the $\sigma_-$ field has always a large and positive effective mass-squared, pinning it to zero. Thus, during inflation and at the *initial* stages of symmetry breaking, this model behaves just like the standard two field hybrid model discussed in the last section. We have only to apply the constraint $g^2 = 2\lambda$ and identify the Higgs field with $\sigma_+$.

We emphasize that the parallel between (5.26) and the standard two field hybrid potential (5.1) is useful only for analyzing the initial stage of symmetry breaking and for establishing the constraints on the inflationary model. In particular, the vacuum structure of the two theories is very different. The standard model has a unique vacuum up to the $Z_2$ symmetry while the potential (5.26) possess a continuously degenerate vacuum along the hyperbola $\sigma_+^2 - \sigma_-^2 = 2$ in addition to the $U(1)$ symmetry. For a proper analysis beyond this stage, we must return to the potential (5.24) and consider all six, real bosonic degrees of freedom. In section 5.2.1, we will present a linear analysis of the equations for small fluctuations around the background $\sigma_\pm$ and $\phi$ fields. We find that the description in terms of a homogeneous background plus small fluctuations breaks down very quickly. This is due to a new tachyonic effect which we call *tachyonic preheating*. Tachyonic preheating results in the rapid growth of modes with $k > l_c^{-1}$ and is distinct from the initial symmetry breaking instability. In section 5.2.2 we confirm our expectations with a nonlinear analysis of the full field dynamics.

### 5.1.4 The D-term Model

The simplest model of D-term hybrid inflation [75] consists of three (left) chiral superfields: the inflaton and two fields oppositely charged under a local $U(1)$. The potential for this model comes from the superpotential

$$W = \sqrt{2}g\,\Phi\Sigma_+\Sigma_- \ , \tag{5.27}$$

and the D-term

$$D = \frac{\sqrt{\lambda}}{2}\left(2|\Sigma_+|^2 - 2|\Sigma_-|^2 - v^2\right) \ , \tag{5.28}$$

where the fields $\Sigma_\pm$ have charges $\pm\sqrt{\lambda}$ and the Fayet-Illiopolous term is $\frac{\sqrt{\lambda}}{2}v^2$. These give rise to the potential

$$\begin{aligned} V &= V_{\mathrm{F}} + D^2 \qquad (5.29)\\ &= 2g^2\left(|\Phi|^2|\Sigma_+|^2 + |\Phi|^2|\Sigma_+|^2 + |\Sigma_+|^2|\Sigma_-|^2\right) + \frac{\lambda}{4}\left(2|\Sigma_+|^2 - 2|\Sigma_-|^2 - v^2\right)^2 , \end{aligned}$$

where we have used the same notation for each left chiral superfield and its corresponding complex scalar component.

The potential (5.29) has many features in common with the F-term potential (5.25). Inflation can occur when $\langle|\Phi|\rangle$ acquires a large value. This gives $\langle\Sigma_+\rangle$ and $\langle\Sigma_-\rangle$ a large effective mass, driving them to zero. Again, this is a false vacuum state; in this case the true vacuum corresponds to $\langle\Phi\rangle = \langle\Sigma_-\rangle = 0$ and $\langle|\Sigma_+|\rangle = \frac{v}{\sqrt{2}}$. The slow-roll potential, $V_{\rm sr}(\Phi)$, will drive $\langle|\Phi|\rangle$ towards zero. For $|\Phi|^2 < |\Phi_c|^2 = \frac{\lambda v^2}{2g^2}$, $\langle\Sigma_+\rangle$ acquires a tachyonic mass, leading to spontaneous symmetry breaking. $\langle\Sigma_-\rangle$, on the other hand, remains pinned at zero.

We see that the potential (5.29) is independent of the phases of the fields. Inside a quasi-homogeneous patch, we may choose the fields to be real and define $\sigma_\pm \equiv \sqrt{2}|\Sigma_\pm|$ and $\phi \equiv \sqrt{2}|\Phi|$, again allowing for canonical kinetic terms. In terms of these fields, the potential (5.29) reduces to the form

$$V_{\rm D} = \frac{\lambda}{4}\left(\sigma_+^2 - \sigma_-^2 - v^2\right)^2 + \frac{g^2}{2}\left(\phi^2\sigma_+^2 + \phi^2\sigma_-^2 + \sigma_+^2\sigma_-^2\right) \,. \tag{5.30}$$

As in the F-term model, when $\sigma_-$ is forced to zero, the potential takes the form of the standard two field hybrid model (5.1), with arbitrary coupling parameters $g^2$ and $\lambda$. We find the size of quasi-homogeneous patches to be $l_c \sim \mu^{-1}$.

Like the F-term model, the potential (5.30) should only be used to study inflation and the initial stage of symmetry breaking. In section 5.3 we analyze the dynamics of all six real bosonic degrees of freedom of the potential (5.29), both as linearized equations for fluctuations and through a full non-linear analysis. In this case, the motion of the background fields is more complicated than the F-term case. Nevertheless, we find that tachyonic preheating occurs for a broad range of the parameter $\frac{g^2}{\lambda}$.

## 5.2 Preheating in the F-term Model

In this section we present an analysis of preheating in the three field F-term model of hybrid inflation. After the stage of symmetry breaking (i.e. after $\phi$ reaches the bifurcation point), the expansion of the Universe and the slow-roll potential $V_{\rm sr}$ can be neglected. In this approximation, the full equations for the three complex fields in the F-term model, which follow from the potential (5.24), are

$$\begin{aligned} \ddot{\Phi} - \nabla^2\Phi + 4\lambda\left[|\bar{\Sigma}|^2 + |\Sigma|^2\right]\Phi &= 0\,, \\ \ddot{\Sigma} - \nabla^2\Sigma + 4\lambda\left[|\Phi|^2 + |\bar{\Sigma}|^2\right]\Sigma &= \lambda v^2\bar{\Sigma}^*\,, \end{aligned} \tag{5.31}$$

$$\ddot{\bar{\Sigma}} - \nabla^2\bar{\Sigma} + 4\lambda\left[|\Phi|^2 + |\Sigma|^2\right]\bar{\Sigma} = \lambda v^2 \Sigma^* \,.$$

Our strategy will be first to consider the evolution of the background fields and their fluctuations separately. Under the assumption that the fluctuations are small, we will linearize their equations. We will find, however, that a tachyonic instability generates fluctuations so rapidly that backreaction should be incorporated within the first oscillation. Thus, we find that a quantitatively correct description requires a lattice calculation, the results of which are described in the last subsection.

### 5.2.1 F-term: Linearized Theory

We have already seen in section 5.1.3 that the background fields after the stage of symmetry breaking can be reduced to the real, quasi-homogeneous fields $\sigma_\pm(t)$ and $\phi(t)$ in a given patch. We make the substitutions

$$\frac{1}{\sqrt{2}}\left[\Sigma(x,t) \pm \bar{\Sigma}(x,t)\right] \equiv \Sigma_\pm(x,t) = \frac{1}{\sqrt{2}}\left(\sigma_\pm(t) + \delta\sigma^r_\pm(x,t) + i\delta\sigma^i_\pm(x,t)\right) \,,$$
$$\Phi(x,t) \equiv \frac{1}{\sqrt{2}}\left(\phi(t) + \delta\phi^r(x,t) + i\delta\phi^i(x,t)\right) \,,\tag{5.32}$$

where $\delta\sigma^r_\pm$, $\delta\phi^r$ stand for fluctuations in the real parts of the fields, and $\delta\sigma^i_\pm$, $\delta\phi^i$ are fluctuations of the imaginary parts. As usual, the factors of $\frac{1}{\sqrt{2}}$ in (5.32) are necessary to maintain minimal kinetic terms for the field components. Furthermore, as it is convenient to work with dimensionless variables, in this section we will redefine the space-time variables $(\tilde{x},\tilde{t}) \equiv \left(\sqrt{\lambda}v\right)(x,t)$ and fields $\varphi \equiv \phi_c^{-1}\phi$, $\tilde{\sigma}_\pm \equiv \phi_c^{-1}\sigma_\pm$. This rescaling will allow us to remove all dimensionful parameters from our equations. In these variables, it will be helpful to remember that the bifurcation point corresponds to $\varphi = 1$,$\tilde{\sigma}_\pm = 0$ and the global minimum of the potential (5.25) corresponds to $\varphi = 0$ and $\tilde{\sigma}_+^2 - \tilde{\sigma}_-^2 = 2$.

The equations for the homogeneous background components–$\varphi(t)$ and $\tilde{\sigma}_\pm(t)$–follow from (5.31) and the definitions (5.32). They are

$$\ddot{\tilde{\sigma}}_\pm + \left[\varphi^2 \mp 1 \pm \frac{1}{2}\left(\tilde{\sigma}_+^2 - \tilde{\sigma}_-^2\right)\right]\tilde{\sigma}_+ = 0 \,,$$
$$\ddot{\varphi} + \left(\tilde{\sigma}_+^2 + \tilde{\sigma}_-^2\right)\varphi = 0 \,,\tag{5.33}$$

where we have neglected the back-reaction of produced fluctuations. This nonlinear, coupled set of equations admits a simple analytic solution; it is easy to check

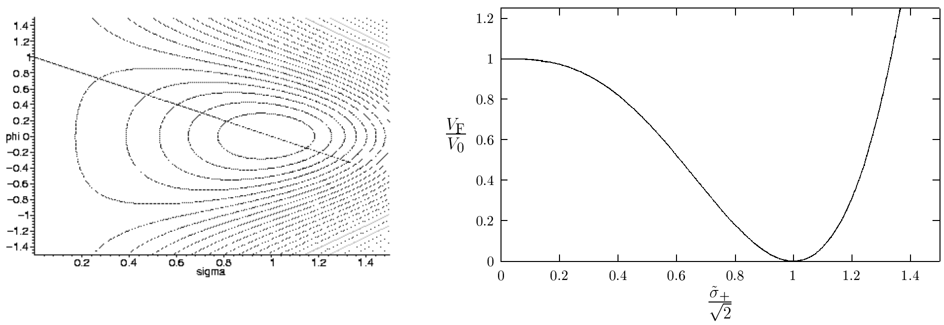


Figure 5.1: The left panel shows a contour plot of the F-term potential (5.26). The horizontal axis shows $\tilde{\sigma}_+/\sqrt{2}$ and the vertical shows $\varphi$. The solid line shows the solution (5.34). The right panel shows the potential along the solution $\varphi(t) = 1 - \frac{\tilde{\sigma}_+}{\sqrt{2}}$ (along the line of the left panel). The $\tilde{\sigma}_+$ field oscillates between a little above 0 and a maximum near $\frac{4\sqrt{2}}{3}$. The maximum curvature occurs at $\tilde{\sigma}_+ = \frac{\sqrt{2}}{3}$.

that the combination

$$\varphi(t) + \frac{1}{\sqrt{2}}\tilde{\sigma}_+(t) = 1 \ , \qquad\qquad \tilde{\sigma}_-(t) = 0 \ , \tag{5.34}$$

is a solution of equations (5.33). As expected, the background field $\tilde{\sigma}_-$ is frozen to zero due to its high mass, while $\varphi$ and $\tilde{\sigma}_+$ are oscillating along the valley with exact anti-phase, see the left panel of figure 5.1. Next, let us write down equations for fluctuations for all six real degrees of freedom around the background given by equations (5.33). Because we have chosen the background fields in our initial patch to be purely real, there is no mixing between fluctuations of the real and imaginary components of the fluctuations.

For the Fourier modes of the fluctuations of the real components we have

$$\left( \partial_{\tilde{t}}^2 + \kappa^2 + \mathcal{M}_{\rm r}^2 \right) \begin{pmatrix} \delta\sigma_{k+}^r \\ \delta\sigma_{k-}^r \\ \delta\phi_k^r \end{pmatrix} = 0 \ , \tag{5.35}$$

where the rescaled dimensionless momentum is $\kappa^2 = \frac{k^2}{\lambda v^2}$, and the mass matrix is

$$\mathcal{M}_{\rm r}^2 = \begin{pmatrix} \varphi^2 - 1 + \frac{1}{2}\left(3\tilde{\sigma}_+^2 - \tilde{\sigma}_-^2\right) & -\tilde{\sigma}_+\tilde{\sigma}_- & 2\varphi\tilde{\sigma}_+ \\ -\tilde{\sigma}_+\tilde{\sigma}_- & \varphi^2 + 1 - \frac{1}{2}\left(\tilde{\sigma}_+^2 - 3\tilde{\sigma}_-^2\right) & 2\varphi\tilde{\sigma}_- \\ 2\varphi\tilde{\sigma}_+ & 2\varphi\tilde{\sigma}_- & \tilde{\sigma}_+^2 + \tilde{\sigma}_-^2 \end{pmatrix} \tag{5.36}$$

Substituting here the solution (5.34), we find

$$\mathcal{M}_{\rm r}^2 = \begin{pmatrix} -\sqrt{2}\tilde{\sigma}_+\left(1-\sqrt{2}\tilde{\sigma}_+\right) & 0 & \sqrt{2}\tilde{\sigma}_+\left(\sqrt{2}-\tilde{\sigma}_+\right) \\ 0 & 2-\sqrt{2}\tilde{\sigma}_+ & 0 \\ \sqrt{2}\tilde{\sigma}_+\left(\sqrt{2}-\tilde{\sigma}_+\right) & 0 & \tilde{\sigma}_+^2 \end{pmatrix} \tag{5.37}$$

This matrix has eigenvalues $\{\sigma_+^2, \sqrt{2}\tilde{\sigma}_+, -\sqrt{2}\tilde{\sigma}_+\left(2-\frac{3}{\sqrt{2}}\tilde{\sigma}_+\right)\}$. This last eigenvalue represents a tachyonic mass for $0<\tilde{\sigma}_+<\frac{2\sqrt{2}}{3}$ with a minimum at $\tilde{\sigma}_+=\frac{\sqrt{2}}{3}$. We expect that fluctuations $\delta\sigma_{k-}^r$ will remain stable while both the fluctuations $\delta\sigma_{k+}^r$ and $\delta\phi_k^r$ will grow exponentially when $\tilde{\sigma}_+<\frac{2\sqrt{2}}{3}$. The maximum momentum of an unstable mode is $\frac{2}{3}\sqrt{\lambda}v$.

Similarly, for the fluctuations of the imaginary components we have

$$\left(\,\partial_{\tilde{t}}^2+\kappa^2+\mathcal{M}_{\rm i}^2\,\right)\begin{pmatrix} \delta\sigma_{k+}^i \\ \delta\sigma_{k-}^i \\ \delta\phi_k^i \end{pmatrix}=0 \tag{5.38}$$

where the mass matrix is

$$\mathcal{M}_{\rm i}^2 = \begin{pmatrix} \varphi^2+1+\frac{1}{2}\left(\tilde{\sigma}_+^2+\tilde{\sigma}_-^2\right) & -\tilde{\sigma}_+\tilde{\sigma}_- & 0 \\ -\tilde{\sigma}_+\tilde{\sigma}_- & \varphi^2-1+\frac{1}{2}\left(\tilde{\sigma}_+^2+\tilde{\sigma}_-^2\right) & 0 \\ 0 & 0 & \tilde{\sigma}_+^2+\tilde{\sigma}_-^2 \end{pmatrix} \tag{5.39}$$

Again, upon substituting the solution 5.34, we find

$$\mathcal{M}_{\rm i}^2 = \begin{pmatrix} 2-\sqrt{2}\tilde{\sigma}_+\left(1-\frac{\tilde{\sigma}_+}{\sqrt{2}}\right) & 0 & 0 \\ 0 & -\sqrt{2}\tilde{\sigma}_+\left(1-\frac{\tilde{\sigma}_+}{\sqrt{2}}\right) & 0 \\ 0 & 0 & \tilde{\sigma}_+^2 \end{pmatrix} \tag{5.40}$$

which, as expected, is diagonal. The mass-squared of $\delta\sigma_{k-}^i$ fluctuations is tachyonic for $0<\tilde{\sigma}_+<\sqrt{2}$ and minimal for $\tilde{\sigma}_+=\frac{1}{\sqrt{2}}$. The momenta as large as $\frac{1}{2}\sqrt{\lambda}v$.

Our initial conditions should be such that $\tilde{\sigma}_-(0)=0$ and the linearized equations of motion show that this will remain true inside our patch. Thus, as promised, the background depends only on $\varphi$ and $\tilde{\sigma}_+$. Furthermore, we see from (5.35) and (5.38) that, at least in the linear approximation, only the fluctuations of $\tilde{\sigma}_{k+}^r$ and $\varphi_k^r$ will be coupled.

Table 5.2 lists the initial conditions for several parameter sets (see the paragraph under equation (5.22)). Recall that $g^2=2\lambda$ for the F-term models.

| $v(\text{ GeV})$ | $\lambda$ | $\varphi(0)-1$ | $\tilde{\sigma}_+(0)$ |
|---|---|---|---|
| $10^{14}$ | $10^{-01}$ | $5\cdot 10^{-03}$ | $3\cdot 10^{-03}$ |
| $10^{14}$ | $10^{-02}$ | $5\cdot 10^{-04}$ | $3\cdot 10^{-04}$ |
| $10^{12}$ | $10^{-01}$ | $5\cdot 10^{-03}$ | $3\cdot 10^{-03}$ |
| $10^{12}$ | $10^{-02}$ | $5\cdot 10^{-04}$ | $3\cdot 10^{-04}$ |

Table 5.2: The initial values of the $\varphi = \phi_c^{-1}\phi$ and $\tilde{\sigma}_+ = \phi_c^{-1}\sigma_+$ fields for some of the parameters in Table 5.1. Note that $g^2 = 2\lambda$ for the F-term models.

Although the effective mass-square of fluctuations is negative in the tachyonic regime, we can still use the standard adiabatic particle number

$$n_k = \frac{1}{2\omega_k}\left(|\dot{\chi}_k|^2 + \omega_k^2|\chi_k|^2\right) - \frac{1}{2} \tag{5.41}$$

at all times if we apply the prescription $\omega_k^2 = |k^2+m^2|$. This will correspond to the true particle number near the minima of the potential where the effective mass-squared is positive. If the evolution is adiabatic, this will still be a meaningful number in the tachyonic regime. We will choose vacuum-like positive frequency initial conditions for the Fourier modes of the fluctuations $\delta\sigma_\pm^{r,i}$ and $\delta\phi^{r,i}$ as though they were initially massless. That is, we choose their amplitudes $\propto 1/\sqrt{2k}$.

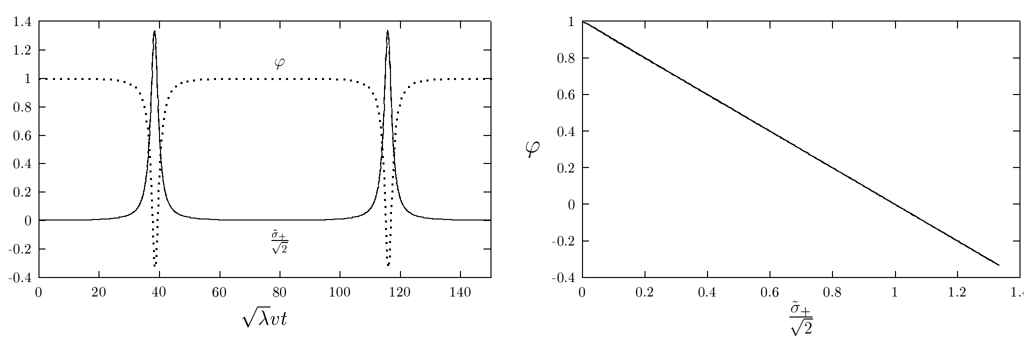


Figure 5.2: The left panel shows the evolution of the background fields $\frac{\tilde{\sigma}_+(t)}{\sqrt{2}}$ (dotted curve) and $\varphi(t)$ (solid curve) after symmetry breaking for the F-Term model with $\lambda = 10^{-2}$. The right panel shows several oscillations of the fields. They lie very near the line $\varphi + \frac{\tilde{\sigma}_+(t)}{\sqrt{2}} = 1$.

We now present the results of our linearized analysis. In figure (5.2) we show a numerical solution for the background fields $\tilde{\sigma}_+$ and $\varphi$ in the case $\lambda = 10^{-2}$, $v = 10^{14}\,\text{GeV}$. The left panel shows the time evolution of the two fields. They oscillate periodically in anti-phase with one another. The period in this case is about $74/\sqrt{\lambda}v$. In the right panel we show that the fields do, in fact, evolve along the line $\varphi + \frac{\tilde{\sigma}_{\pm}}{\sqrt{2}} = 1$ in field space.

It is straight forward to solve the fluctuation equations (5.35) and (5.38) in the presence of this background. In figure (5.3) we plot the number of produced particles after one whole inflaton oscillation. The left panel shows $n_k$ for the real parts of the fluctuation fields while the right panel is the same for the imaginary parts. We see that the fluctuations are enormously amplified by the tachyonic instability. As expected, $\delta\sigma^r_{k+}$ and $\delta\phi^r_k$ are similarly excited. We expected $\delta\sigma^r_{k-}$ fluctuations not to be amplified by the tachyonic effect. Nevertheless, the left panel of figure (5.3) shows that they are excited. This is due to two reasons. First, because of our initial conditions, the fields do not evolve exactly along the line (5.34). Thus, there is some residual coupling between $\delta\sigma^r_{k-}$ fluctuations and the exponentially amplified modes. Second, there is particle production due to regular parametric resonance as the background fields shoot through their minima.

Fluctuations of the imaginary parts behave similarly. The right hand panel of figure (5.3) shows that $\delta\sigma^i_{k-}$ fluctuations are significantly amplified, as expected. Also, $\delta\sigma^i_{k+}$ and $\delta\phi^i_k$, which are not tachyonically unstable, are amplified. Again, this is due both to residual mode coupling and the effect of parametric resonance as

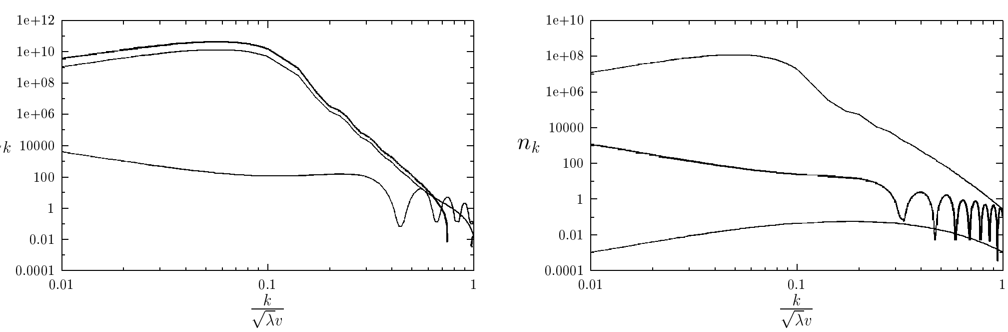


Figure 5.3: The right panel shows the occupation number $n_k$ of fluctuations in the real parts of the fields after one complete inflaton field oscillation, $\sqrt{\lambda}vt = 74$ in figure 5.2. From top to bottom, these results are for $\delta\sigma^r_{k+}$ , $\delta\phi^r_k$, and $\delta\sigma^r_{k-}$. The left panel shows the same thing for the imaginary parts. From top to bottom are $\delta\sigma^i_{k-}$ , $\delta\sigma^r_{k+}$, and $\delta\phi^r_k$ occupation numbers. The large amplitudes indicate that backreaction must be included in our calculations.

the background fields shoot through their minima. The reason the unstable modes grow so large is two-fold. Not only do they have a tachyonic mass for part of a background field oscillation, but this mass is also tachyonic near the turning points of the background fields. Thus, the effect of the tachyonic mass is strengthened by the increased time spent in the tachyonic region.

One thing is abundantly clear from figure (5.3): the occupation numbers of fluctuations rise very rapidly and to very large values with momenta as large as $k_{\rm max} \sim 0.1\sqrt{\lambda}v$. This means that the effects of backreaction should be incorporated essentially from the very beginning. Indeed, we can estimate the energy in fluctuations to be approximately $k^4_{\rm max} n_k \sim 10^6\, \lambda^2 v^4 \gg V_0$.

One might attempt to incorporate the effects of particle production by simply solving the self consistent mean field equations instead of our linearized ones. Thus, one would include in the effective mass of fluctuations a Hartree term $\sum_i g_i^2 < \delta\chi_i^2 >$, where the $\chi_i$ are each of the fluctuation fields and the $g_i^2$ are effective coupling constants. In this procedure, one would also incorporate the effect of these terms into the evolution equations for the background fields. This formalism is energy conserving so, as fluctuations grow, the amplitudes of the background fields decrease. For large enough fluctuations, or small enough background amplitudes, the tachyonic effect no longer occurs.

The problem with this self-consistent mean field approach (the Hartree approximation or any other mean field construction) is that the fluctuations are strongly correlated: they have large amplitudes and they interact strongly with each other. The physical reason for this is simple. SSB is an inherently non-linear, non-perturbative, irreversible phenomenon. Once a domain structure or string network is formed at $t \sim \mu^{-1}$, this structure is not static. The domains and strings will interact with each other, with themselves, and with "the background". In the asymptotic future, we know that the width of a domain wall (in the two-field case) or the diameter of a global string (in the F-term case) will depend on the mass of the Higgs field, $m_h$, *at its minimum* [7, 76]. Hence, we expect that, as the defects evolve, modes with $k \sim m_h = \sqrt{2\lambda}v$ will be very important. Note that this is entirely independent of the question of the initial separation scale for defects. This scale is $\mu^{-1} \sim (\sqrt{\lambda g^2}v)^{-1}$, in our case, ($g^2 = 2\lambda$ for the F-term model) and can be much larger than the characteristic width of the defects. Nevertheless, Fourier space is non-local; even if there is no defect near by, potentials that lead to SSB such as we consider here, lead to strong correlations and inhomogeneities on scales $k \lesssim \sqrt{\lambda}v$.

Fortunately, the large occupation numbers for fluctuations mean that we can use *classical* relativistic field theory to describe them. Basically, the fluctuations amplified by the SSB process initially will behave like classical waves that interact with each other. This classical system of waves can be put on a lattice and solved in real space. Thus, backreaction and correlations can be taken into account naturally. This is what we will do in the next section.

### 5.2.2 F-term: Lattice Solution

To fully solve the nonlinear equations in these models, it is necessary to put the fields on a three dimensional lattice. The lattice is an $N^3$ cubic grid of points with arrays representing the values of all the fields and their time derivatives at each point. The equations may then be solved using finite differencing for spatial derivatives. Our lattice program, LATTICEEASY [67], uses a staggered leapfrog algorithm in which the field values and their time derivatives are calculated at alternating times separated by a half time-step. We solved equations (5.31) using the rescaled, dimensionless variables $(\tilde{x}, \tilde{t}) \equiv \left(\sqrt{\lambda} v\right)(x, t)$, $(\tilde{\phi}, \tilde{\sigma}, \tilde{\bar{\sigma}}) \equiv \frac{1}{\phi_c}(\phi, \sigma, \bar{\sigma}) = \frac{\sqrt{2}}{\phi_c}(\Phi, \Sigma, \bar{\Sigma})$. In terms of these variables the equations of motion become

$$\begin{aligned}
\ddot{\tilde{\phi}} - \nabla^2\tilde{\phi} + \left[|\tilde{\bar{\sigma}}|^2 + |\tilde{\sigma}|^2\right]\tilde{\phi} &= 0\,, \\
\ddot{\tilde{\sigma}} - \nabla^2\tilde{\sigma} + \left[|\tilde{\phi}|^2 + |\tilde{\bar{\sigma}}|^2\right]\tilde{\sigma} &= \tilde{\bar{\sigma}}^*\,, \\
\ddot{\tilde{\bar{\sigma}}} - \nabla^2\tilde{\bar{\sigma}} + \left[|\tilde{\phi}|^2 + |\tilde{\sigma}|^2\right]\tilde{\bar{\sigma}} &= \tilde{\sigma}^*\,.
\end{aligned} \tag{5.42}$$

Initially the homogeneous component of $\phi$ (i.e. the zero mode) was set to one in dimensionless units. The homogeneous components of the field derivatives and the homogeneous components of the $\sigma$ fields were all set to zero initially. The real and imaginary components of all the fields began with vacuum fluctuations for which each mode in Fourier space was set with a Gaussian distribution with expectation value

$$\langle |f_k|^2 \rangle = \frac{1}{2k}. \tag{5.43}$$

and a random phase. An inverse Fourier transform converted these modes to values in real space, where the evolution equations were solved.

All the results shown in this paper used a grid of $128^3$ points with a total box size $L = 136$ in rescaled distance units. In all cases energy was conserved to within 3% over the entire run. The F-term results shown in this section were for $\lambda = 2.5 \times 10^{-5}$.

We expected the r.m.s. fields to follow the line (5.34). Simulations show that the homogeneous fields $\tilde{\phi}$ and $\tilde{\sigma}_+$ initially followed this trajectory but, within one oscillation of the inflaton field, fluctuations grew too large to speak meaningfully of the fields as homogeneous oscillators. These fluctuations grew in such a way that $\tilde{\sigma} = \tilde{\bar{\sigma}}^*$ almost exactly throughout the simulation. In other words $\delta\tilde{\sigma}_+^r$ and $\delta\tilde{\sigma}_-^i$ were excited while $\delta\tilde{\sigma}_+^i$ and $\delta\tilde{\sigma}_-^r$ were not. Because of this we only plot the fields $\tilde{\phi}$ and $\tilde{\sigma}$; it's understood in all the results that $\tilde{\bar{\sigma}}$ equals $\tilde{\sigma}^*$.

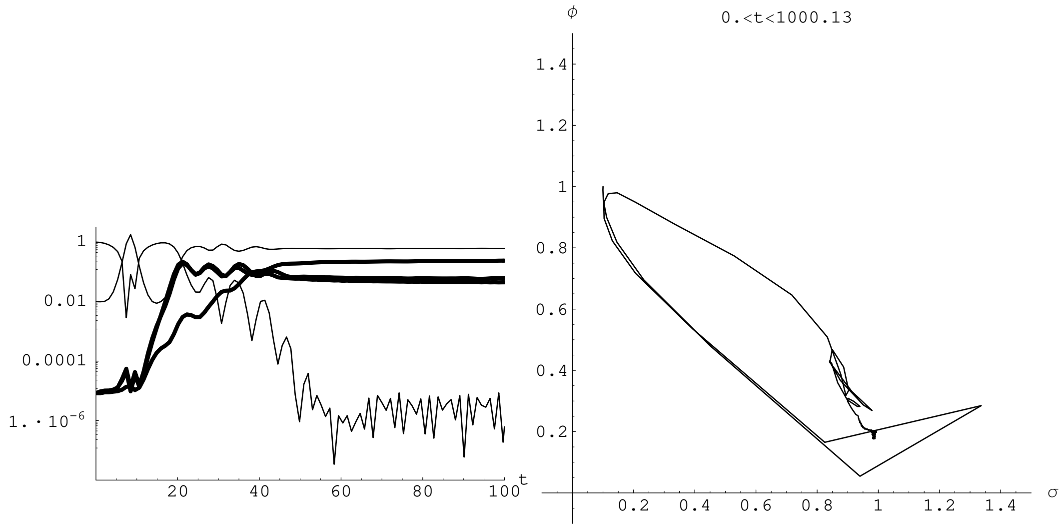


Figure 5.4: Left panel: Means and variances. The squared means $\langle\tilde{\phi}^r\rangle^2$ and $\langle\tilde{\sigma}^r\rangle^2$ are ordinary solid lines while the field variances $\langle\delta f^2\rangle$ are thick lines. The mean of $\tilde{\phi}^r$ starts at 1, oscillates once, and then decays. The mean of $\tilde{\sigma}^r$ grows in anti-phase to $\tilde{\phi}^r$. The variances of $\tilde{\phi}^r$ and $\tilde{\sigma}^r$ are nearly indistinguishable. The variance of $\tilde{\sigma}^i$ grows later but reaches a higher value than the other variances. The means of $\tilde{\phi}^i$ and $\tilde{\sigma}^i$ and the variance of $\tilde{\phi}^i$ were not significantly excited and aren't shown here. Right panel: the r.m.s. values $\langle\sqrt{|\tilde{\sigma}|^2}\rangle$ (horizontal axis) and $\langle\sqrt{|\tilde{\phi}|^2}\rangle$ (vertical axis) for the F-term model.

The left panel of figure 5.4 shows the evolution of the homogeneous fields $\langle\tilde{\phi}^r\rangle^2$ and $\langle\tilde{\sigma}^r\rangle^2$ and the fluctuations of $\tilde{\phi}^r$, $\tilde{\sigma}^r$, and $\tilde{\sigma}^i$. The inflaton undergoes one oscillation before decaying completely. Meanwhile $\tilde{\sigma}^r$ grows in anti-phase. (The small spike in the oscillation of $\langle\tilde{\phi}^r\rangle^2$ appears because the field mean was squared for the log plot, so it appears to grow when the mean briefly becomes negative.) While the inflaton decays, fluctuations of $\tilde{\phi}^r$ and $\tilde{\sigma}^r$ grow exponentially. Fluctuations of $\tilde{\sigma}^i$ grow a little later but ultimately become much larger than the fluctuations of $\tilde{\sigma}^r$. This difference is not surprising. The final distribution of $\tilde{\sigma}$ in the complex plane is closely concentrated around the unit circle. Because the mean value is at $\tilde{\sigma} = 1$ the majority of the spread is in the imaginary direction.

Fluctuations of $\tilde{\phi}^i$ do grow during the simulation, but the rate is so small that the growth would be undetectable if we included these fluctuations in figure 5.4. Extrapolating that growth forward it should take about $150,000$ dimensionless time units for the fluctuations of $\tilde{\phi}^i$ to reach 1.

The right panel of figure 5.4 shows the trajectory followed by the r.m.s. values of $\tilde{\phi}$ and $\tilde{\sigma}$. In the first oscillation, the trajectory closely follows equation (5.34).

Once fluctuations begin to grow, however, the r.m.s. values are correspondingly shifted upwards. The r.m.s. value of $\tilde{\sigma}$ ends very close to its minimum at $|\tilde{\sigma}| = 1$ but the spread in $\tilde{\phi}$ around its mean value of 0 gives it a nonzero r.m.s. value.

## 5.3 Preheating in the D-term Model

In this section we will analyze the evolution of D-term models after the end of inflation the same way we did for the F-term model. Neglecting the expansion of the universe, the field equations arising from the potential (5.30) are

$$\begin{aligned} \ddot{\Phi} - \nabla^2\Phi + 2g^2\left[|\Sigma_+|^2 + |\Sigma_-|^2\right]\Phi = 0 \ , \\ \ddot{\Sigma}_\pm - \nabla^2\Sigma_\pm + \left[2g^2|\Phi|^2 \mp \lambda v^2 + 2\lambda|\Sigma_\pm|^2 + 2g^2\left(1 - \frac{\lambda}{g^2}\right)|\Sigma_\mp|^2\right]\Sigma_\pm = 0 \ . \end{aligned} \tag{5.44}$$

First we consider the equations for the homogeneous background fields and linear perturbations around them. We calculate the amplification of linear fluctuations and find that backreaction due to the tachyonic instability becomes important very quickly and for arbitrary values of the parameter $\frac{g^2}{\lambda}$. Next we show the results of lattice simulations for D-term hybrid models with different values of $\frac{g^2}{\lambda}$.

### 5.3.1 D-term: Linearized Theory

Consider a patch of the universe where the complex fields $\Phi$, $\Sigma_+$ and $\Sigma_-$ are nearly homogeneous. Because the potential (5.29) is independent of the phases of the fields, we can, without lost of generality, set the initial values of the imaginary components to zero. We make the following substitutions for the background fields and fluctuations around them.

$$\begin{aligned} \Phi(x,t) &= \frac{1}{\sqrt{2}}\left(\phi(t) + \delta\phi^r(x,t) + i\delta\phi^i(x,t)\right) \ , \\ \Sigma_\pm(x,t) &= \frac{1}{\sqrt{2}}\left(\sigma_\pm(t) + \delta\sigma_\pm^r(x,t) + i\delta\sigma_\pm^i(x,t)\right) \ . \end{aligned} \tag{5.45}$$

Again, it is convenient to work with dimensionless variables, in this section we will redefine the space-time variables $(\tilde{x}, \tilde{t}) \equiv \left(\sqrt{\lambda}v\right)(x,t)$ and fields $\varphi \equiv \phi_c^{-1}\phi$, $\tilde{\sigma}_\pm \equiv \phi_c^{-1}\sigma_\pm$. This rescaling will allow us to remove all dimensionful parameters from our equations. In these variables, it will be helpful to remember that the bifurcation point corresponds to $\varphi = 1, \tilde{\sigma}_\pm = 0$ and the global minimum of the potential (5.29) corresponds to $\varphi = \sigma_- = 0$, $\tilde{\sigma}_+ = \sqrt{\frac{g^2}{\lambda}}$.

The equations for the background fields, neglecting the back-reaction of fluctuations, are

$$\begin{aligned}
\ddot{\tilde{\sigma}}_+ + \left[\varphi^2 - 1 + \left(1 - \frac{\lambda}{g^2}\right)\tilde{\sigma}_-^2 + \frac{\lambda}{g^2}\tilde{\sigma}_+^2\right]\tilde{\sigma}_+ = 0\ ,\\
\ddot{\tilde{\sigma}}_- + \left[\varphi^2 + 1 + \left(1 - \frac{\lambda}{g^2}\right)\tilde{\sigma}_+^2 + \frac{\lambda}{g^2}\tilde{\sigma}_-^2\right]\tilde{\sigma}_- = 0\ ,\\
\ddot{\varphi} + \left(\tilde{\sigma}_+^2 + \tilde{\sigma}_-^2\right)\varphi = 0\ .
\end{aligned} \tag{5.46}$$

For the Fourier modes of the fluctuations of the real components of the fields we obtain

$$(\,\partial_0^2 + \kappa^2 + \mathcal{M}_{\mathrm{r}}^2\,)\begin{pmatrix}\delta\tilde{\sigma}_{k+}^r\\ \delta\tilde{\sigma}_{k-}^r\\ \delta\phi_k^r\end{pmatrix} = 0 \tag{5.47}$$

where the mass matrix is

$$\mathcal{M}_{\mathrm{r}}^2 = \begin{pmatrix} \varphi^2-1+\left(1-\frac{\lambda}{g^2}\right)\tilde{\sigma}_-^2+3\frac{\lambda}{g^2}\tilde{\sigma}_+^2 & 2\left(1-\frac{\lambda}{g^2}\right)\tilde{\sigma}_+\tilde{\sigma}_- & 2\varphi\tilde{\sigma}_+\\ 2\left(1-\frac{\lambda}{g^2}\right)\tilde{\sigma}_+\tilde{\sigma}_- & \varphi^2+1+\left(1-\frac{\lambda}{g^2}\right)\tilde{\sigma}_+^2+3\frac{\lambda}{g^2}\tilde{\sigma}_-^2 & 2\varphi\tilde{\sigma}_-\\ 2\varphi\tilde{\sigma}_+ & 2\varphi\tilde{\sigma}_- & \tilde{\sigma}_+^2+\tilde{\sigma}_-^2 \end{pmatrix} \tag{5.48}$$

For the fluctuations of the imaginary components we have

$$(\,\partial_0^2 + \kappa^2 + \mathcal{M}_{\mathrm{i}}^2\,)\begin{pmatrix}\delta\tilde{\sigma}_{k+}^i\\ \delta\tilde{\sigma}_{k-}^i\\ \delta\phi_k^i\end{pmatrix} = 0 \tag{5.49}$$

where the mass matrix is

$$\mathcal{M}_{\mathrm{i}}^2 = \begin{pmatrix} \varphi^2-1+\left(1-\frac{\lambda}{g^2}\right)\tilde{\sigma}_-^2+\frac{\lambda}{g^2}\tilde{\sigma}_+^2 & 0 & 0\\ 0 & \varphi^2+1+\left(1-\frac{\lambda}{g^2}\right)\tilde{\sigma}_+^2+\frac{\lambda}{g^2}\tilde{\sigma}_-^2 & 0\\ 0 & 0 & \tilde{\sigma}_+^2+\tilde{\sigma}_-^2 \end{pmatrix} \tag{5.50}$$

We solve the equations for the background fields and fluctuations for the D-term hybrid model numerically. Again we use positive frequency vacuum initial conditions for the fluctuations. The behavior of the background oscillations depends on the ratio $\frac{g^2}{\lambda}$. In all cases the background field $\tilde{\sigma}_-(t)$ remains zero, so we can work with two real quasi-homogeneous fields: $\tilde{\sigma}_+(t)$ and $\varphi(t)$. In figures 5.5, 5.7, and 5.9 we plot the evolution of the background fields $\varphi$ and $\tilde{\sigma}_+$ for several values of the parameter $\frac{g^2}{\lambda}$. In each figure, the left panel shows the time

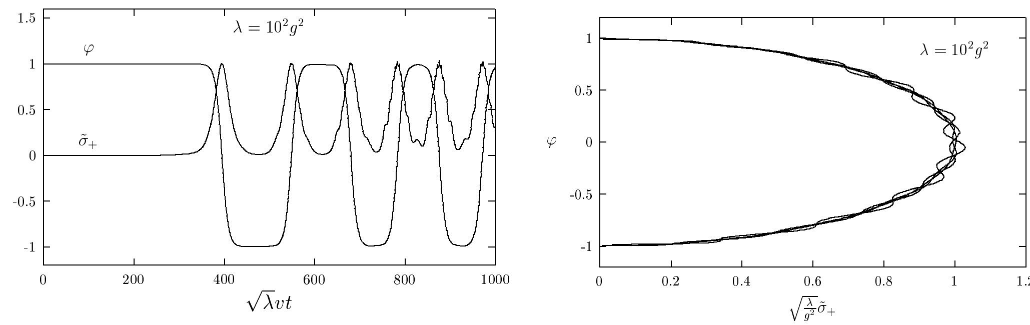


Figure 5.5: Evolution of the two background fields in the D-term model with $\lambda = 10^2 g^2$. In this case, the $\varphi$ field dominates the oscillations with the $\tilde{\sigma}_+$ field making smaller amplitude oscillations.

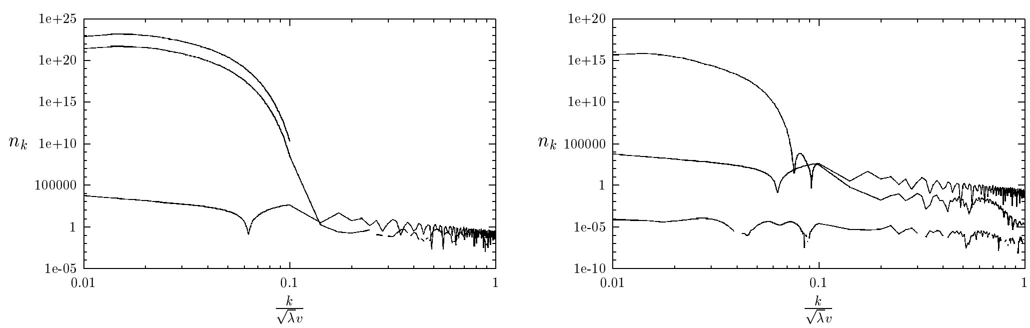


Figure 5.6: Amplification of fluctuations in the D-term theory with $\lambda = 10^2 g^2$. The left panel shows the occupation number for fluctuations of the real parts of the fields. Top to bottom are $\delta\sigma^r_{k+}$, $\delta\phi^r_k$, and $\delta\sigma^r_{k-}$. The right panel is for the imaginary parts. Top to bottom are $\delta\sigma^i_{k+}$, $\delta\sigma^i_{k-}$, and $\delta\phi^i_k$.

evolution of the fields while the right panel shows the fields' trajectories in the $(\varphi, \tilde{\sigma}_+)$ plane. The occupation numbers of fluctuations for these models are shown in figures 5.6, 5.8, and 5.10. In each case, the left panel shows the fluctuations on the real parts while the right panel is for fluctuations in the imaginary part. In every case, the growth of fluctuations is tremendous, indicating that backreaction must be incorporated.

In each case, we have chosen $v = 10^{14}\,\mathrm{GeV}$, but this was not important for the results. In figure 5.5, we show the case $\lambda = 10^{-3}$ , $g^2 = 10^{-1}$. We see that the oscillations are dominated by the $\tilde{\sigma}_+$ field. Note that the true vev of $\tilde{\sigma}_+$ is at $\sqrt{\frac{g^2}{\lambda}} = 10$, but we have scaled this out in the figure. Figure 5.6 shows the occupation number of particles created after just one complete oscillation of the $\tilde{\sigma}_+$

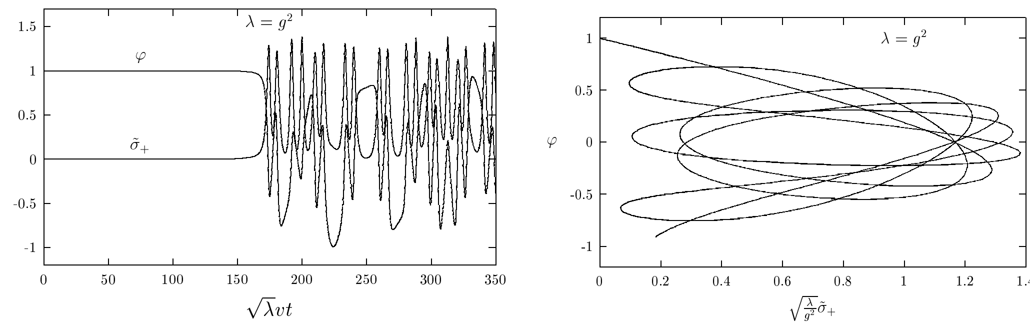


Figure 5.7: Evolution of the two background fields in the D-term model with $\lambda = g^2$. In this case, neither field dominates the oscillations which are quite chaotic.

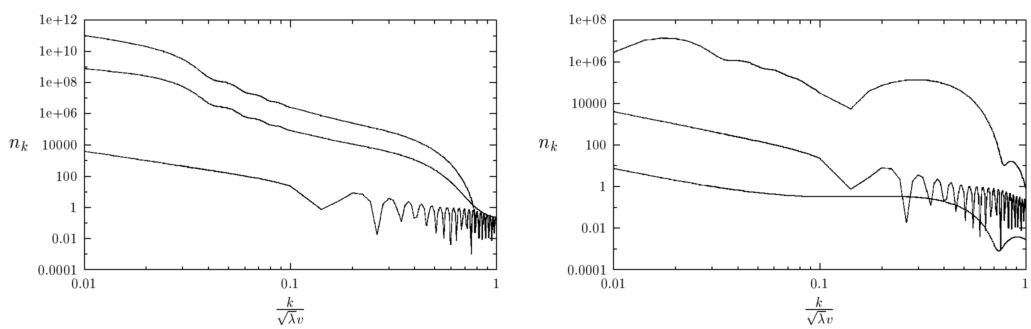


Figure 5.8: Amplification of fluctuations in the D-term theory with $\lambda = g^2$. The left panel shows the occupation number for fluctuations of the real parts of the fields. Top to bottom are $\delta\sigma^r_{k+}$, $\delta\phi^r_k$, and $\delta\sigma^r_{k-}$. The right panel is for the imaginary parts. Top to bottom are $\delta\sigma^i_{k+}$, $\delta\sigma^i_{k-}$, and $\delta\phi^i_k$.

field. Figure 5.7 is for the case $\lambda = 10^{-2} = g^2$. The oscillations when $g^2 \sim \lambda$ are not dominated by either field and are quite chaotic. Figure 5.8 shows the occupation number of particles in this case. As neither field dominates, we have chosen an arbitrary time shortly after the start of oscillations ($t = 187\sqrt{\lambda}v$). Figure 5.9, we show the case $\lambda = 10^{-1}$ , $g^2 = 10^{-3}$. We see that the oscillations are dominated by the $\varphi$ field along an ellipse in field space. $\tilde{\sigma}$ makes small oscillations along the path. Note that the true vev of $\tilde{\sigma}_+$ is at $\sqrt{\frac{g^2}{\lambda}} = 0.1$, but we have scaled this out in the figure. Figure 5.10 shows the occupation number of particles created after one complete oscillation of the $\varphi$ field.

Note that, once again, in every case modes are excited at least up to $k = 0.1\sqrt{\lambda}v$. In the cases with $\frac{g^2}{\lambda} \gtrsim 1$, the negative curvature of the potential is greatest

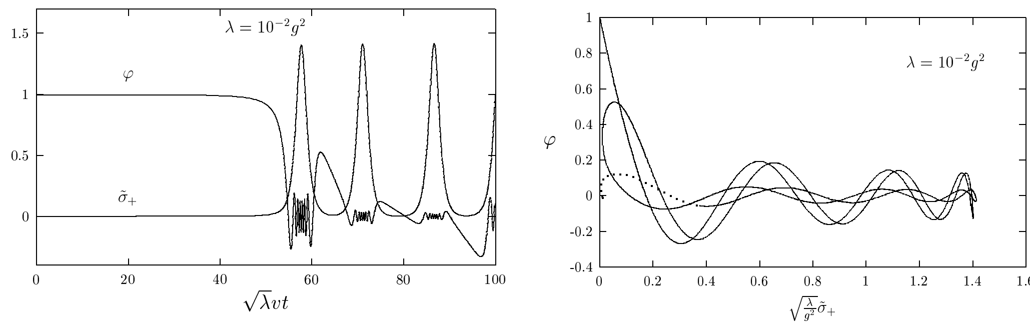


Figure 5.9: Evolution of the two background fields in the D-term model with $\lambda = 10^{-2}g^2$. In this case, the $\tilde{\sigma}_+$ field dominates the oscillations with the $\varphi$ field making smaller amplitude oscillations.

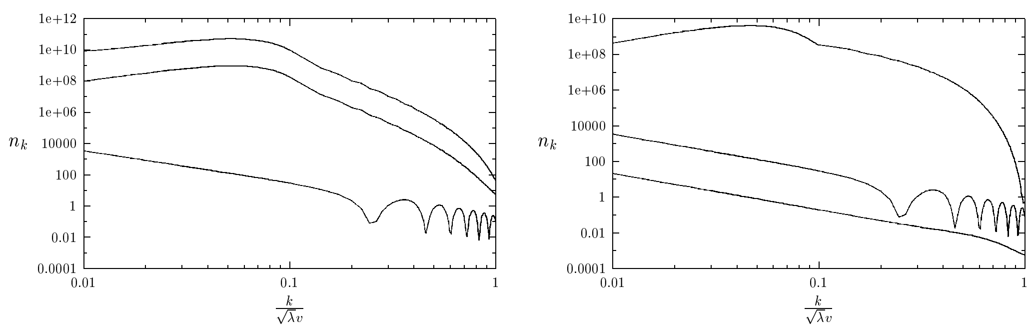


Figure 5.10: Amplification of fluctuations in the D-term theory with $\lambda = 10^{-2}g^2$. The left panel shows the occupation number for fluctuations of the real parts of the fields. Top to bottom are $\delta\sigma^r_{k+}$, $\delta\phi^r_k$, and $\delta\sigma^r_{k-}$. The right panel is for the imaginary parts. Top to bottom are $\delta\sigma^i_{k+}$, $\delta\sigma^i_{k-}$, and $\delta\phi^i_k$.

near the bifurcation point. As a result, the modes most strongly amplified are actually hard modes $k \sim \sqrt{\lambda}v$ that are generated due to the tachyonic instability immediately after the bifurcation point, see figures 5.6 and 5.8. This occurs because large $\tilde{\sigma}$ oscillations push the fields into the region where the tachyonic effect is strongest. Amplification of the fluctuations is stronger in this case than for $\lambda \gtrsim g^2$.

Over all, for all values of $\frac{g^2}{\lambda}$ the picture is similar: preheating in the D-term models is tachyonic and very strong, and one has to take the backreaction of fluctuations into account. We can again estimate the energy in fluctuations. In each case it is many orders of magnitude greater than that available from $V_0$.

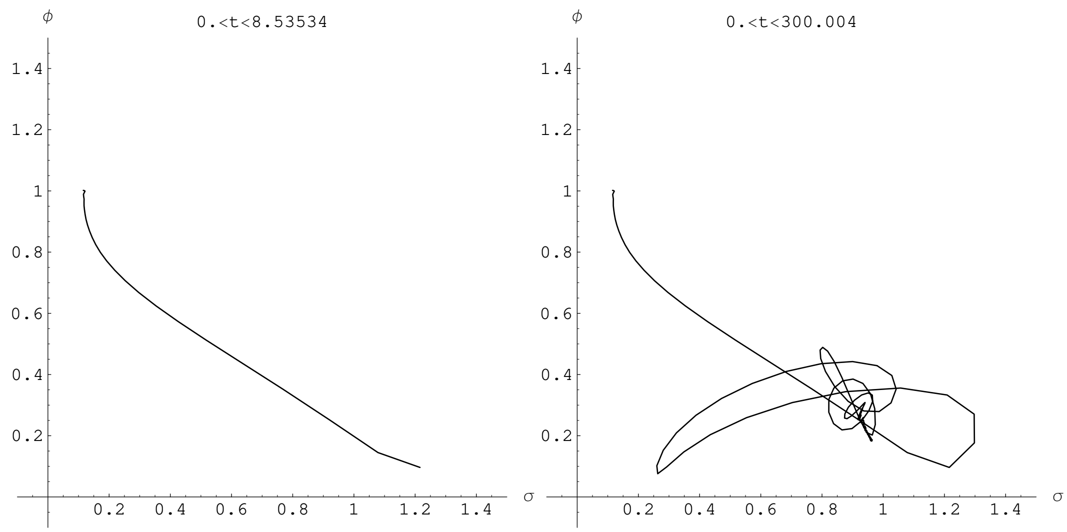


Figure 5.11: The r.m.s. values $\langle\sqrt{|\tilde{\sigma}_+|^2}\rangle$ (horizontal axis) and $\langle\sqrt{|\varphi|^2}\rangle$ (vertical axis) for D-term inflation with $g^2 = \lambda$.

### 5.3.2 D-term: Lattice Solution

We performed a series of lattice simulations of D-term models with different values of $\frac{g^2}{\lambda}$. The methods used in the lattice simulations were discussed in section 5.2.2. As in the F-term case, the initial values of the homogeneous components for the $\sigma$ fields were set to zero and for the $\varphi$ field to 1. As expected, in all versions of D-term inflation that we considered, the field $\tilde{\sigma}_-$ was never significantly excited. It is not shown in the plots below.

As in F-term inflation, $\langle\tilde{\sigma}^r_+\rangle$ grows while $\langle\varphi^r\rangle$ falls, all within the first oscillation of the inflaton. The variances of $\tilde{\sigma}^r_+$ and $\tilde{\sigma}^i_+$ grow at the same time and fluctuations of $\varphi^r$ grow shortly afterwards.

For $g^2 = 10^2\lambda$ the minimum of the potential is at $\tilde{\sigma}_+ = 10$ rather than $\tilde{\sigma}_+ = 1$, so the means and fluctuations of $\tilde{\sigma}_+$ grow much larger than $\varphi$ in this model. For this model the fluctuations of $\varphi^r$, $\tilde{\sigma}^r_+$, and $\tilde{\sigma}^i_+$ grow much sooner than the mean value $\langle\tilde{\sigma}^r_+\rangle$. Once the mean of $\tilde{\sigma}^r_+$ grows, the variance of $\tilde{\sigma}^r_+$ shrinks for the reasons discussed in section 5.2.2. The values of $\langle(\delta\tilde{\sigma}^i_+)^2\rangle$ and $\langle(\delta\sigma^r_+)^2\rangle$ were nearly identical by the end of the run.

Although fluctuations of $\varphi^i$ and $\tilde{\sigma}_-$ did not grow appreciably during the time of the run, they were growing slowly for the $g^2 = \lambda$ model. Extrapolating that growth forward $\varphi^i$ and $\sigma_-$ would reach 1 at $t \approx 75,000$ and $t \approx 200,000$ respectively. In the $g^2 = 10^2\lambda$ model these fields had a small burst of initial growth and then decreased slowly throughout the rest of the run.

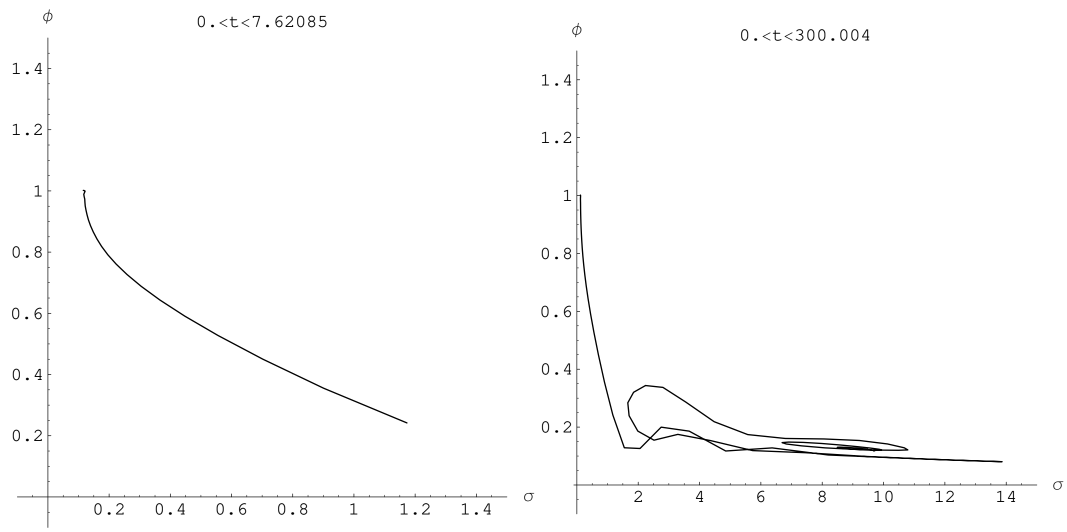


Figure 5.12: The *r.m.s.* values $\langle\sqrt{|\sigma|^2}\rangle$ (horizontal axis) and $\langle\sqrt{|\phi|^2}\rangle$ (vertical axis) for D-term inflation with $g^2 = 10^2\lambda$.

Figure 5.11 shows the trajectory of the r.m.s. values of $\varphi$ and $|\tilde{\sigma}_+|$ for $g^2 = \lambda$. The initially smooth trajectory is chaotic much like the linear solution shown in figure 5.7. As energy is lost to fluctuations, however, the trajectory quickly becomes trapped near the minimum of the potential. The $\tilde{\sigma}_+$ field makes what at most could be called two oscillations.

In figure 5.12 we show the trajectories of the r.m.s. values of $\varphi$ and $|\tilde{\sigma}_+|$ for $g^2 = 10^2\lambda$. We see that the field quickly moves towards its vev, having dissipated its energy into fluctuations. This should be compared with figure 5.9.

Figure 5.13 shows the process of spontaneous symmetry breaking and tachyonic preheating in D-term inflation for $g^2 = 10^{-2}\lambda$. This time, we have plotted a histogram showing the number of lattice sites (vertical axis) with the corresponding field values (horizontal plane). As in figure 5.5, we see that the fields move along the ellipse $\varphi^2 + \frac{\lambda}{g^2}\tilde{\sigma}_+^2 = 1$. The probability distribution relaxes quickly to the minimum of the effective potential, within a single oscillation.

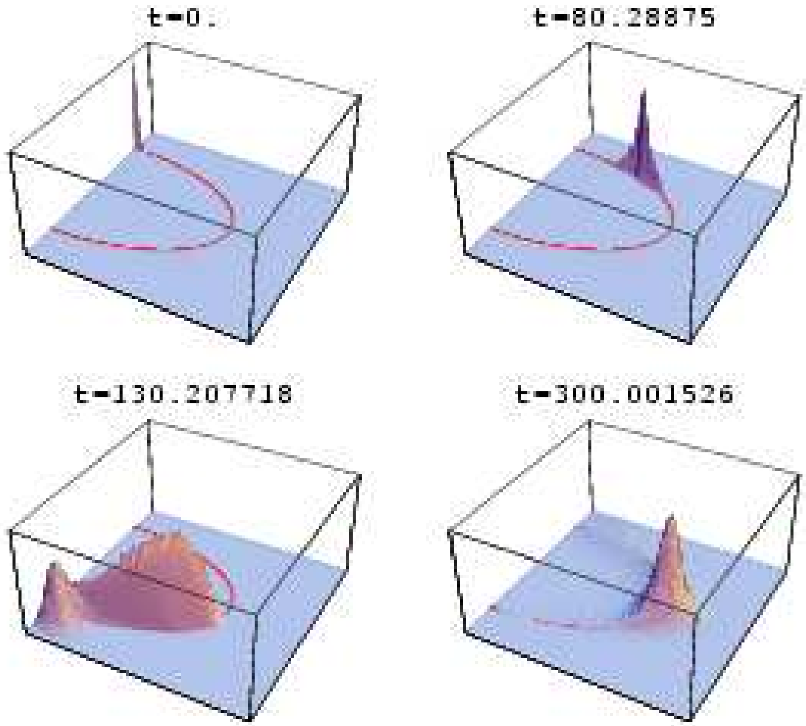


Figure 5.13: A histogram plot of the process of symmetry breaking and tachyonic preheating in the D-term hybrid inflation model for $g^2 \ll \lambda$. The field distribution moves along the ellipse $\varphi^2 + \frac{\lambda}{g^2}\tilde{\sigma}_+^2 = 1$ from the bifurcation point $\varphi = 1$, $\tilde{\sigma}_+ = 0$. It makes only one oscillation before settling near its true vev at $\varphi = 0$, $\tilde{\sigma}_+ = \sqrt{\frac{g^2}{\lambda}}$. Note, however, the large dispersion in the fields around this point at late times.

## 5.4 Discussion

Thus we see that tachyonic preheating is a typical feature of hybrid inflation. The production of bosons in this regime is non-perturbative, very fast, and efficient, but it is usually not related to parametric resonance. Instead it is related to the production and scattering of classical waves of the scalar fields. Of course, one should keep in mind that there may exist some particular versions of hybrid inflation in which tachyonic preheating is inefficient, e.g. because of fast motion of the field $\phi$ near the bifurcation point.

So far we have discussed tachyonic preheating in the inflaton sector of hybrid models, which leads to the decay of the homogeneous fields and the excitation of their fluctuations. Preheating in the non-inflaton sector and the subsequent development of equilibrium in hybrid models were considered in [39]. Light bosonic fields interacting with scalars from the inflaton sector are dragged into the process of preheating. Excitations of these fields rapidly acquire large occupation numbers and further evolve into equilibrium together with the scalars from the inflaton sector.

The tachyonic nature of preheating in hybrid inflation implies, in particular, that instead of the production of gravitinos by a coherently oscillating field [57, 77], in hybrid inflation one should study gravitino production due to the scattering of classical waves of the scalar fields produced by tachyonic preheating. Our results may also be important for the theory of the generation of the baryon asymmetry of the universe at the electroweak scale [78].

# Chapter 6

# Conclusion

In this thesis we have reviewed some results in the theory of preheating after inflation. We began with an investigation of the development of parametric resonance in the conformally invariant theories of the type $\frac{1}{4}\lambda\phi^4 + \frac{1}{2}g^2\phi^2\chi^2$. We found that the development of parametric resonance in these theories does not depend on the expansion of the universe, and can be classified in terms of the ratio $\frac{g^2}{\lambda}$. This ratio determines the structure of the stability/instability bands for the equations describing the resonance. We found that the strength of the resonance with respect to $\chi$-particle production is a non-monotonic function of $\frac{g^2}{\lambda}$. The non-monotonic dependence of the characteristic exponent $\mu$ on the ratio $\frac{g^2}{\lambda}$ suggests that there exists an "unnatural selection" rule: The particles which are most intensively produced during preheating are not the ones which have the strongest coupling to the inflaton field, but those for which the characteristic exponent $\mu(\frac{g^2}{\lambda})$ is the greatest.

In the conformally invariant theories, the expansion of the universe does not hamper the resonance, so it ends only due to the backreaction of the produced particles. We found that there are several different mechanisms which may terminate the parametric resonance. First of all, creation of particles leads to a decrease in the amplitude of oscillation of the field $\varphi = a\phi$, which otherwise would remain constant. This leads to a proportional decrease in the frequency of oscillations in terms of the conformal time $\eta$, which may shift the position of the instability band towards smaller momenta. There is also an opposing effect which increases the frequency of oscillations due to the interaction of the homogeneous inflaton field with the produced particles. Finally, quantum fluctuations of the fields $\phi$ and $\chi$ acquire contributions to their masses, which changes their spectra. A combination of all these effects leads to restructuring of the instability bands. This terminates the amplification of the leading modes which have been growing from the very beginning of preheating. We found that our simple estimates ignoring the process of rescattering of produced fluctuations gave results in good numerical agreement with the results of computer simulations of reheating in the theory $\frac{1}{4}\lambda\phi^4$ performed in [37] where all of these effects, including rescattering, have been taken into account.

We also found that the addition of even a small mass term would completely change the character of the resonance, leading to stochastic resonance. We developed "phase diagrams" showing how p/reheating will develop for different parameter ranges in the more general theories $\pm\frac{1}{2}m_\phi^2\phi^2 + \frac{1}{4}\lambda\phi^4 + \frac{1}{2}g^2\phi^2\chi^2$. These diagrams allow a synthesis of the results from several different studies of preheating. One of the important results is that the complete perturbative decay of the inflaton will only occur in the theories of this type with spontaneous symmetry breaking.

We then investigated the role of fermions in preheating for the conformal theory. Again, we found that the expansion of the universe played no role and that fermion production could be described by a simple "master equation" similar to the master equation in the bosonic case. Although the Pauli principle prevents the unbounded growth in fermion occupation number, we found that fermions are typically created in a manner very different from what would be expected perturbatively. We developed analytic results for the production of fermions in the conformal case and when expansion can otherwise be neglected. We found that a considerable fraction of the inflaton's energy can be transfered to fermions in only a few inflaton oscillations.

We next studied fermion production when the expansion of the universe could not be neglected. In this case, the analytic results found previously could not be applied, but we were able to extend the method of successive parabolic scatterings to fermion production. We found that, just as in the bosonic case, fermions can be created spontaneously due to the non-adiabatic evolution of their effective mass. By treating the phase accumulated between successive scatterings as a random variable, we were able to estimate the final spectrum of massive fermions in the expanding universe.

One very important result is that supermassive fermions with $m_\psi \lesssim h\phi_0 \lesssim 10^{17}\,\mathrm{GeV}$ can be produced. This is different from the bosonic case where massive bosons are limited by $m_\chi \lesssim \sqrt{g\phi_o m_\phi} < 10^{15}\,\mathrm{GeV}$. This implies, for example, that only fermionic preheating can be responsible for leptogenesis via the non-equilibrium production of SUSY GUT fermions with SUSY GUT masses $m_\psi \sim 10^{16}\,\mathrm{GeV}$ [17]. The GUT bosons could not be produced. Furthermore, such supermassive fermions may survive as relic particles contributing to the cold dark matter of the universe [16],[17].

Finally, we turned to the problem of reheating after hybrid inflation. We found that, contrary to earlier expectations, there is no stage of homogeneous oscillations for the inflaton and Higgs fields. A new effect, tachyonic preheating, destroys the coherence of the inflaton sector fields and leads to large amplitude, long wavelength fluctuations of these fields, just as if parametric resonance had occurred. We showed that the rapid growth of fluctuations makes a linearized mean field analysis useless after just one oscillation of the "background" fields. Because the large amplitude bose fields can be treated like classical waves, we were able to analyze reheating in hybrid inflation using lattice simulations. These simulations confirmed that no prolonged stage of coherent background oscillations occurs and that most of the false vacuum energy of the Higgs field is transfered to fluctuations within the first two oscillations. This new effect was termed tachyonic preheating and we saw that it will occur for a wide range of the parameter $\frac{g^2}{\lambda}$.

As a final comment, we would like to note that the insights gained by studying preheating after inflation have uses in other contexts. Fundamental scalar fields are ubiquitous in modern cosmology and particle physics. They have been introduced by cosmologists and particle theorists alike to solve various problems in fundamental theory. In addition to the inflaton field, other important scalar fields include the axion which particle theorists introduced to solve the strong CP problem of QCD, supersymmetric *sparticles* which are motivated by string theory and the SUSY solution to the hierarchy problem of the Standard Model, moduli, polonyi, dilaton, and radion fields introduced by supergravity and string theory, and of course the Standard Model Higgs field.

It is natural, particularly in the context of inflationary cosmology, for some of these scalar fields to be displaced from their true vevs and undergo coherent oscillations at some epoch in the early universe. The methods of preheating would then be applicable to these fields as well. In fact, parametric resonance has already been considered for axions [79] and moduli [80]. We expect tachyonic preheating will be important as well.

# Appendix A

# Notation

Throughout this thesis we use units such that $\hbar = c = 1$. We work with the Planck mass defined as

$$M_p \;=\; G^{-1/2} \;\approx\; 1.22 \cdot 10^{19}\,\mathrm{GeV}\,. \tag{A.1}$$

We will only be concerned with flat FRW metrics of the form

$$g_{\mu\nu} = \mathrm{diag}\{+1, -a^2(t), -a^2(t), -a^2(t)\}\,, \tag{A.2}$$

where $a(t)$ is the scale factor of the universe. Notice that our signature convention is that of Landau and Lifshitz [81]–the usual one in particle physics.

We use the Dirac-Pauli representation of the Dirac matrices. In terms of the usual Pauli spin matrices $\sigma^i$, these are

$$\gamma_0 = \begin{pmatrix} 1 & 0 \\ 0 & -1 \end{pmatrix} \quad , \quad \gamma_i = \begin{pmatrix} 0 & \sigma^i \\ -\sigma_i & 0 \end{pmatrix} \quad , \quad \gamma_5 = \begin{pmatrix} 0 & 1 \\ 1 & 0 \end{pmatrix}\,, \tag{A.3}$$

so that $\gamma_0$ and $\gamma_5$ are Hermitian and the $\gamma_i$'s are anti-Hermitian. Furthermore, we define $\gamma_{\mu\nu} = \frac{1}{2}(\gamma_\mu\gamma_\nu - \gamma_\nu\gamma_\mu)$. The helicity operator is defined in terms of the spin matrix $\hat{\mathbf{k}} \cdot \Sigma$ where

$$\Sigma^i = \begin{pmatrix} \sigma^i & 0 \\ 0 & \sigma^i \end{pmatrix}\,. \tag{A.4}$$

The vierbein $e^a_\mu$ of basis vectors is used to covariantize the Dirac equation, c.f. [82, 81]. In terms of these ortho-normal basis vectors, the metric may be written $g_{\mu\nu} = \eta_{ab} e^a_\mu e^b_\nu$, where $\eta_{ab} = \mathrm{diag}\{+1, -1, -1, -1\}$ is the flat space metric. We take the four basis vectors to be

$$e^0_\mu = \delta^0_\mu \qquad , \qquad e^i_\mu = a(t)\delta^i_\mu\,. \tag{A.5}$$

We define curved space Dirac matricies as $\bar{\gamma}_\mu = e^a_\mu \gamma_a$, where the un-barred gammas are the flat space ones above. Note that $\{\bar{\gamma}_\mu, \bar{\gamma}_\nu\} = g_{\mu\nu}$.

The connection coefficients may be written

$$\begin{aligned}\Gamma^\rho_{\mu\nu} &= \frac{1}{2} g^{\rho\sigma} \left[2 g_{\sigma(\mu,\nu)} - g_{\mu\nu,\sigma}\right] \\ &= \delta^\rho_i \delta^i_{(\mu} \delta^0_{\nu)} \left(\frac{\dot{a}}{a}\right) \text{, no sum on } i\,.\end{aligned} \tag{A.6}$$

The covariant derivative on Dirac spinors contains the spin connection: $D_\mu = \partial_\mu + \Gamma^{(1/2)}_\mu$, where $\Gamma^{(1/2)}_\mu$ is given by

$$\begin{aligned}\Gamma^{(1/2)}_\mu &= \frac{1}{4} \omega^{ab}_\mu \gamma_{ab} = \frac{1}{4} \gamma_{ab} \left(g^{\nu\rho} e^a_\nu e^b_{\rho;\mu}\right) \\ &= \frac{3}{2} \left(\frac{\dot{a}}{a}\right) \delta^0_\mu\,,\end{aligned} \tag{A.7}$$

where " ; " represents the covariant derivative with connection coefficients (A.6).

# Bibliography


[1] A. Linde, Contribution to the Proceedings of PASCOS 2001 , hep-th/0107176.

[2] A. Guth, Phys. Rev. **D23**, 347 (1981).

[3] A. Linde, Phys. Lett. **B108**, 389 (1982).

[4] A. Albrecht and P. Steinhardt, Phys. Rev. Lett. **48**, 1220 (1982).

[5] A. D. Dolgov and A. D. Linde, Phys. Lett. **B116**, 329 (1982).

[6] L. F. Abbott, E. Fahri, and M. Wise, Phys. Lett. 29 (1982).

[7] A. Linde, *Particle Physics and Inflationary Cosmology* (Harwood, Chur, Switzerland, 1990).

[8] J. Traschen and R. Brandenberger, Phy. Rev. **D42**, 2491 (1990).

[9] L. Kofman, A. Linde, and A. A. Starobinsky, Phys. Rev. Lett. **73**, 3195 (1994).

[10] E. Kolb and M. Turner, *The Early Universe* (Addison-Wesley, New York, 1990).

[11] P. B. Greene, L. Kofman, A. Linde, and A. A. Starobinsky, Phys. Rev. **D56**, 6175 (1997), hep-ph/9705347.

[12] P. B. Greene and L. Kofman, Phys. Lett. **B448**, 6 (1999), hep-ph/9807339.

[13] J. Baacke, K. Heitmann, and C. Pätzold, Phys. Rev. **D58**, 125013 (1998), hep-ph/9806205.

[14] P. B. Greene and L. Kofman, Phys. Rev. **D62**, 123516 (2000), hep-ph/0003018.

[15] L. Kofman, A. Linde, and A. A. Starobinsky, Phy. Rev. **D56**, 3258 (1997), hep-ph/9704452.

[16] P. B. Greene, in *Proceedings of COSMO-98, Nov. 1998*, Ed. D. Caldwell (AIP Press, NY, 1999).

[17] G. Giudice, M. Peloso, A. Riotto, and I. Tkachev, JHEP 9908 (1999), hep-ph/9905242.

[18] G. Felder, J. García-Bellido, P. B. Greene, L. Kofman, A. Linde, and I. Tkachev, Phys. Rev. Lett. **87**, 011601 (2001), hep-ph/0012142.

[19] G. Felder, J. García-Bellido, P. B. Greene, L. Kofman, A. Linde, and I. Tkachev, , in preparation.

[20] A. Linde, Phys. Lett. **B129**, 177 (1983).

[21] N. B. Narozhnyi and A. I. Nikishov, Sov. Phys. JETP 427 (1974).

[22] M. V. Mostepanenko and V. M. Frolov, Sov. J. Nucl. Phys. 885 (1974).

[23] V. S. Popov, Sov. J. Nucl. Phys. 1140 (1974).

[24] A. A. Grib, S. G. Mamayev, and V. M. Mostepanenko, *Vacuum Quantum Effects in Strong Fields* (Friedmann Laboratory, St. Petersburg, 1994).

[25] A. D. Dolgov and D. P. Kirilova, Sov. J. Nucl. Phys. 172 (1990).

[26] L. Kofman, in *Proceedings of the 8th Canadian Conference on General Relativity and Relativistic Astrophysics*, McGill University, June 10-12, 1999 (AIP, NY, 2000).

[27] V. Zanchin, A. Maia Jr., W. Craig, and R. Brandenberger, Phy. Rev. **D57**, 4651 (1998), hep-ph/9709273.

[28] B. Basset, Phy. Rev. **D58**, 021303 (1998), hep-ph/9709443.

[29] V. Zanchin, A. Maia Jr., W. Craig, and R. Brandenberger, Phy. Rev. **D60**, 023505 (1999), hep-ph/9901207.

[30] G. Felder, L. Kofman, and A. Linde, Phys. Rev. **D59**, 123523 (1999), hep-ph/9812289.

[31] B. R. Greene, T. Prokopec, and T. G. Roos, Phys. Rev. **D56**, 6484 (1997).

[32] F. da Rocha Vaz Bandeira de Melo, R. H. Brandenberger, and A. M. Junior, (2001), hep-ph/0110003.

[33] J. Ellis and D. N. Nanopoulos, Phys. Lett. **B116**, 133 (1982).

[34] K. Olive, Phys. Rep. 308 (1990).

[35] T. Moroi, Ph.D. Thesis (Mar. 1995), hep-ph/9503210.

[36] D. Chung, E. Kolb, and A. Riotto, Phys. Rev. **D60**, 063504 (1999), hep-ph/9809453.

[37] S. Y. Khlebnikov and I. I. Tkachev, Phys. Rev. Lett. **77**, 219 (1996), hep-ph/9603378.

[38] S. Y. Khlebnikov and I. I. Tkachev, Phys. Rev. Lett. **79**, 1607 (1997), hep-ph/9610477.

[39] G. Felder and L. Kofman, Phys. Rev. **D63**, 103503 (2001), hep-ph/0011160.

[40] S. Khlebnikov, L. Kofman, A. Linde, and I. Tkachev, Phys. Rev. Lett. **81**, 2012 (1998), hep-ph/9804425.

[41] I. Tkachev, S. Khlebnikov, L. Kofman, and A. Linde, Phys. Lett. **B440**, 262 (1998), hep-ph/9805209.

[42] Y. Shtanov, J. Traschen, and R. Brandenberger, Phy. Rev. **D51**, 5438 (1995).

[43] L. Kofman, in *Relativistic Astrophysics: A Conference in Honor of Igor Novikov's 60th Birthday*, Eds. B. Jones and D. Marcovic (Cambridge University Press, Cambridge Mass., 1997).

[44] D. Boyanovsky *et al.*, Phy. Rev. **D51**, 4419 (1995).

[45] D. Boyanovsky, H. J. de Vega, R. Holman, and J. F. J. Salgado, Phy. Rev. **D54**, 7570 (1996).

[46] D. I. Kaiser, Phy. Rev. **D56**, 706 (1997), hep-ph/9702244.

[47] T. Prokopec and T. G. Roos, Phy. Rev. **D55**, 3768 (1997), hep-ph/9610400.

[48] L. Kofman, A. Linde, and A. A. Starobinsky, Phys. Rev. Lett. 1011 (1996).

[49] A. Erdelyi, ed., *Higher Transcendental Functions, vol. 3* (Bateman Manuscript Project, McGraw-Hill, New York, 1955).

[50] M. Abramowitz and I. Stegun, *Handbook of Mathematical Functions* (Dover, New York, 1965).

[51] D. Kaiser, Phys. Rev. **D57**, 702 (1998), hep-ph/9707516.

[52] L. D. Landau and E. M. Lifshitz, *Quantum Mechanics (Non-relativistic theory)* (Pergamon Press, London, 1993).

[53] L. Kofman, A. Linde, and A. A. Starobinsky, unpublished .

[54] A. Riotto and I. Tkachev, Phy. Lett. **B385**, 57 (1996), hep-ph/9604444.

[55] S. Y. Khlebnikov and I. I. Tkachev, Phys. Lett. **B390**, 80 (1997), hep-ph/9608458.

[56] J. Baacke and C. Pätzold, Phys. Rev. **D62**, 084008 (2000), hep-ph/9912505.

[57] R. Kallosh, L. Kofman, A. Linde, and A. Van Proeyen, Phys. Rev. **D61**, 103503 (2000), hep-th/9907124.

[58] D. Chung, E. Kolb, A. Riotto, and I. Tkachev, Phys. Rev. **D62**, 043508 (2000), hep-ph/9910437.

[59] A. Linde, Phys. Lett. **B259**, 38 (1991).

[60] A. Linde, Phys. Rev. **D49**, 748 (1994).

[61] J. García-Bellido and A. Linde, Phys. Rev. **D57**, 6065 (1998).

[62] M. Bastero-Gil, S. King, and J. Sanderson, Phys. Rev. **D60**, 103517 (1999).

[63] J. García-Bellido, S. Mollerach, and E. Roulet, JHEP 034 (2000), hep-ph/0002076.

[64] D. A. Kirzhnits and A. D. Linde, Phys. Lett. **B42**, 471 (1972).

[65] D. A. Kirzhnits and A. D. Linde, Ann. Phys. 195 (1976).

[66] D. Boyanovsky *et al.*, Phys. Rev. **D56**, 3929 (1997).

[67] G. Felder and I. Tkachev, unpublished , lATTICEEASY URL: http://physics.stanford.edu/gfelder/latticeeasy/.

[68] D. Lyth and A. Riotto, Phys. Rept. **314**, 1 (1999), hep-ph/9807278.

[69] R. Jeannerot and J. Lesgourgues, Phys. Rev. **D62**, 023514 (2000).

[70] G. Felder, L. Kofman, and A. Linde, (2001), hep-th/0106179.

[71] A. Linde, Nucl. Phys. **B372**, 421 (1992).

[72] J. García-Bellido and D. Wands, Phys. Rev. **D54**, 7181 (1996), astro-ph/9606047.

[73] E. J. Copeland *et al.*, Phys. Rev. **D49**, 6410 (1994).

[74] J. R. Battye and J. Weller, Phys. Rev. **D61**, 043501 (1996), astro-ph/9810203.

[75] P. Binetruy and G. Dvali, Phys. Lett. **B388**, 241 (1996).

[76] C. Hill, H. Hodges, and M. Turner, Phys. Rev. **D37**, 263 (1988).

[77] G. F. Giudice, I. Tkachev, and A. Riotto, JHEP 009 (1999), hep-ph/9907510.

[78] J. García-Bellido, D. Grigoriev, A. Kusenko, and M. Shaposhnikov, Phys. Rev. **D60**, 123504 (1999).

[79] P. B. Greene, L. Kofman, and A. A. Starobinksy, Nucl. Phys. **B543**, 423 (1999), hep-ph/9808477.

[80] G. F. Giudice, A. Riotto, and I. Tkachev, JHEP 020 (2001), hep-ph/0103248.

[81] L. D. Landau and E. M. Lifshitz, *The Classical Theory of Fields* (Pergamon Press, London, 1993).

[82] N. D. Birrell and P. C. W. Davies, *Qunatum Fields in Curved Space* (Cambridge University Press, New York, 1982).